Aus dem Fachbereich Medizin

der Johann Wolfgang Goethe-Universität

Frankfurt am Main

betreut in der

Dr. Senckenbergischen Anatomie

Institut für Anatomie I

(Klinische Neuroanatomie)

Direktor: Prof. Dr. Thomas Deller

The plasticity-related protein Synaptopodin in the dentate gyrus and area CA2 of the mouse hippocampus

Dissertation

zur Erlangung des Doktorgrades der Medizin

des Fachbereichs Medizin

der Johann Wolfgang Goethe-Universität

Frankfurt am Main

vorgelegt von

Michael Rietsche

aus Karlsruhe

Frankfurt am Main, 2023

Dekan: Prof. Dr. Stefan Zeuzem

Referent: Prof. Dr. Thomas Deller

Korreferent: Prof. Dr. Georg Auburger

Tag der mündlichen Prüfung: 01.08.2024

Index

IV

1 Introduction

1.1 The anatomy of the mouse hippocampus

Since Patient H.M. in 1957 lost his ability to store new memories after bitemporal neurosurgical resections of the hippocampus[1], the mammalian hippocampus (HC) has been considered an essential brain structure for learning and memory[2,3]. In both rodents and primates the hippocampus is highly interconnected with parahippocampal cortices and, collectively, these brain regions are often referred to as the hippocampal formation[4]. As the basic neuroanatomy is quite conserved, with some expectable species-dependent differences, rats and mice have been used to study this brain region and have become widely used neuroscientific animal models[4] for the analysis of structure-function relationships in the hippocampus.

The mouse HC has been described as a "banana-shaped" structure[5] which curves from the septal nuclei all the way down to the temporal lobe (so-called "septo-temporal axis" of the hippocampus). It consists of two main parts, the cornu ammonis (CA) and the dentate gyrus (DG)[4]. In a frontal section through the brain, the dorsal HC (dHC) is cut almost perpendicular to the septo-temporal axis of the HC and both CA and DG are visible as two interleaved C-/V-shaped structures on Nissl-stained sections (Figure 1 A). The DG is further subdivided into three layers: the polymorphic cell layer (*pl*), also called the dentate hilus (*h*), the granule cell layer (*gcl*) harboring the somata of the dentate granule cells (GC), and the molecular layer (*ml*), which is filled up with the cone-shaped dendritic trees of the GCs[5-7] and their afferent axons. In the dHC, the granule cell layer envelops the hilus and the most proximal CA3 in a V-shaped fashion (Figure 1 A). The suprapyramidal blade – dorsal to CA3 – is separated from CA1 by the hippocampal fissure (*hf*). The infrapyramidal blade lies ventral to CA3. The apex of the V-shaped formation is called the crest.[5] The molecular layer is divided further into 3 sub-layers (Figure 8), based on the different afferents terminating in this layer. In the inner molecular layer (IML), axons from hilar mossy cells terminate on proximal GC dendrites[8]. The middle molecular layer (MML) receives input from layer II of the medial entorhinal cortex (MEC), the outer molecular layer (OML) is targeted by layer II of the lateral entorhinal cortex (LEC)[4,5,9].

Lorente de Nó[10] described the anatomy of the CA region in detail. He identified three CA-subregions[4] on the basis of the morphology of their principal neurons, the pyramidal cells. The CA1 region is characterized by densely-packed small neuronal somata[4], which form a single cell layer in the mouse. CA3, which is located closest to the hilar region of the dentate gyrus, harbors pyramidal cells with large somata and huge spiny protrusions called thorny excrescences. Thorny excrescences are the postsynaptic elements of complex GC-CA3 synapses formed in the stratum lucidum (*sl*) between mossy fibers and CA3 pyramidal cells[11,12]. Positioned between area CA1 and area CA3 is area CA2, which will be described in more detail in chapter 1.4. Both, area CA2 and area CA3 are further subdivided into subfields along the proximo-distal axis of the hippocampus based on differences in the innervation of these subfields by GC-axons, i.e. the mossy fibers (see legend to Figure 1 for further details). All three CA-subregions exhibit at least 4 layers: the principal cell layer is the pyramidal cell layer (*pcl*). Between this layer and the surface of the hippocampus lies stratum oriens (*so*). Between the pcl and the hippocampal fissure stratum radiatum (*sr*) and stratum lacunosum-moleculare (*slm*) are found (Figure 1 A and B). In CA3 and CA2b mossy fibers terminate on pyramidal neurons and form an additional layer right above the pcl called stratum lucidum (*sl*)[4].
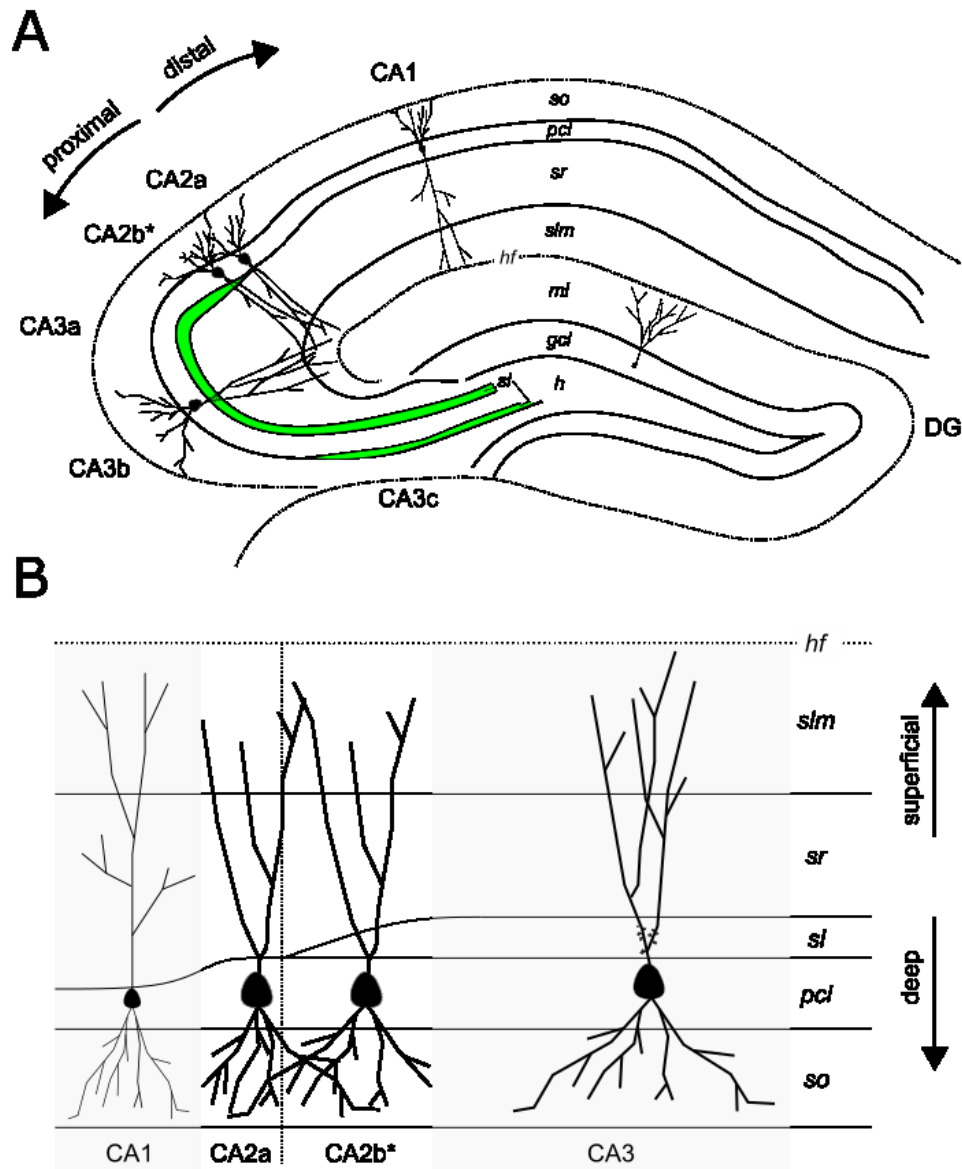
Figure 1: The hippocampus proper, made up by the CA and the DG. A: Diagram of the septal mouse hippocampus in a frontal brain section, indicating the CA-subregions and some principal cells. CA3 is subdivided along the proximo-distal axis[4,13,14]: CA3c is defined as the region with an additional infrapyramidal *sl* (green). CA3a is seen as the area where the *sl* starts to narrow down. CA3b is interposed between CA3a and CA3c. *h*: dentate hilus. *gcl*: granule cell layer. *ml*: molecular layer. *slm*: stratum lacunosum moleculare. *sr*: stratum radiatum. *sl*: stratum lucidum (green), mainly occupied by mossy fibers. *pcl*: pyramidal cell layer. *so*: stratum oriens. *hf*: hippocampal fissure, separating the *ml* from the *slm*. B: Lorente de Nó (1934) distinguished 3 CA-subregions based on their morphology: CA3-pyramidal neurons have large somata and exhibit thorny excrescences in *sl*. CA2-pyramidal neurons also show large somata, but lack thorny excrescences. CA1-pyramidal neurons show smaller somata than CA2 and CA3 neurons. A and B: * = recently defined CA2b-subregion receiving DG-input via the most distal *sl*, which is tapering out. (see also chapter 1.4 and Figure 2).

1.2 Dendritic spines and their subtypes

Dendritic spines, first described by Ramon y Cajal in 1888, are small membranous extensions distributed along the dendritic trees of many neurons in mammals, such as rodents (e.g. mice) or humans[15-17]. Dendritic spines receive the majority of excitatory glutamatergic afferents in telencephalic circuits[16-20]. Although dendritic spines have been described over a century ago, their role in memory and learning is not fully understood.

Spines are highly dynamic structures and they can change their shape and size within very short time intervals[20-23]. This allows spines to adapt their geometry and their cytosolic architecture to presynaptic activity. Spine size changes are associated with long lasting increases (long term potentiation, LTP) and long-lasting decreases of synaptic strength (long-term depression, LTD)[17,24].

Dendritic spines mature postnatally, presumably in an input-dependent manner[25]. Based on the analysis of fixed tissues, several different spine shapes or "spine classes" were defined: Filopodia-like protrusions (F), stubby-shaped spines (S), thin-shaped spines (T) and mushroom-shaped spines (M)[25-28]. Filopodia-like protrusions (F) are long, thin, serpent-like protrusions tapering off at the tip[16,19,20,27]. They are seen as the initial protrusion formed typically during neuronal development[25] with a high turnover and eventually developing into more mature spine shapes[29]. They also exist in the mature brain, mostly under specific conditions, e.g. after brain injury[29]. Stubby-shaped spines are hill- or cone-shaped protrusions without a spine neck, tapering off at the tip, showing a much longer transverse than longitudinal diameter[20,27,30,31]. Stubby spines form the predominant type in the early stages of postnatal development and also in mature neurons they are seen as an immature spine type, e.g. a spine undergoing pruning or maturation[32]. Some recent data obtained with super-resolution microscopy, e.g. STED, indicate that some stubby spines observed in confocal or bright-field microscopy are in fact mushroom-shaped spines with their spine head positioned too close to the dendritic shaft to be resolved as separate structures[33]. Another pitfall occurs if analysis takes place in projected images, e.g. in Golgi-stained material, as large mushroom-spines positioned along the z-axis in front or behind the dendritic shaft may imitate stubby spines[34]. Nevertheless, stubby-shaped spines do exist in the mature brain as they can be found regularly at the ultrastructural level, probably appearing in the process of

spine pruning or re-growth[27,28,32]. Thin- and Mushroom-shaped spines typically protrude in a more or less hill-shaped manner from the dendritic shaft, the spine base[35], then narrowing down to the so-called spine neck, and finally expanding again into a more or less large protrusion at the tip, the spine head[26,28,36]. Spine head size is the main – and probably the only valid – distinctive feature to classify spiny protrusions exhibiting a spine neck[19]: Thin spines have relatively small spine heads, while Mushroom spines show a larger spine head[19,20,27]. However, both spine classes are able to change spine head size dynamically in very short timeframes[20]. As a consequence, Thin and Mushroom spines form a continuum of mature spines with a wide range of spine head sizes, making it impossible to subjectively draw the border between both spine classes[19]. Consequently, interconversion of Thin and Mushroom shaped spines can readily occur at synapses depending on afferent activity.

The entire spectrum of spine shapes described above[15,19,20,28] was observed during experiments for this thesis. Taking into account the current concept of spines as a dynamic continuum[19,20], in this thesis dendritic spines were sorted only into three groups, as proposed by Berry et al 2017[20]: (I) Mature spines, i.e. every spine with a spine neck, thus encompassing the "Thin and Mushroom continuum". As stated above, these spines most probably do form a functional synapse, with spine head size correlating to synaptic strength and spine stability[20,22,24,28,30]. (II) Immature spines, including the spectrum of spines without a spine neck, comprising the "Filamentous and Stubby continuum". These spines presumably do not form strong excitatory synapses[20]. (III) The category of non-classifiable spines contains all spines, which could be verified as dendritic spines and were included in the spine density count but which could not be reliably assigned to either Group I or II (for details, please see chapter 2.6.1 and Figures 9-11).

Spine density describes the number of dendritic spines observed along a given length of dendritic segment. As the vast majority of excitatory synapses are formed with spines, spine density is commonly used as an estimate for the number of excitatory synapses of a given dendritic segment[20].

Spine head size has been correlated with synaptic strength and the area of the postsynaptic density (PSD), which in turn correlates with the number of AMPA receptors[19,31,37,38]. Besides the postsynaptic membrane, cytosolic organelles play

an important role for synaptic transmission and synaptic strength. The endoplasmatic reticulum (ER) is regularly found in dendritic spines. The complexity of spine ER is variable[39] and it has been linked to different kinds of synaptic plasticity[40-44]. Mechanistically it could act as a local calcium store[44,45], as a site of local protein synthesis[44,46] or as a regulator of trafficking of postsynaptic molecules[47,48]. Spine head size was shown to increase after LTP-induction, a phenomenon now termed structural LTP (sLTP)[21,24,47,49]. Whereas small spines are regarded as the reservoir for structural plasticity, large spines are considered important for memory traces[50].

1.3 The actin-binding protein Synaptopodin (SP) and its role beyond the spine apparatus (SA) in learning and memory

Synaptopodin (SP) is an actin-modulating protein first described by Mundel et al. (1997) in rodents, with a ~84 % identical sequence between mouse and human SP on the protein level[51]. SP exists in two organ-specific isoforms: The renal 110 kDa isoform is found in podocytes of the kidney, whereas the neuronal 100 kDa isoform is found in telencephalic neurons[51,52]. In this thesis, only the neuronal 100 kDa isoform was investigated, hence "SP" always refers to the brain-specific isoform, if not stated otherwise. SP is an almost linear protein due to the high percentage of proline equally distributed along the molecular structure, thus preventing globular protein domains[51-53]. SP-protein expression was reported to be age-dependent, starting postnatally in mice[51,54]. During maturation, protein expression increases[54], stays constant during adulthood, and is down-regulated in 15 months old C57BL/6 mice[55]. In the hippocampus of the adult brain, SP clusters are distributed in a layer- and region-specific fashion[56-59]. In principal neurons of the hippocampus, such as dentate granule cells or pyramidal cells of the CA, SP is sorted into three subcellular compartments: Dendritic spines, the axon initial segment, and the soma. Immunoreactive SP-clusters are found in dendritic spines[58], where SP was shown to be an essential component of a spine-specific organelle, the spine apparatus (SA)[60,61]. In the axon initial segment (AIS), SP is needed to form cisternal organelles[62-67]. In the soma of GCs, SP was shown to be associated with perinuclear endoplasmic reticulum[68]. All work conducted for this thesis focused on the spinous subcellular compartment of SP and its organelle, the SA[36,42].

The SA consists of two ultrastructurally visible components: Stacked cisterns of ER interleaved with electron dense material[36]. This electron dense material could be shown to be immunoreactive for SP[56,69]. The sER forms an intracellular membranous system of cisternes, tubules, and vesicles[44] and the SA-cisterns are connected with it. As the dendritic ER network does not enter all spines, three subsets of spines were proposed based on their sER content[17]: 1) spines without any sER (usually small spines), 2) spines containing unstacked sER but no SA, 3) spines with stacked sER cisterns called SA which typically exhibit a larger spine head[39,56,70]. The ratio of SP-positive (SP+) spines, i.e. spines containing cytosolic SP in head, neck and/or base, could be shown to vary in a layer-specific manner[58,71]. The ratio of SP+ spines was proposed to be an adequate estimate of dendritic spines containing a SA[58].

In a loss-of-function approach using SP-deficient mice (SP-KO), many sER-containing spines were found, but no spines containing the SA could be observed[60]. Therefore, it was suggested that SP, located in the dense material of the SA, is essential to form the SA-defining stacks of sER[17,60]. Synaptic plasticity was found to be reduced in SP-KO mice[17,47,60,72-74]. It could be shown that forming SA organelles is one important, but not the only function of SP. It is interacting with the actin cytoskeleton, which is crucial for spine formation, spine shape and sLTP[21] in a direct manner via stabilizing F-actin[51,75]. More indirectly, SP binds to actin-modulating molecules such as alpha-actinin-2, Cdc42, RhoA, or myosin V[17,52,76-79]. Adding to this, recent findings by Yap, Drakew, Smilovic, Rietsche et al. (2020) linked SP with the long term stability of dendritic spines, showing that SP stabilizes dendritic spines and that the presence of fluorescent SP-clusters in SP+ spines indicates spines of high stability[22]. On a mechanistic level, this could be due to SP interacting with the central pool of stable actin in the spine core[21,80-83]. Taken together, these findings show the important role of SP and the SA organelle in dendritic spines and synaptic plasticity, and thus on learning and memory[17,18,84,85].

However, it is still unknown what impact the overexpression or the lack of SP would have on of certain important spines parameters of GC dendrites of adult male mice, such as spine head size, spine head size distribution or the ratio of SP+ spines. SP mRNA is probably expressed somaticly[51,56] and then translocated into subcellular compartments. Besides a constitutive SP-

expression found in most telencephalic spiny neurons, transcription of SP was shown to be upregulated after synaptic activation[59,86].

In addition, behavioral stimulation via a new environment lead to an SP-upregulation in activity-regulated cytoskeleton protein (Arc)-positive ensembles of GCs in adult male mice[68]. Arc is a well-established immediate early gene (IEG) in the DG[87,88]. IEGs "are transiently and rapidly induced in response to stimulation"[87(p1631)].

1.4 Dorsal CA2 and social recognition memory

Morphologically, pyramidal neurons (also referred to as pyramidal cells, pc) in both CA2 and CA3 have large somata[4,14]. Lorente de Nó (1934) first noted that a small subgroup of large pc adjacent to the CA1-region were lacking thorny excrescences[10,89], thus differentiating them morphologically from CA3 pc. Thorny excrescences are the postsynaptic sites of the complex DG-CA3 synapse positioned in the *sl* delineated by bundles of mossy fibers[11,12]. Classically, CA2 was neuroanatomically defined as the subregion between CA3 and CA1 containing large pc's but lacking a *sl* and thorny excrescences and thus it was concluded that CA2 does not receive mossy fiber-input (Figure 1 B)[90]. In recent years, however, CA2-specific molecular markers have been identified, including regulator of G-protein signaling 14 (RGS 14) or purkinie-cell-protein 4 (PCP 4)[91,92]. At least in C57BL/6-mice, this molecular definition expanded the former narrow CA2 region towards CA3, including a considerable portion of the former most distal CA3a, where the *sl* does still exist, but is tapering out[89,92,93] (Figures 1, 3 and 20). Thus, a change in nomenclature has been proposed, renaming the classical CA2 without *sl* as CA2a, and the former most-distal CA3c as CA2b[89]. In CA2b, DG-axons were shown to form functional synapses with CA2b-pc's[92]. However, to the author's knowledge no study has so far demonstrated thorny excrescences on molecularly defined CA2-pc in CA2b.

The dorsal CA2-subregion (dCA2) receives extra- and intrahippocampal afferents in a layer-specific manner[89,94] (Figure 2). Dendrites of CA2 neurons in *sr* form excitatory synapses with Schaffer collaterals arising from CA3 pc's[95,96]. Dendrites of CA2 neurons in *slm* are targeted by axons from layer II of the medial EC (MEC) and lateral EC (LEC)[92,97,98]. The *sl* of dCA2b also receives mossy fiber input from the DG[92]. The *so* of CA2, as in all CA-subregions, receives recurrent collateral

input[4,14], contains somata of interneurons and receives axonal collaterals of bistratified interneurons[4]. Extrahippocampal axons from the supramammillary nucleus (SUM) were shown to terminate in the *so* and *pcl* of CA2 and CA3a[99], with Substance P providing one of the numerous neuromodulators reaching the CA2-region from extrahippocampal sources[89]. Another example are vassopressinergic fibers from the hypothalamic periventricular nucleus (PVN)[100,101].
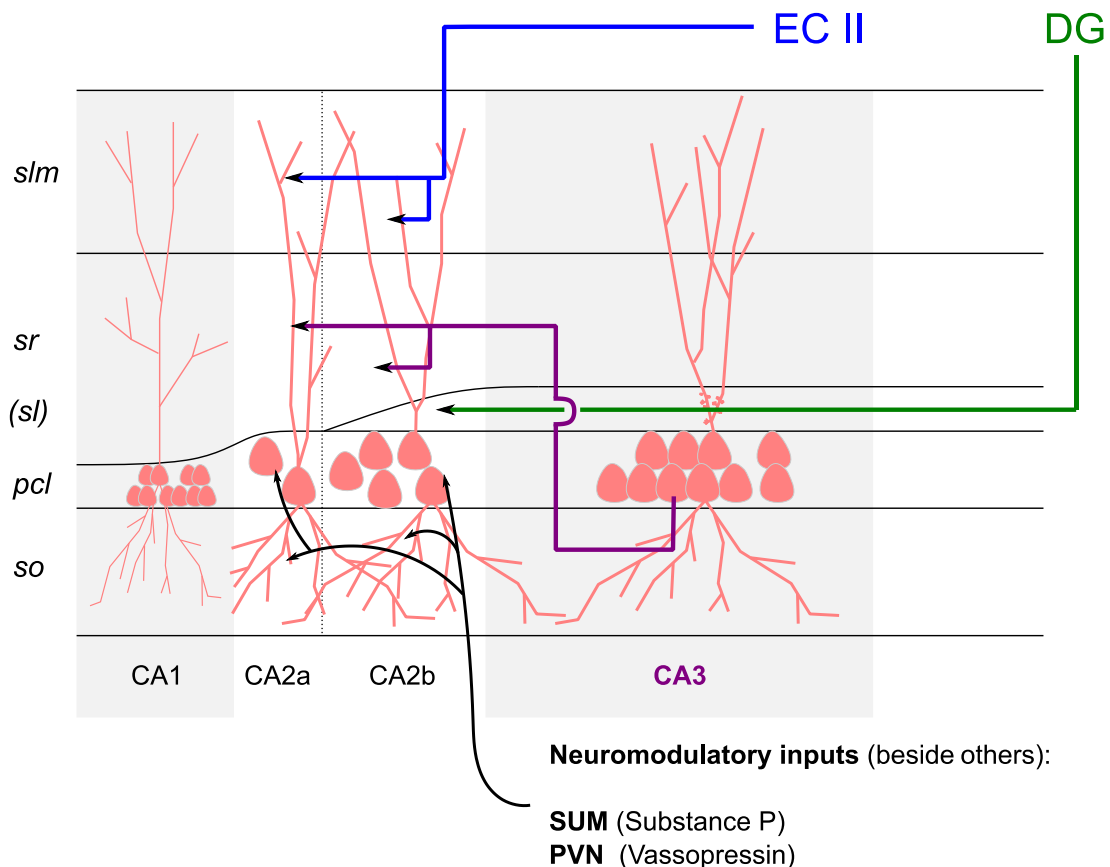
Figure 2: Schematic diagram showing major afferents to dCA2. In stratum radiatum (*sr*), dCA2-pc's receive glutamatergic input from ipsilateral and contralateral CA3-pc's (purple). In stratum lacunosum-moleculare (*slm*), axons from the ipsilateral ECII (blue) forms glutamatergic EC-CA2 synapses. In stratum lucidum (*sl*) of CA2b, mossy fibers from the ipsilateral DG target proximal dendrites in the *sl* of dCA2, which is typically is tapering out proximo-distally. Contralateral dCA2 also targets *sr* of ipsilateral dCA2 (not shown). Various neuromodulators from various subcortical nuclei target dCA2 (black), such as the supramammillary nucleus (SUM) or the paraventricular nucleus (PVN). Although detailed data is sparse, at least SUM-fibers were shown to mainly target the pyramidal cell layer (*pcl*) and Stratum oriens (*so*). EC II = Layer II of the Entorhinal Cortex. DG = dentate gyrus.

It could be shown in the last decades that in dCA2, synaptic plasticity such as LTP is tightly regulated in a lamina-specific manner[102-104]. CA3-CA2 synapses in *sr* were shown to be resistant to classical LTP-induction[96] due to robust Ca^{2+}-buffering[105], postsynaptic signaling pathways limiting plasticity (also involving the molecular CA2-markers PCP 4 and RGS 14)[105,106] and due to the perineural nets (PNN), which is a specialized form of extracellular matrix (ECM) surrounding excitatory CA2-synapses[107,108]. In contrast in the *slm*, a strong LTP at excitatory ECII-CA2 synapses could be easily elicited[109]. Most recently, LECII-projections to *slm* of dCA2 were shown to regulate social recognition memory[97]. The dCA2-subregion is crucial for social recognition memory formation[110]. Social recognition memory was described as "the ability of an animal to remember a conspecific"[110], which is essential to behave correctly in social contexts for both humans and vertebrates such as rodents[111]. Concerning social recognition memory dynamics, it could be shown that dCA2 is necessary for the formation, encoding, consolidation and the recall of social recognition memory[112]. In addition, Meira et al. (2018) discovered the projections of dCA2 to deep ventral CA1 (vCA1), and more downstream, the vCA1-projection to the shell of the Nucleus accumbens (NAc), which is essential for social recognition memory dynamics[112]. Interestingly, vCA1 seems to store social recognition memory engrams[113] (Figure 3).

Besides the role of CA2 in social recognition memory, it has been suggested that CA2 works as a hub distributing information[114,115]. More recently, additional functions of CA2 have been proposed, such as computing novelty or saliency[116], temporal sequence-learning[117], working memory[118] and hippocampal sharp-wave-ripples which are important for memory consolidation[114].
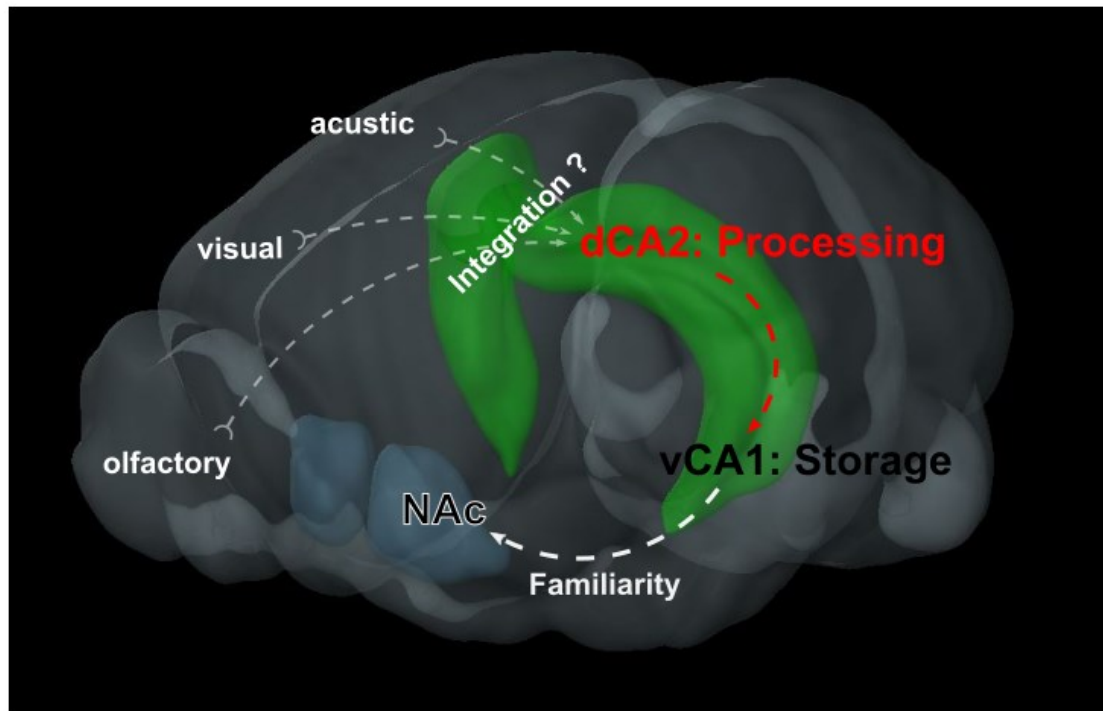
Figure 3: Neuronal circuits involved in social recognition memory. A conspecific mouse could be identified and recognized via multimodal inputs, such as olfactory, visual and/or auditory cues. dCA2 is important for information processing (formation, encoding, consolidation and recall of social memory[112]). vCA1 stores social memory engrams[113,119]. vCA1-pc's use three main pathways for efferent projections, e.g. onto the shell of NAc.[120] vCA1-NAc(Shell) projections are important for social memory strorage[113]. Adapted from: Allen Mouse Brain Atlas, mouse.brain-map.org and atlas.brain-map.org, in a 3D representation with the Brain Explorer 2[121]. Based on Watarai et al. (2021)[119].

Although most CA2-studies were carried out in male animals, a recent study that included male and female mice revealed a CA2 neuronal activity-dependent sexual dimorphism of behavioural fear responses[122] (see also chapter 1.5). Another sexual dimorphism concerning the dendritic trees of CA2-pc's could be shown in guinea pigs[123]: After Golgi-impregnation, Bartesaghi et al. (1999) observed in both male and female animals four morphologically distinct CA2-pc (termed Ma, Mb, Mc and B). The morphometry of Ma, Mb and B neurons showed significant sex differences, mostly in favor of larger morphometry in males: soma dimension, shaft thickness, number of distal branches, number apical of apical branches (Ma and Mb only). In contrast, female B neurons showed more branches at their proximal apical and basal dendritic tree. Due to this findings, Bartesaghi et al. (1999) proposed "...that the synaptic function in field CA2 is sexually dimorphic"[123(p270)], and requested more specific studies on this topic, as

well as Dudek, Alexander and Farris (2016) did more recently[89]. Similarly, little is known about differences of spine densities and spine head sizes on apical and basal pc-dendrites in the molecularly defined dCA2[89]. Likewise, the distribution of intracellular components of spines, e.g. the plasticity-related protein SP, has not yet been studied in the CA2 region.

1.5 Sexual dimorphisms in dendritic spine morphology, synaptic plasticity, SP expression and social recognition memory

Biomedical research is often conducted on male animals or young male human patients[124,125]. In the light of the important sex-specific differences that have been uncovered during the last decades, awareness for this topic has increased and there have been efforts to reduce the so-called "gender-gap" in biomedical research[126-128].

Focusing on dendritic spine density, the pioneering work of Woolley et al. (1990) showed estrous cycle-dependent fluctuations in the apical compartment in CA1 of the rat[129], which was followed by decades of research concerning sex-hormones and their influence on learning and memory and synaptic plasticity[130]. Concerning dendritic spines, the focus was mostly set on spine density.[131]

In vertebrates, two main sources of sex hormones have to be distinguished: (a) Peripheral production of androgens, namely testosterone, and estrogens, e.g. 17β-estradiol[132], and, (b) central synthesis of steroid hormones by neurons in the CNS itself, via neuronal aromatase[133], also called sex neurosteroids[134]. As corticosteroids in general, serum-estradiol is able to cross the blood brain barrier (BBB) via transmembrane diffusion[135]. However, to what extent the cycle-dependent, assumingly estrogen-dependent changes of dendritic spine density are driven via peripheral hormone levels or local synthesis of neurosteroids remains under vivid discussion[132,134].

Importantly, neither cortex nor the cerebellum shows cycle-dependent changes in spine density[136], thus leaving the hippocampus of the rat as the only known site of cycle-dependent changes of spine densities[134,137]. Intrahippocampally, region- and layer-specific sex-differences have been shown[138,139]. Only recently, similar studies were performed in mice. Brandt et. al (2020) could show that, in contrast to Woolley's findings in the rat, adult female mice did not show a cycle-

dependent fluctuation of spine density on apical CA1-dendrites[140] if all predefined spine classes (following Sorra and Harris, 2000[141]) were included. However, a cycle-dependent fluctuation was found for spines with a large spine head, defined by the authors as >0.6 µm diameter, across the 4 estrous cycle-stages (metestrus, diestrus, proestrus, estrus). Interestingly, peak spine density of large spines was found in diestrus. Males showed a significantly lower density of large spines with >0.6 µm head diameter, compared to females (all cycle stages pooled) [140]. These findings point to a species-dependent difference in estrous cycle-dependent changes of spine density, which is of importance as a number of studies include both rats and mice when investigating sex-specific differences in the hippocampus.

However, sex-dependent variances introduced by female rodents were shown to be far less than it has been assumed for a long time[142,143]. Interestingly, male mice housed in groups have been shown to exhibit very different levels of serum-testosterone, dependent on social dominance or subordinance[144]. In general, if a potential sex difference is suspected, it was proposed to consider controlling female animals included for neuroscientific experiments for their current stage of the estrous cycle[145].

Female mice have an average 4-5 day cycle[146,147]. The number of defined estrous cycle stages varies in literature[148]. For this thesis, the following 4 stages are used: diestrus, proestrus, estrus, metestrus[149]. Cycle stage can be determined *in vivo* using vaginal cytology[150]. Blood levels of sex hormones such as estradiol and progesterone fluctuate during the rodent estrous cycle, as indicated in Figure 4[151].
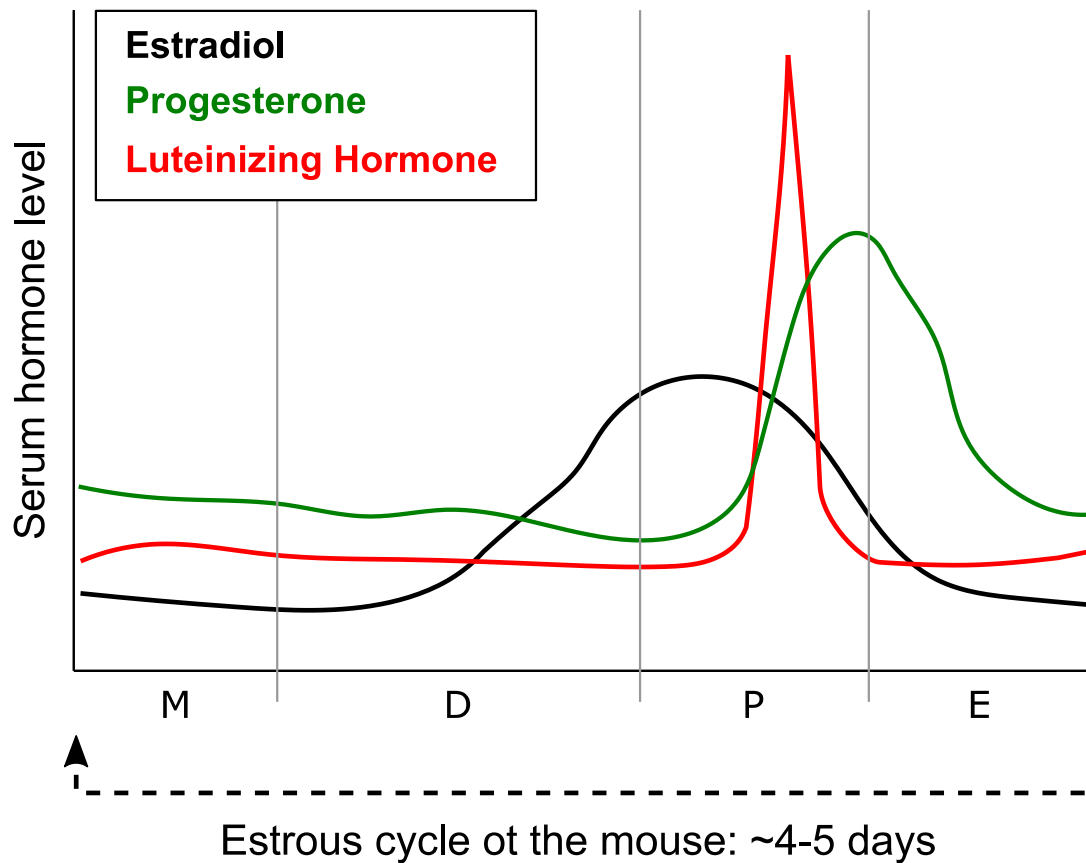
Figure 4: Serum hormone levels throughout the rodent estrous cycle. Schematic displaying the serum hormone levels of Estradiol (black), Progesterone (red) and Luteinizing Hormone (green) throughout the rodent estrous cycle, based on Goldman et al. (2007)[151]. M = Metestrus. D = Diestrus. P = Proestrus. E = Estrus.

Long-lasting increase of spine head size due to synaptic stimulation has been termed structural long-term potentiation (sLTP)[152]. LTP has been shown to be sex-specifically controlled in male and female hippocampus of mice: Estrogens influence LTP in females, androgens influence LTP in males[153]. However, no study investigating spine head size as a potential proxy for sLTP[21], spine density, and spine morphology has been carried out in adult male and female <u>mice</u> *ex vivo*, concerning the molecularly defined dCA2-region.

In dissociated hippocampal neurons derived von E18 Wistar rats, neurons of female animals expressed significantly more spines with a head-diameter >0.6 µm (the authors' definition of mushroom spines in the respective study), whereas spines with a head diameter <0.6 µm (defined by the authors as thin spines) were found more often in males than in females[154].

In hippocampal neurons of both sexes, estrogens are synthesized by the enzyme aromatase, with testosterone as a substrate[155]. SP was shown to be highly responsive to estrogens[156,157]. Mechanistically, Ca^{2+} transients from internal stores were shown to control aromatase activity in hippocampal neurons of adult mice, whereas aromatase regulates SP expression[158]. Interestingly, this regulation seems to take place in a sex-independent manner: after drug-induced aromatase inhibition in WT-mice, immunoreactivity of SP was downregulated in both male and female mice in a similar fashion. The same phenomenon was observed in male and female aromatase-knock out mice[158]. In *sr* of dCA1, a higher fluorescence of SP puncta was shown in adult female mice, compared to adult males[158]. In contrast, at the EM-level the number of SA did not show any differences between male and female adult mice in *sr* of CA1[140]. Notably, in both of these studies females were not controlled for estrous cycle-stage.

As mentioned before, dCA2 is crucial for social recognition memory, the ability to remember a conspecific, which is vital for any individual in social contexts. Behavioral differences in social memory and social exploration are known in both humans and in rodents[111,159]. In addition, recent findings showed sex-specific differences in CA2-dependent fear-conditioning[122]. Anatomically, cytoarchitectural sexual dimorphism of the apical dendritic tree of CA2-pc's has been shown in guinea pigs[123]. Early studies already indicated layer-specific differences in estrogen-level-dependent spine density, as only apical dendrites in *slm* of CA1 showed cycle-dependent changes in spine density in the rat, whereas in the *so*, i.e. the basal compartment, the cycle-dependent fluctuations were not significantly different[129]. However, nothing is known so far concerning sex-specific differences on the level of dendritic spines in the molecularly defined dCA2.

1.6 Aims of this thesis

SP/SA play an important role in synaptic plasticity as well as learning and memory. The present thesis focused on two under-investigated aspects of SP in the hippocampus: First, the impact of different expression levels of SP (gain-of-function, loss-of-function) on spine morphology were investigated in the DG *ex vivo* in male adult mice. Second, SP analysis and spine morphometry was expanded towards sex-specific differences in dCA2 in adult male and female mice, since SP is regulated by the activity of aromatase, the essential enzyme for estrogen-synthesis[158].

1.6.1 Gain-of-function and loss-of-function of SP in the dentate gyrus

The first aim of this thesis was to investigate the impact of SP-overexpression on spine density, spine morphology, and the distribution of SP in GC-dendrites (i.e. the ratio of SP+ spines and the SP-cluster size of SP+ spines) in SP-overexpressing adult male mice (CSPtg). Therefore, adult male SP-overexpressing mice and wild-type animals (WT) were perfused and individual GCs were intracellularly labeled with fluorescent dye and immunostained for SP. A robust spine analysis algorithm was established and used for the morphometric analysis of spines in confocal z-stacks of GC dendrites in the OML of the DG. SP-cluster sizes and the ratio of SP+ spines were quantified and correlated with the respective spine head size at the single spine-level.

Previous studies in SP-deficient adult male mice revealed deficits in synaptic plasticity of CA1-pc's, while spine density remained unchanged.[60] However, *ex vivo* data from adult mouse dentate GCs is still missing. Therefore, the second aim of this thesis was to investigate the impact of SP-deficiency on the spine head size and spine density of GC. Adult male SP-deficient SP-KO and WT animals mice were perfused and individual GCs were intracellularly labeled with fluorescent dye. Again, spine analysis was performed in confocal z-stacks of GC-dendrites in the OML of the DG.

The specific questions were as follows:

1. Does SP-overexpression change spine density in the OML? What happens under SP-deficiency?

2. What impact does SP-overexpression or SP-deficiency have on spine head size?

3. Does the ratio of SP+ spines change and in what manner?

4. Is there a difference of SP-puncta size in SP+ spines in CSPtg-mice, compared to the control group?

5. Does SP-puncta size and spine head size correlate in control animals? If yes, in what manner? And does that change under SP-overexpression?

6. Is there a difference in spine head size of SP+ and SP− spines?

1.6.2 CA2-Subregion

CA2 is essential for social recognition memory[110]. Sex-dependent behavioral differences in social recognition are known in humans as well as in rodents[111,159]. Recent findings showed sex-specific differences in CA2-dependent fear-conditioning[122]. Anatomically, a cytoarchitectural sexual dimorphism of CA2-pc's has been shown in guinea pigs[123]. In male mice, dCA2 receives layer-specific synaptic input from intra- and extrahippocampal brain regions[89,110]. A layer-specific regulation of plasticity at axo-spinous synapses was shown in the apical compartment[96,109,160]. Also, a lamina-dependent distribution of SP[71] has been shown for CA1 and CA3 in the male mouse hippocampus[58]. However, similar data is missing for CA2. Most previous studies were carried out in male animals only, and few microanatomical studies have been published on the apical and basal compartments of pc's in the molecularly defined CA2 region[89].

Therefore, the next aim of this thesis was to investigate potential sex-specific differences in spine density, spine morphology, and SP distribution in the dCA2-subregion of adult male and female animals, in a lamina-specific manner. The following aims and questions were addressed with regard to dCA2 cells:

1. Establishing the intracellular injection-technique of fluorescent dye in fixed tissue[161,162] to label individual cells *ex vivo* in adult mouse brains.

2. Is there a layer-specific difference in spine density or spine head size between apical and basal dendrites? If so, does it occur in a similar fashion in adult male and female (diestrus) mice?

3. Is there a sex-specific difference in spine density or spine head size in the apical part of the dendritic tree, i.e. *sr*? Can sex-dependent differences be identified in the basal compartment, i.e. *so*?

4. Do spines show structural correlates for the layer-specific regulation of synaptic plasticity, i.e. differences in spine head size in *sr* vs. *so*?

5. Are there any sex-specific differences in the distribution of SP between dendrites of male and female (diestrus) mice located in stratum oriens?

6. Are there similar spine head size differences between SP+ and SP– spines in dCA2 compared to the DG? Does SP cluster-size correlate with spine head size on the single spine-level?

2 Materials and Methods

2.1 Animals

Adult mice used to investigate dentate GC in fixed tissue were bred and housed at MfD GmbH, Wendelsheim. Animals were maintained on a 12 hr light/dark cycle with food and water available ad libitum.

Adult mice used to investigate pyramidal cells of the CA2-subregion in fixed tissue were ordered and subsequently housed at the animal facility of Goethe University Hospital Frankfurt. Female C57/Bl6 mice were housed in groups of 3–5 in standard individually ventilated cages on a 12 h light/dark cycle (lights on at 7:00) under controlled ambient conditions (21 ± 1 °C, 55 ± 5% humidity). All mice were habituated to the facility for at least 7 days before perfusion and aged between 10-12 weeks, separated by gender, mating did never occur. Food and water were available ad libitum. Animal care and all experimental procedures were conducted in accordance with the Directive of the European Communities Council of 24 November 1986 (86/609/EEC) and German animal welfare laws (TierSchG and TSchV), had been declared to the Animal Welfare Officer of the Medical Faculty (Wa-2014–35) and were approved by the Darmstadt regional council. Every effort was made to minimize the distress and pain of animals.

2.1.1 Dentate gyrus: CFP-SP-transgenic (CSPtg), SP-deficient (SP-KO) and WT adult male mice (all C57BL/6 background)

In gain-of-function experiments, adult male mice overexpressing SP (CSPtg, n = 6 animals) were investigated, their WT litter mates were used as control animals (WT, n = 6 animals). CSPtg mice express an additional eCFP-tagged allele of Synaptopodin under the Thy1.2-promotor on a C57BL/6J genetic background (Figure 5). They were generated by Del Turco et al. (unpublished) by pronucleus injection of an eCFP-tagged SP construct, similarly as described for Thy1-GFP/SP mice elsewhere[61]. Due to the Thy1.2-promotor, expression of the eCFP-tagged SP occurs specifically in neurons[163,164]. CSPtg animals therefore carry three alleles of SP, one eCFP-tagged allele in addition to the two alleles of mouse brain SP already existing in the C57BL/6J WT mouse, leading to an increased expression of SP in CSPtg mice compared to WT animals (gain-of-function).
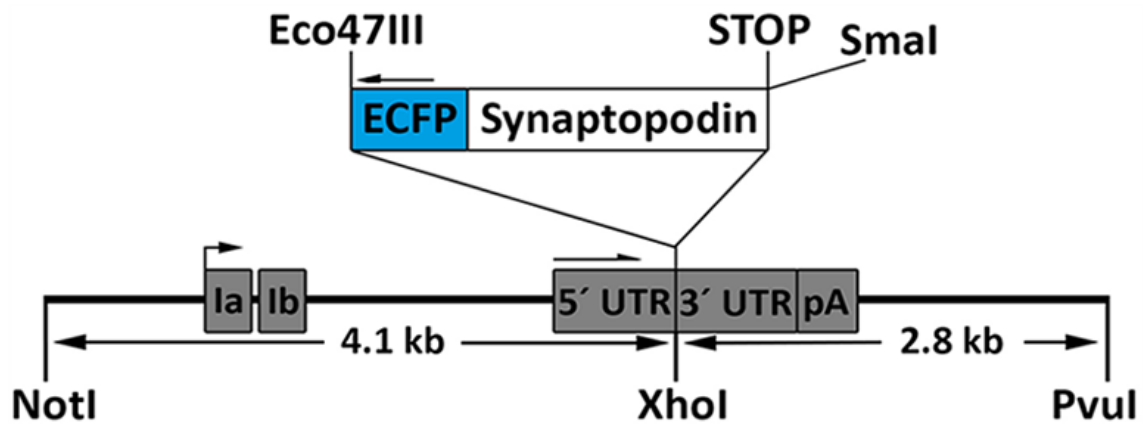
Figure 5: Diagram of the genetic construct used to generate transgenic CSPtg mice. A fragment of the Thy1.2 expression cassette (NotI-PvuI) includes essential sequences for expression. The eCFP-tagged mouse SP cDNA was cloned into the XhoI site of the expression cassette. Gray boxes mark the exons of the Thy1.2 gene. The arrow at exon Ia indicates the transcription start site. pA = polyadenylation sequence; UTR = untranslated region. Del Turco*, Paul*, Rietsche et al., unpublished.

In loss-of-function experiments, adult male mice lacking SP[60] (SP-KO, C57BL/6J background, n = 8 animals) and WT animals as controls (Synpo +/+, C57BL/6J background, n = 8 animals) were investigated.[22] In the same study, male adult mice expressing eGFP-tagged SP under the Thy1-promoter were also investigated (Thy1-eGFP-SP x SP-KO, eGFP-SP-tg, C57BL/6J background, n = 6 animals)[22,61]. As homozygote Thy1-eGFP-SP transgenic mice were crossbred with SP-deficient mice[53], the resulting eGFP-SP-tg mice carry only one allele of eGFP-SP, resulting in moderate SP mRNA-expression levels[22,61].

2.1.2 CA2-Subregion: Female adult mice in the diestrus stage of the estrous cycle and male adult mice (both C57Bl/6J)

Adult male and female mice in the diestrus stage of the estrous cycle (C57BL/6J WT animals, 10-12 weeks old) were used to study pyramidal cells in the dorsal area of CA2 (dCA2). Basal dendrites in *so* of dCA2 pyramidal cells were investigated in n = 6 male and in n = 6 female animals. In a subset of these animals, apical dendrites in *sr* of dCA2 pyramidal cells were investigated (male: n = 4 animals, female: n = 3 animals). For female animals, the diestrus stage of the estrous cycle was determined using vaginal cytology[150] by Prof. Dr. David Slattery and Dr. Aet O'Leary (Group of Translational Psychiatry, Department of Psychiatry, Psychosomatic Medicine and Psychotherapy, University Hospital,

Goethe University, Frankfurt, Germany). Only female animals in the diestrus stage of the estrous cycle were included in the study, as dendritic spine density[129] and spine head size[140] can fluctuate during the course of the estrous cycle.

2.2 Tissue preparation

2.2.1 Dentate gyrus

For intracellular injections of dentate GC, adult male animals were first killed with an overdose of 0.1 ml Pentobarbital-Natrium i.p. (Merial GmbH, Narcoren, 16 g/100 ml) and subsequently perfused intracardially using a gravity-based perfusion system. Tail biopsies were obtained from each animal after death and before fixation to reconfirm genotypes via PCR. To obtain optimal tissue for intracellular injections, the cardiovascular system was rinsed first with 0.1 M phosphate-buffered saline (PBS, pH 7.4) at room temperature (RT) for 1-2 min, followed by perfusion with 4 % paraformaldehyde in 0.1 M PBS (PFA, pH 7.4, RT) for 4 minutes. Brains were taken out immediately and post-fixed in 4 % PFA in 0.1 M PBS for 18 hours at 4°C. After washing 2 times with ice-cold 0.1 M PBS (pH 7.4), 250 μm-frontal slices containing the dorsal hippocampus were obtained with a vibratome (Leica VT 1000 S). Slices were stored in 0.1 M PBS at 4°C until intracellular injections were performed.

2.2.2 CA2-Subregion

For investigation of CA2-pc, adult mice were intracardially perfused using a perfusion pump (Fisher Scientific, Model # 78-91001) by Prof. Dr. David Slattery and Dr. Aet O'Leary (Group of Translational Psychiatry, Department of Psychiatry, Psychosomatic Medicine and Psychotherapy, University Hospital, Goethe University, Frankfurt, Germany). The cardiovascular system was rinsed first with 0.1 M PBS at room temperature (RT) for 1-2 min, followed by 4 % PFA in 0.1 M PBS for 4 min (males) and 3 min (females). This was done to adjust for sex-specific differences in body weight at the same age, leading to a comparable fixation of brain tissue in both genders and thus achieve optimal tissue conditions for intracellular injections with fluorescent dye.[165] Brains were taken out immediately and post-fixed in 4 % PFA in 0.1 M PBS, at 4°C up to 18 h. Subsequently, brains were washed 3 times with ice-cold 0.1 M PBS and 250 μm sections of dorsal area CA2 (dCA2) were obtained using a vibratome (Leica VT 1000 S).

In contrast to dentate granule cells or pyramidal neurons in the CA1-subregion, it turned out to be difficult to label entire pc in the CA2-subregion in strictly frontal slices. Consistent with previous observations[166], in strictly frontal sections the apical dendrites of dCA2-pc were visible, but rapidly "dived" into deeper layers of the section when the soma was injected at the rostral surface, making it often impossible to judge the quality of the labeling in the apical compartment. When a soma of a dCA2-pc was injected from the caudal surface, pc close to the surface did not even show apical dendrites, some somata injected more deeply showed short trunks of apical dendrites. In contrast, in *so* basal dendrites were visible when injections were performed from the caudal surface, and by observation in higher numbers as when injections were performed at the rostral surface. Therefore, I concluded that the dendritic trees of dCA2-pc are not orientated strictly frontally but are tilted, i.e. the apical compartment is orientated caudally, whereas the basal compartment is orientated rostrally (Figure 6).
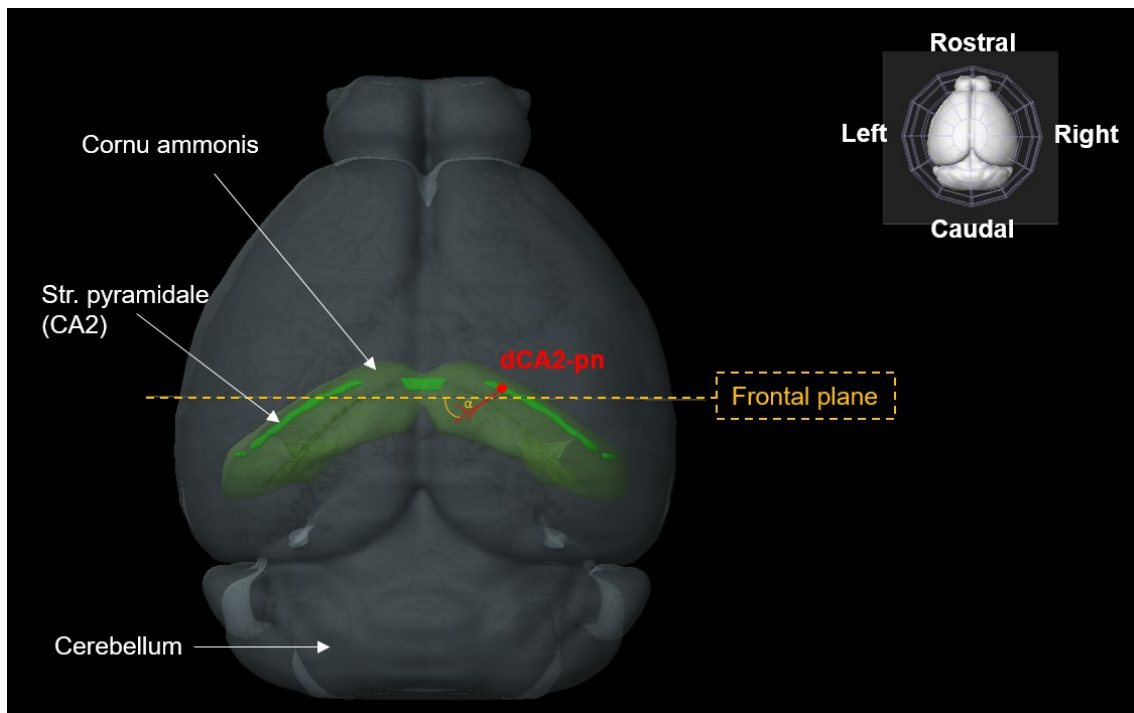
Figure 6: Spatial orientation of pyramidal neurons of the dorsal CA2. Dorsal view on a 3D-reconstruction of the mouse brain. Red: Spatial orientation of an intracellularly injected dCA2-pc with the apical dendritic tree, as observed in frontal sections. Basal dendrites not shown. α = ~ 30° (estimated in n = 4 neurons from n = 2 animals: 1 male, 1 female). Transparent green: Cornu ammonis. Light green: Stratum pyramidale of the CA2-subregion. Adapted from: Allen Mouse Brain Atlas, mouse.brain-map.org and atlas.brain-map.org, in a 3D representation with the Brain Explorer 2[121].

As a result, the cutting plane had to be adjusted to yield sections that included complete dendrites. In the optimal case for intracellular injections of fluorescent dyes in fixed tissue, the dendritic tree of the target cell is oriented horizontally to the surface of a section, thus facilitating assessment of injection quality, as less tissue obscures the fluorescence of dendrites. Confocal image stacks are taken in parallel to the surface of the section (i.e. in parallel to the cover slip), therefore dendrites running in parallel to the surface facilitate imaging and analysis of dendrites and dendritic spines. In addition, the chance to preserve the dendritic tree during re-slicing is increased and therefore the re-attribution of the dendritic order of a given dendritic segment is facilitated. To optimize the cutting plane at the vibratome, and hence the spatial orientation of dCA2-pc in fixed brain sections, a custom-made platform was built (Figure 7 A).
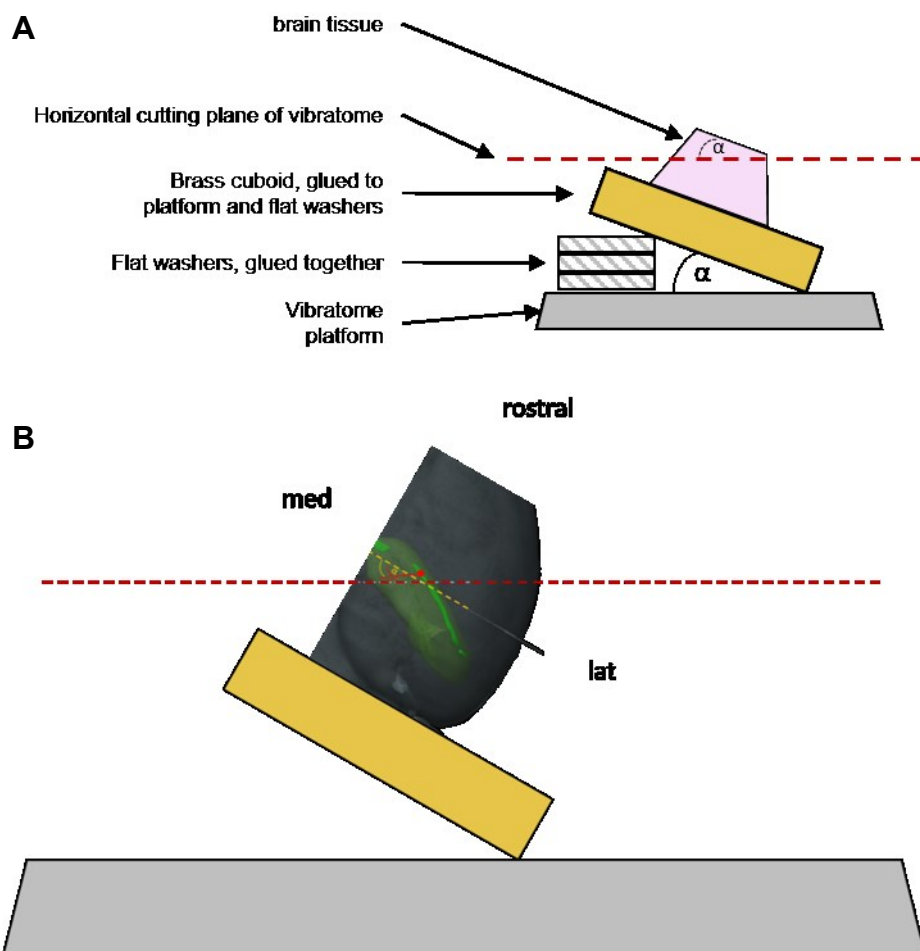
Figure 7: Custom-made vibratome platform to optimize cutting plane for intracellular injections of pyramidal neurons in dCA2. A: Schematic representation of the custom-made platform to cut brain tissue in a defined angle α (α = 30° already improved intracellular injections in dCA2). B: A right brain hemisphere glued onto the vibratome platform, displaying the spatial

orientation of injected dCA2-pc. Gray polygon: Vibratome baseplate. Yellow rectangle: Brass cuboid. Red dotted line: Cutting plane of vibratome. med = medial. lat = lateral. In part adapted from: Allen Mouse Brain Atlas, mouse.brain-map.org and atlas.brain-map.org, in a 3D representation with the 3D – Brain Explorer 2.[121]

To obtain 250 µm sections containing dCA2 in an optimal cutting plane for intracellular injections, brains were processed as follows: (1) Using a cutting matrix to standardize frontal sectioning (Alto Coronal Brain Matrix, Mouse 45-75 Gram; 1mm), the cerebellum and the olfactory bulbs including the most rostral part of the cortex were cut off with a razor blade. Afterwards, a median-sagittal cut was performed to divide both hemispheres. The right hemisphere was marked by cutting away some basal cortex. (2) Each hemisphere was embedded upright, i.e. the caudal cut surface downwards, the rostral cut surface up, in 5 % Agar (PanReac AppliChem, Agar powdered pure/Food grade) in 0.1 M PBS. (3) Embedded hemispheres where glued onto the custom-made vibratome platform with the medial cut surface orientated uphill (Figure 7 B), and 250 µm thick sections containing the dorsal hippocampus were obtained. The agar was removed and sections were stored in 0.1 M PBS at 4°C until intracellular injections were performed.

2.3   Intracellular labeling of identified neurons in fixed tissue

2.3.1   Dentate gyrus

Using the intracellular injection technique of fluorescent dye in fixed tissue[161,167], individual dentate granule cells (GC) were labeled in the suprapyramidal blade of the dentate gyrus (DG) with 0.75 mM Alexa 568-Hydrazide (Thermo Fisher Scientific, Alexa Fluor® 568 Hydrazide). A 250 µm thick slice containing the dorsal hippocampus was placed in a custom-built, transparent, and grounded chamber filled with ice-cold 0.1 M PBS. The chamber was mounted on a fixed-stage tower system (Science Products, Patch Clamp Tower System). An epifluorescent microscope (Olympus BX51WI; Olympus) attached to a x-y translation table (Science Products, VT-1 xy Microscope Translator) and a 10x objective with a long working distance (Olympus LMPlanFLN10x, NA 0.25, WD 21mm; Olympus) were used for visualization (Figure 8 A). Sharp quartz-glass microelectrodes with a filament (Sutter Instruments; O.D: 1.0 mm, I.D.: 0.7 mm; 10 cm length; Art. Nr.: QF100-70-10) were produced using a laser puller (Sutter P-2000, Sutter Instruments). The tip of a microelectrode was loaded with

0.75 mM Alexa Fluor 568-Hydrazide (A568, Thermo Fisher Scientific) in HPLC-grade water (VWR Chemicals, HiPerSolv CHROMANORM) and subsequently back-filled with 0.1 M LiCl in HPLC-grade H2O. Microelectrodes were attached to an electrophoretic setup via a silver wire and a 500 MΩ resistance (Figure 8 B). A square voltage (1 mV, 1 Hz) was applied using a voltage generator (Gwinstek SFG-2102; Gwinstek) and visualized on an oscilloscope (Gould; 20 Ms/sec Oscilloscop [DSO] 1602) The tip of the microelectrode was navigated over the GCL (suprapyramidal blade) using a micromanipulator (Märzhäuser Wetzlar, Manipulator DC-3K) and epifluorescent microscopy (Olympus BX51WI). As adult-newborn granule cells are typically located deep in the GCL, i.e. close to the hilus[168], and as they can differ from adult granule cells[169], intracellular injections were performed in the superficial half of the GCL whenever possible, i.e. close to the molecular layer. The electrode was advanced into the tissue under visual control using epifluorescent microscopy. Once the impalement of a soma was observed, the offset was set to negative and the cell filled for at least 10 minutes or until no further labeling was observed. (Figure 8 C). I was able to label several dentate granule cells in the same slice while minimizing overlaps of dendritic trees. Injected sections were fixed with 4 % PFA in PBS overnight at 4°C under lightprotection. Subsequently, slices were washed with ice-cold 0.1 M PBS 3 times. Brain sections from SP-KO, eGFP-SP-tg mice and their respective control animals were whole-mounted in DAKO (Dako North America Inc., Dako Fluorescence Mounting Medium), with the injected somata orientated to the coverglass[22]. Brain sections from CSPtg mice and their control animals were stored in 0.1 M PBS (4°C, lightprotected) for re-slicing and immunostaining. In general, only GC with dendrites reaching the hippocampal fissure (hf) were included for analysis.
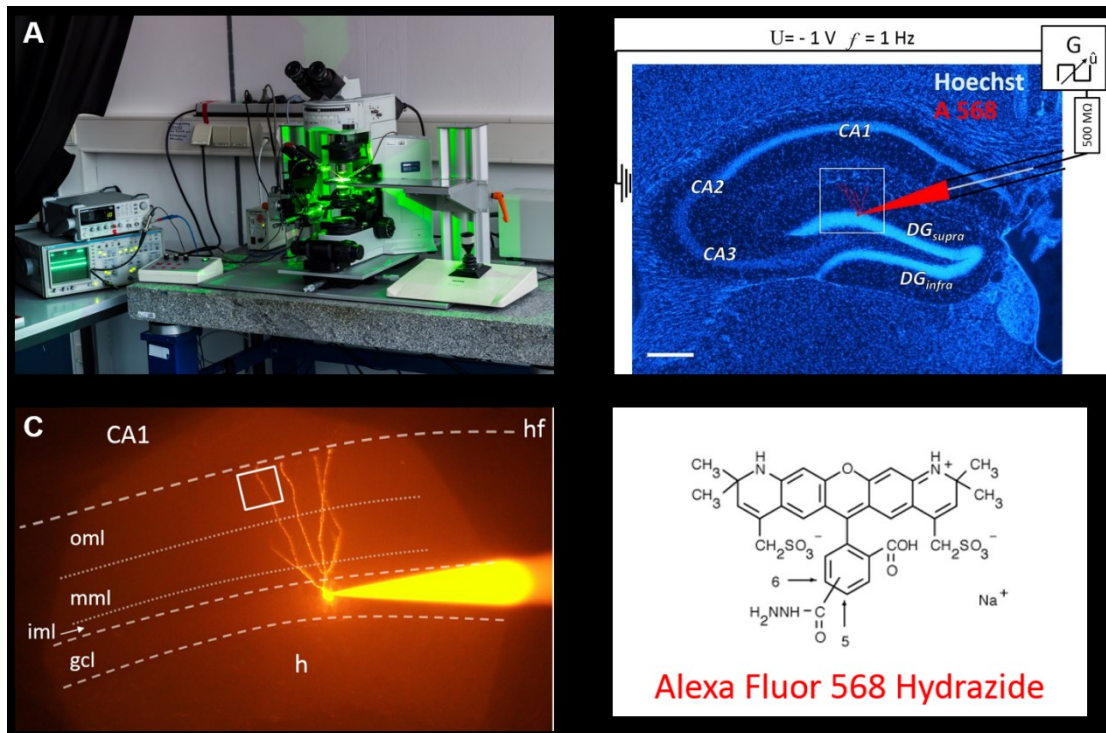
Figure 8: Intracellular injection of fluorescent dye in fixed tissue. A: Electrophoretic setup placed on a vibration-damped table. B: A sharp quartz-glass microelectrode, tip-loaded with 0.75 mM Alexa Fluor 568-Hydrazide (A568) and back-filled with 0.1 M LiCl was attached to an electrophoretic setup via a silver wire and a 500 MΩ resistance. A square voltage (1 mV, 1 Hz) was applied using a voltage generator and visualized on an oscilloscope (A, left). Under visual control using epifluorescence microscopy, the microelectrode was lowered into the target area of a 250 μm brain section (here: granule cell layer, suprapyramidal blade of dentate gyrus). C: Once a soma was penetrated, the cell was filled until no further labeling was observed. Epifluorescent image from the area indicated in B. A dentate GC being injected with A568. Most of the dendritic tree is labeled up to the hippocampal fissure (hf). White box marks the location used for confocal imaging. D: Molecular structure of Alexa Fluor 568 Hydrazide, which can be fixed with PFA. (adapted from: ThermoFisher Scientific). CA1, CA2, CA3 = Subregions CA1-CA3 of the cornu ammonis. DG_{supra} = suprapyramidal blade of dentate gyrus. DG_{infra} = infrapyramidal blade of dentate gyrus. oml = outer molecular layer. mml = middle molecular layer. iml = inner molecular layer. gcl = granule cell layer. h = hilus of dentate gyrus.

2.3.2 CA2-Subregion

To facilitate targeting the pyramidal cell layer (pcl) of CA2, sections were incubated with Hoechst 1:5000 (Sigma-Aldrich, bisBenzimide H 33342 trihydrochloride) in 0.1 M PBS for 10 minutes at RT and washed twice with 0.1 M PBS. As described elsewhere[91,170,171], borders of dCA2 are quite distinguishable using nuclei staining, as "[...]progressing from CA1 to CA2, the cell density in the

pyramidal cell layer abruptly decreases, and, progressing from CA2 to CA3, the thickness in that layer subtly increases."[170] Sections were positioned in a grounded, custom-made basin filled with 0.1 M PBS and mounted on a fixed-stage tower system (Science Products, Patch Clamp Tower System). For visualization, an Olympus BX51WI microscope (Olympus) attached to an x-y translation table (Science Products, VT-1 xy Microscope Translator) and a 10x objective with a long working distance (Olympus LMPlanFLN10x, NA 0.25, WD 21mm; Olympus) was used. Sharp quartz glass electrodes containing a filament (Sutter Instruments QF100-70-10; O.D: 1.0 mm, I.D.: 0.7 mm; 10 cm length) were produced with a Sutter P-2000 laser puller (Sutter Instruments). Electrode tips were filled with 0.75 mM A568 in HPLC-grade H_2O (VWR Chemicals, HiPerSolv CHROMANORM) and backfilled with 0.1 M LiCl in HPLC-grade H_2O. Under visual control by alternate use of fluorescent channels (nuclei-staining vs. A568), the electrode was lowered into the pcl of dCA2 while applying a negative square voltage pulse (-1 V, 1 Hz) via a silver wire in line with a 500 MOhm resistance using a motorized 3D micromanipulator (Märzhäuser Wetzlar, Manipulator DC-3K). Once a soma of a pyramidal neuron (pc) was penetrated, cells were filled for at least 10 minutes or until no further labeling was observed. Several injections were carried out from proximal CA1 across CA2 until distal CA3 in the same section to maximize the number of intracellularly injected pyramidal neuron, post-hoc molecularly identified as dCA2-pc. 250 µm thick sections containing intracellularly labeled pyramidal neurons were fixed with 4 % PFA in PBS overnight (4°C, light protected) and washed twice with 0.1 M PBS. To document the morphology of complete dendritic trees of the injected neurons before re-slicing, sections were temporarily mounted on glass slides in 0.1 M PBS, with the injected somata orientated towards the cover-glass, and confocal z-stacks were taken, using a confocal microscope (Olympus FV1000, Olympus) and a 20x objective (UPlanSApo, NA 0.75, Olympus) with a step size of 1-2 µm. To avoid photo-bleaching, reduced image size was used if necessary, e.g. of 512x512 or 256x256 pixels, when image quality was sufficient to determine the order of the dendrite. Right after imaging, sections were unmounted, rinsed with 0.1 M PBS and stored at 4°C in PBS for immunostaining.

2.4 Immunohistochemistry

2.4.1 Dentate gyrus

Brain sections from CSPtg-mice (250 µm) and their control animals with individually labeled GCs were embedded in 5% Agar in 0.1 M PBS and re-sliced to 40 µm thick sections on the vibratome (VT1000 S, Leica). To visualize SP, free-floating 40 µm sections were washed 3 times for 5 minutes in 0.05 M Tris-buffered saline (TBS) containing 0.1 % Triton X-100 and 0.01 % NaN_3 and incubated with a blocking buffer (0.5 % Triton X-100, 0.01 % NaN_3 and 5 % bovine serum albumin [BSA] in 0.05 M TBS) for 30 min at RT to reduce unspecific binding. Sections were incubated with a primary antibody (guinea pig anti-Synaptopodin; Synaptic Systems), diluted 1:2000 in a solution of 0.5 % Triton X-100, 0.01 % NaN and 1 % BSA in 0.05 M TBS for 68 hours at RT. After washing 3 times for 5 minutes (0.1 % Triton X-100 and 0.01 % NaN_3 in 0.05 M TBS), sections were incubated with a secondary antibody (donkey anti-guinea pig A 488, Dianova) diluted 1:2000 in a solution of 0.1 % Triton X-100, 0.01 % NaN_3 and 1 % BSA in 0.05 M TBS for 4 hours at RT. Finally, sections were washed 3 times for 5 minutes with 0.05 M TBS containing 0.01 % NaN_3 at RT and mounted in Fluorescence Mounting Medium (Dako, Dako North America Inc.).

Injected 250 µm thick sections from SP-KO animals and their control animals were whole-mounted in Fluorescence Mounting Medium (Dako, Dako North America Inc.) and not further processed before confocal imaging. The same applies for injected 250 µm thick sections from eGFP-SP-tg mice. These data were acquired together with Dinko Smilović (D.S.), who did perform tissue preparation, intracellular injections of dentate granule cells, confocal imaging and the quantification of spine head sizes (blind to genotype, following the protocol outlined in chapter 2.6.1). My own contributions consisted of establishing the experimental techniques stated above, the training of D.S., intracardial perfusion of animals, tissue preparation, intracellular injections of dentate granule cells and statistics (data published in Yap, Rietsche et al. 2020[22]).

2.4.2   CA2-Subregion

Brain sections (250 µm) with individually labeled pc were embedded in 5 % agar in 0.1 M PBS and re-sliced to 40 µm thick sections using a vibratome (VT1000 S, Leica). To verify A568-injected pyramidal neurons as dCA2-pc[92] using the molecular marker Purkinje Cell Protein 4 (PCP4)[93] and to label SP, free-floating 40 µm sections were washed three times in 0.05 M TBS containing 0.1 % Triton X-100 and 0.01 % NaN_3 and incubated with a blocking buffer (0.5 % Triton X-100, 0.01 % NaN_3 and 5 % BSA in 0.05 M TBS) for 30 min at RT. Subsequently, sections were incubated with primary antibodies for 68 h at RT (rabbit anti-PCP4 polyclonal, 1:1000, Atlas Antibodies; guinea-pig anti-Synaptopodin, 1:2000, Synaptic Systems), diluted in a solution of 0.5 % Triton X-100, 0.01 % NaN_3 and 1 % BSA in 0.05 M TBS. Slices were washed 4 times with 0.05 M TBS containing 0.1 % Triton X-100 and 0.01 % NaN_3 and then incubated with secondary antibodies and nuclear staining for 4 h at RT (goat anti-rabbit Alexa 647, 1:1000, Life Technologies; donkey anti-guinea pig Alexa 488, 1:2000, Dianova Jackson Immuno Research; Hoechst 1:50000, bisBenzimide H 33342 trihydrochloride, Sigma-Aldrich), diluted in a solution of 0.1 % Triton X-100, 0.01 % NaN_3 and 1 % BSA in 0.05 M TBS. Finally, slices were washed four times with 0.05 M TBS containing 0.01 % NaN_3 and mounted in Fluorescence Mounting Medium (Dako, Dako North America Inc.).

2.5   Confocal microscopy

2.5.1   Dentate gyrus

For CSPtg-mice and their control animals, confocal z-stacks sized 1024x1024 pixels of identified A568-labeled dendritic segments in the OML immunostained for SP were obtained using a confocal microscope (Nikon Eclipse 80i; Nikon) and a 60x oil immersion objective (NA 1.3; Nikon) with a 5x scan zoom and a step size of 0.25 µm. Image stacks were taken in a predefined corridor at maximum 50 µm away from hf, with a minimum distance of 10 µm from hf. Imaging parameters for SP were kept the same across all image stacks, except an adjustment of gain in a predefined narrow corridor. A568-labeled dendrites were imaged with the dendritic shaft as bright as possible while not oversaturating dendritic spines at the same time[172]. Only dendritic segments with all protrusions completely

captured in the image stack and with an optimal SP signal were included in the analysis. Branching points or overlaps with adjacent dendritic segments were avoided, it was ensured that every spine could be attributed to each segment.

For SP-KO mice, their control animals and eGFP-SP-tg mice, image stacks of A568-labeled dendritic segments from identified, A568-labeled dentate granule cells where acquired in the OML, using a confocal microscope (Olympus FV1000; Olympus) and a 60x oil-immersion objective (UPlanSApo; NA 1.35; Olympus) with a 5x scan zoom and a step size of 0.25 µm. Again, imaging was carried out in an area at least 10 µm and at maximum 50 µm away from hf. Crossing over of adjacent dendrites and branching points were avoided. In eGFP-SP-tg mice, both eGFP-tagged SP and the A568-labeled dendritic segments were imaged with the same imaging parameters for SP across all images. The imaging parameters were set to visualize the dendritic segment as intensely as possible, while not oversaturating any spines. In case of very large and intensely labeled spines, i.e. when oversaturation was unavoidable, a compromise was found between good signal-to-noise ratio and minimal oversaturation. Image stacks from SP-KO mice, their control animals and eGFP-SP-tg mice were deconvolved with Huygens Professional Software (v19.04, Scientific Volume Imaging) using the same parameters for all image stacks.

2.5.2 CA2-Subregion

Image stacks sized 1024x1024 pixels of A568-labeled basal dendritic segments (3rd-6th branching order) in *so* and A568-labeled apical dendritic segments (3rd-6th branching order) in *sr* of PCP4-positive (PCP4+) dCA2-pc were obtained using a confocal microscope (Olympus FV1000; Olympus), a 60x oil-immersion objective (UPlanSApo; NA 1.35; Olympus) with a 5x zoom and a step size of 0.25 µm. Imaging parameters for SP were kept the same for all segments. A568-labeled dendrites were imaged as bright as possible while not oversaturating dendritic spines[172] and subsequently deconvolved with Huygens Professional Software (v19.04, Scientific Volume Imaging), applying the same parameters across all image stacks.

2.6 Image analysis

Prior to analysis, the A568-signal (dendritic structures) was optimized for contrast and brightness, for all segments in the same way, again avoiding oversaturation of spines. The SP-signal always remained unchanged.

The density of dendritic spines, the subtypes of dendritic spines, spine head size, SP-cluster size and the ratio of SP-positive spines (SP+) were quantified in image stacks using Fiji[173] and a pen tablet (Intuos CTH-480, Wacom), always with the investigator blind to genotypes. Manual spine analysis in the CA2-subregion was performed using a Java-based plugin developed in-house by Dr. Tassilo Jungenitz (SpineAnalyzerJ).

2.6.1 Quantification of dendritic spines

First, the beginning and end of a given dendritic segment were defined, making sure the segment was entirely captured in the z-stack and the signal-to-noise ratio was at comparable levels across all dendritic segments included in the analysis. The length of each segment was determined by outlining the dendritic shaft in a maximum-z-projection, quantifying the length of both borders and then building the mean length of the segment from both measurements. A standardized protocol for spine quantification was applied (adapted from Holtmaat et al., 2009[34]). To determine the density of dendritic spines [1/µm], every protrusion crossing a predefined spine threshold with at least 1 pixel was included (Figure 9), and then assigned to one of the predefined spine groups, as outlined in chapter 1.2: mature spines, immature spines or non-classifiable spines.[19,20,27] (see below and Figures 10 and 11). The spine threshold (orange in Figure 9) was set at a distance of 0.2 µm (pink in Figure 9) from the dendritic shaft (blue in Figure 9), which corresponds to the resolution limit of our confocal microscopes. This way only protrusions extending more than 0.2 µm laterally from the dendritic shaft were quantified, making sure that (1) a given protrusion did really exceed the fluorescence halo of the dendritic shaft, thus minimizing investigator-dependent bias[34], (2) for head size analysis only those protrusions were included that extended laterally (i.e. within the x-y plane of the z-stack), thus minimizing bias by protrusions oriented in the z-direction (see also Figures 9 and 11 C; Holtmaat et al., 2009).

Maximum-z-projection
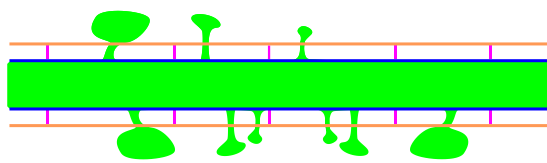
border of
dendritic shaft

spine threshold

limit of spatial resolution
(0.2 μm)

**Single x-y-planes
of z-stack**

included

included

not included

only included for
spine density
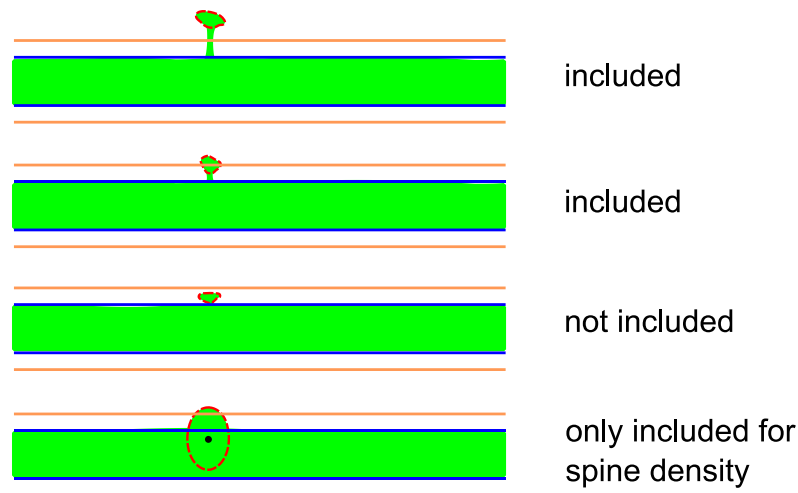
Figure 9: Standardized protocol to quantify spine density and spine head size. The shaft of a dendritic segment (blue) labeled with fluorescent dye (green) and the spine threshold (pink) were defined in a maximum-z-projection image. In a second step, spines were manually identified in the image stack. Every protrusion crossing a predefined spine threshold (orange) with at least 1 pixel was included for spine density analysis and assigned to one of the predefined spine groups (see also Figure 10). The spine threshold was set at a distance of 0.2 μm from the dendritic shaft, which corresponds to the resolution limit of our confocal microscopes (magenta). The maximum cross-sectional area (areamax, red) of a spine head was quantified manually in the respective x-y plane, if it crossed the spine threshold and exceeded the border of the dendritic shaft by ≥ 50%. Black dot = center of areamax. Adapted from Holtmaat el al. (2009) and Jungenitz et al. (2018)[9,34].

As outlined in detail in chapter 1.2, dendritic spines included for analysis were attributed to one of three predefined spine groups[20]: Mature, Immature and non-classifiable spines. Mature spines include all spines exhibiting a spine head, separated from the shaft by a spine neck. This group encompasses two traditional spine classes, i.e. mushroom- and thin-shaped spines. In the early literature, a mushroom-shaped (M) spine was defined as a spine with a large spine head and

a narrow neck[27,28], whereas a thin spine (T) was defined as a spine with a neck and a small head[27,28]. Hence, the spine head size is the main difference between M and T spines[19]. As dendritic spines are highly dynamic structures[20,34] and as spine head size can change in short periods of time *in vivo*[28], it has been pointed out that M and T spines can rapidly interconvert [19,28]. However, the "point of interconversion" cannot be clearly defined, as spine shapes probably form a dynamic continuum[19,20]. Therefore, one main focus was set on spine head quantification, as a direct morphometric measurement[174] for each protrusion with a spine neck, summarizing them as mature spines for the sake of quantification of spine classes in the CA2-subregion of the hippocampus. For this thesis, a spine head was defined as an enlargement at the tip of a spiny protrusion, regularly accompanied with an increase in fluorescence intensity. The spine neck was defined as the thinner connection between the spine head and the dendritic shaft, distinguishing the two (Figure 10). Immature spines[20] include all spines without either a spine neck or a head. Thus, this group encompasses the stubby and filiform spines of the traditional classification of spines (Figure 10).
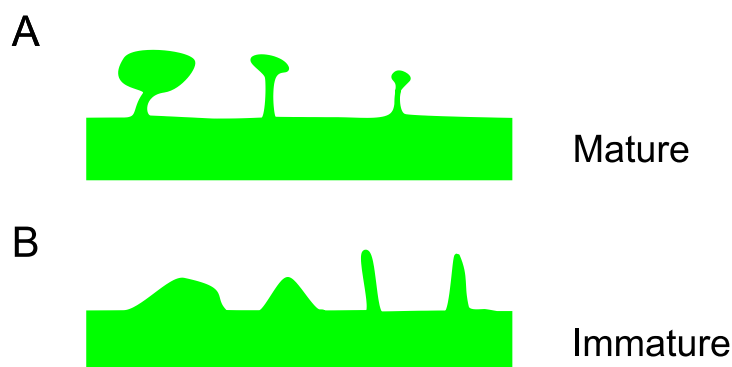
Figure 10: Spine groups. A: Spines with a spine head and spine neck are considered mature spines. These mature spines encompass "mushroom" and "thin" spines of the traditional classification of spines. These spines are believed to form functional synapses[20]. B: Protrusions without a spine neck or clear head[19] were classified as immature spines[20]. These spines encompass the "stubby" and "filiform" spines of the traditional classification of spines.

A meticulous analysis algorithm was developed to reliably quantify the complex three-dimensional structure of dendritic spines in a two-dimensional x-y-plane. The head size of mature spines crossing the spine-threshold (Figure 9) was determined by tracking the spines of a given dendritic segment throughout the image stack[9]. Then, the maximum cross-sectional area (areamax, red in Figure

9) of a spine head was manually quantified, if areamax exceeded the dendritic border by ≥ 50%. This way, only spines spreading lateral enough for valid quantification were included in the analysis (Figure 11).
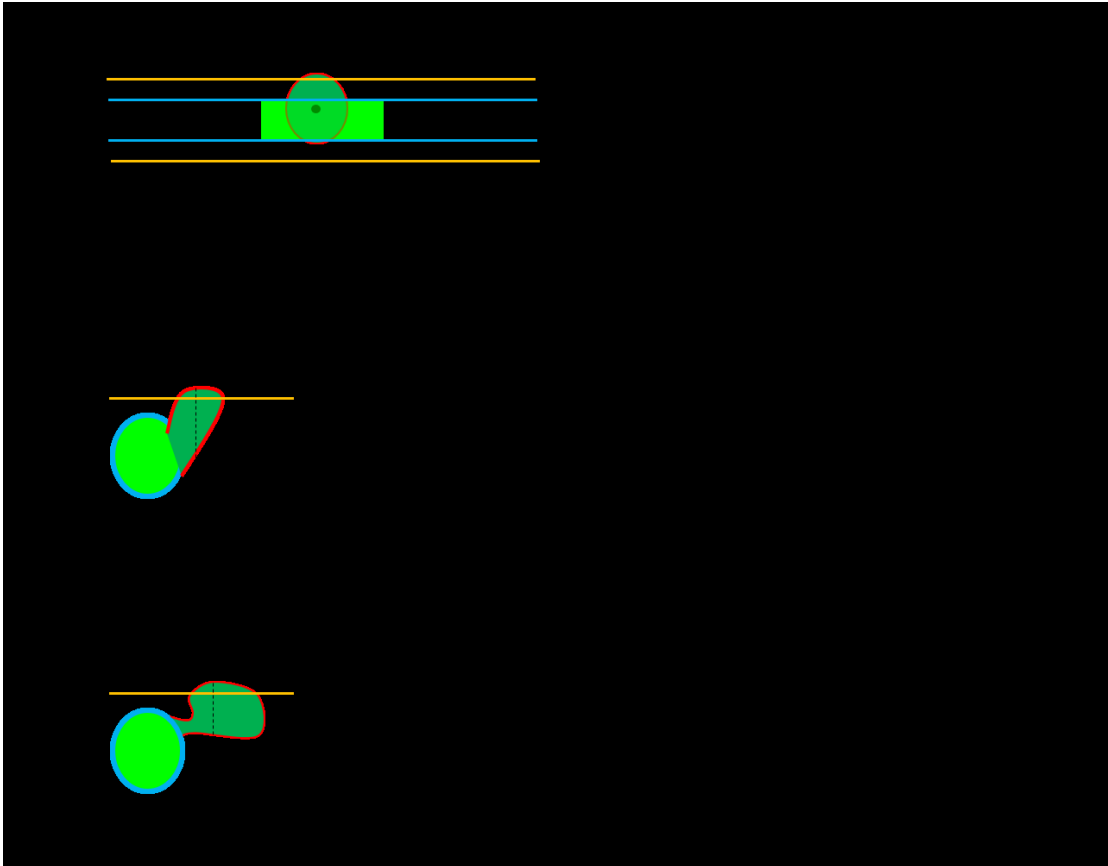
Figure 11: Rationale to include only spines spreading laterally for quantification in the x-y dimension. A: Schematic representation of a single x-y plane from a confocal image stack of a dendritic segment, with a large protrusion running in the z-dimension. Note that areamax (red) of the protrusion crosses the spine threshold (orange), but less than 50 % lies outside the border of the dendritic shaft (blue). For dendritic protrusions oriented in z, it is difficult to judge in x-y images if a given protrusion is a stubby spine without a neck (B) or a spine with a spine neck, which separates the spine head from the dendritic shaft (C).

When performing analysis in two-dimensional x-y image stacks, due to the three-dimensional nature of dendritic spines sprouting along the dendritic shaft, some protrusion are bound to cross the spine threshold (Figure 9), thus meeting criteria to be included for spine density analysis, while being oriented too much in z-dimension to be reliably quantified and/or even reliably classified (Figure 11). Therefore, such spines were counted only for spine density (Figure 9). This avoided the inclusion of stubby-spines in the head size quantification (Figure 11).

Spines that were counted for density but not for spine head size were grouped together and termed "non-classifiable" spines.

2.6.2 Quantification of Synaptopodin

The areamax of SP-clusters co-localizing with identified dendritic spines was quantified using a software macro for image segmentation while applying the same parameters across all image stacks. In the rare case that the macro failed to recognize a SP-cluster, measurements were corrected manually by an investigator blind to genotype. Spines were judged SP-positive (SP+) if the areamax of a SP-cluster co-localized with the spine for more than 50% of its area in x-y, x-z, and y-z Dimension and in 3D-reconstructions, otherwise, they were judged SP-negative (SP–). Finally, the ratio of SP+ spines of a dendritic segment was calculated:

$$\frac{n\ (SP+spines)}{n\ (all\ spines)}\ [\%]$$

In the rare case that multiple SP-punctae co-localized with the same single SP+ spine, the areamax of all SP-punctae were added for correlation to the respective spine head size, in assumption that the whole amount of SP present in a dendritic spine most probably would be able to affect spine head size.

Of note, SP-analyses were performed after finalizing the spine head quantification of all dendritic segments included for analysis. This ensured that the investigator was not only blind to genotype, but also blind to the SP-content of a given spine, further minimizing the risk of a rater bias.

2.7 Statistics

The Graphpad Prism Software (Prism 6, Version 6.07, GraphPad Software, Inc.) was used to test for statistical significance. Mean values of 2 groups were tested for significant difference using the Mann-Whitney U-test. To compare cumulative distributions the Kolmogorov-Smirnov test was applied. For paired data-sets from 2 groups the Wilcoxon matched-pairs signed rank test was used. Statistical significance was defined as $P \leq 0.05$. Asterisks indicate statistical significant differences as follows:* $p \leq 0.05$, ** $p \leq 0.01$, *** $p \leq 0.001$, **** $p \leq 0.0001$. Graphs without showing no significant difference between mean values or cumulative

41

distributions are either not marked by asterisks (blank) or with the comment n.s. = not significant. Error bars represent standard error of the mean (SEM).

2.8 Image processing and Figure composition

For figure composition, Microsoft Powerpoint 2016 software (Microsoft Office Professional Plus 2016), Fiji[173] software and Inkscape sofware (Version 1.1, www.inkscape.org) was used. Images were contrast-adjusted linearly if necessary to optimize visualization. If scaling was applied, only bilinear scaling was used in Fiji. The composition of Figures 12-14 and Figures 16-18 was accomplished together with Dr. Mandy Paul, based on data and images obtained by the author of this thesis.

3 Results

3.1 Dentate gyrus: Effects of SP-overexpression on granule cell dendrites

3.1.1 Overexpression of Synaptopodin in transgenic male mice does not affect the density of dendritic spines

The majority of excitatory synapses in the mammalian brain are formed with dendritic spines as postsynaptic sites[175]. Therefore, the density of dendritic spines formed along a given dendritic segment has been considered the equivalent for the number of glutamatergic synapses impinging on a neuron[20]. Investigations of apical dendrites in CA1 of SP-deficient male mice showed that the absence of SP does not affect spine density in adult male animals[60]. In this earlier study the density of spines of adult mouse GCs was not analyzed.

To address this question, the mean spine density of GC dendrites in the OML was determined. In short, the length of a given granule cell dendritic segment in the OML was determined. Each spiny protrusion was tracked manually in the image stack and counted for spine density if it crossed the predefined spine threshold, irrespective of its shape or class[34]. The spine density [spines/μm] was calculated for each segment and the mean spine density for each animal was determined.

There was no significant difference in mean spine density between SP--overexpressing CSPtg-mice and WT animals (CSPtg: 2.06 spines/μm. WT: 2.05 spines/μm. p = 0.699, Mann-Whitney U-test, Figure 13 A). Consistent with previous findings in CA1 of SP-deficient mice[60], differences in SP expression do not seem to alter the density of GC spines in the OML.

3.1.2 SP-overexpression increases the ratio of SP-positive (SP+) spines *in vivo*

One of the main questions was if and how the overexpression of SP affects the sorting of SP into spines. Specifically, it was of interest to test whether an increase in SP expression levels changes the fraction of spines containing a SP cluster (SP+ spines). As SP was shown to be essential for SA-formation[60], SP+ spines presumably carry a SA or are at least much more prone to do so[176].
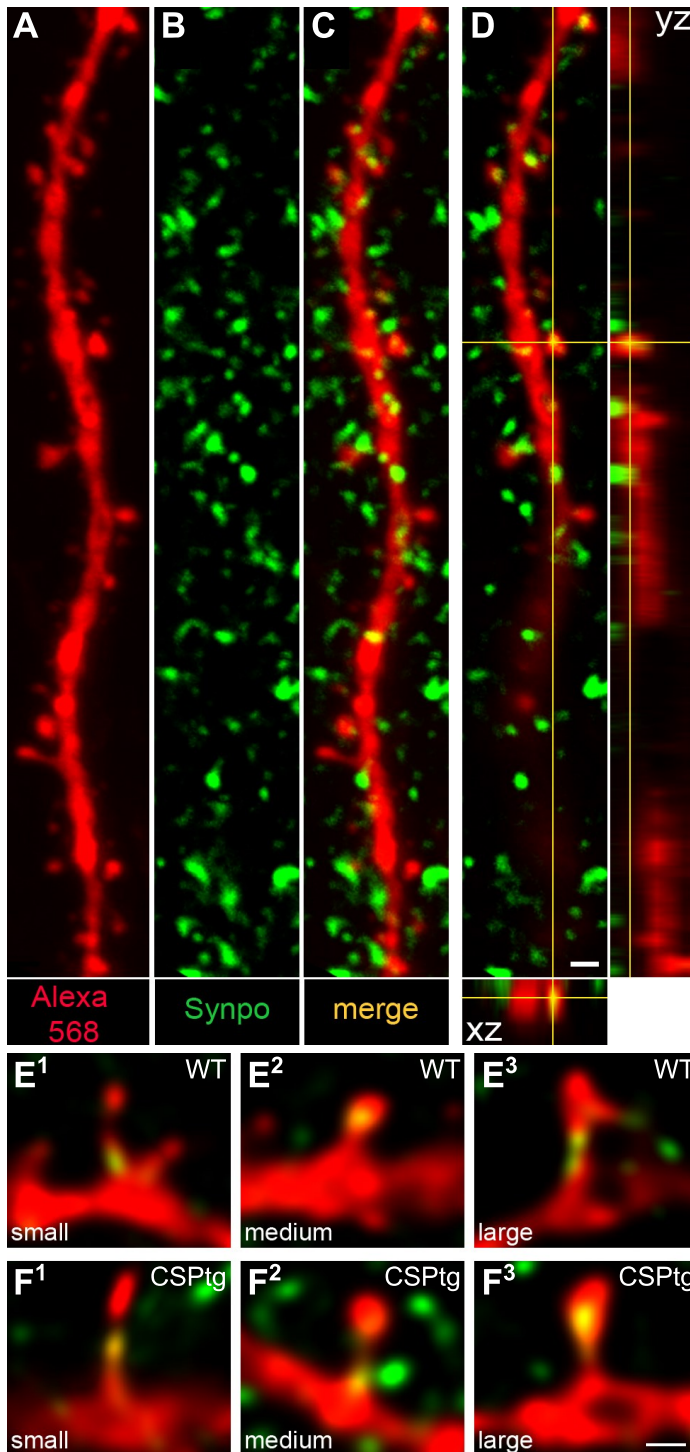
Figure 12: Quantification of the fraction of SP+ spines in dentate granule cell dendrites. A: A568-labeled GC dendrite in the OML (red). B: Immunostaining for SP showing SP-clusters (green). C: Merged image. SP-cluster co-localizing with dendritic spines appear yellow. D: For each given SP+ spine (crosshair), co-localization of the SP-cluster and the spine was verified three-dimensionally in the x-y, x-z, and y-z planes. E-F: SP co-localized with granule cell spines of various head sizes in both WT and CSPtg mice. Scale bars: D = 1 µm. F^3 = 0.5 µm. (Del Turco, Paul, Rietsche et al., unpublished)

To answer this question, the ratio of SP+ spines of granule cell dendrites in the OML was determined in transgenic animals overexpressing SP (CSPtg) and in WT animals expressing wild type levels of SP. In short, spines crossing the spine threshold were judged SP+ if the maximal area (areamax) of a SP-cluster co-localized >50 % in x-y, x-z, and y-z-Dimension and in 3D-reconstructions. Then, the fraction of SP+ spines [%] in a dendritic segment was calculated and the mean for each animal was determined.

SP-overexpressing CSPtg-mice showed a ~2-fold significant increase in the ratio of SP+ spines, compared to control animals (p = 0.0087, Mann-Whitney U-test). On average, CSPtg animals exhibited 20.14 % SP+ spines, whereas in WT mice, 10.94 % of all spines were SP+ (Figure 13 B). In conclusion, these data could show for the first time that an overexpression of SP leads to a ~2-fold increase in SP+ GC spines in the OML of adult male CSPtg mice compared to controls.

3.1.3 Average spine head size is not significantly changed in SP-overexpressing mice

Spine head size correlates with synaptic strength, the size of the PSD-area, and the density of postsynaptic AMPA-receptors[19,31,37,38]. sLTP, i.e. a long-lasting increase in spine head size following LTP-induction, is now a widely accepted concept[177-179]. It was also shown that SP+ spines – probably equipped with a SA – have significantly larger spine heads than SP– spines[47], i.e. spines probably lacking a full-functional SA. A positive correlation between the presence of SP with spine head size had been shown in dissociated cultured hippocampal neurons of the rat[47]. Consistent with this, a positive correlation between the SP puncta size and SP+ spine head size has been shown in organotypic slice cultures of the hippocampus and as well as *ex vivo* in adult male mice expressing SP at a wild type level[22].

However, it remains unknown which effect SP-overexpression in adult mice has on the mean head size of dendritic spines of a neuron, irrespective of their SP-content (i.e. SP+ and SP– spines) and which impact SP-overexpression has on SP+ and SP– spines, respectively.

To address this question, the head sizes of granule cell spines was quantified by determining the areamax of individual spines in image stacks from male transgenic animals overexpressing SP (CSPtg) and WT animals expressing wild type levels of SP, as detailed in the method chapter. Of note, spine head size quantification was performed blind to the SP-content of a given spine and blind to the genotype.

Average spine head size of all quantified spines (i.e. SP+ and SP-) was not significantly different between transgenic and control animals (p = 0.24, Mann-Whitney U-test). Mean spine head size for all spines was 0.116 μm^2 in

CSPtg animals and 0.105 µm^2 in WT mice. Average spine head size of SP+ spines was also not significantly different between transgenic and control animals (p = 0.59, Mann-Whitney U-test). Mean spine head size of SP+ spines was 0.282 µm^2 in CSPtg animals (n = 182 spines). and 0.299 µm^2 in WT mice (n = 103 spines). Finally, average spine head size of SP– spines did not show significant differences between transgenic and control animals (p = 0.59, Mann-Whitney U-test). Mean spine head size of SP– spines was 0.080 µm^2 in CSPtg animals (n = 868 spines). and 0.081 µm^2 in WT mice (n = 928 spines). All results are shown in Figure 13 C.

These data indicate that on average, spine head size remained unchanged in the OML of adult male mice.
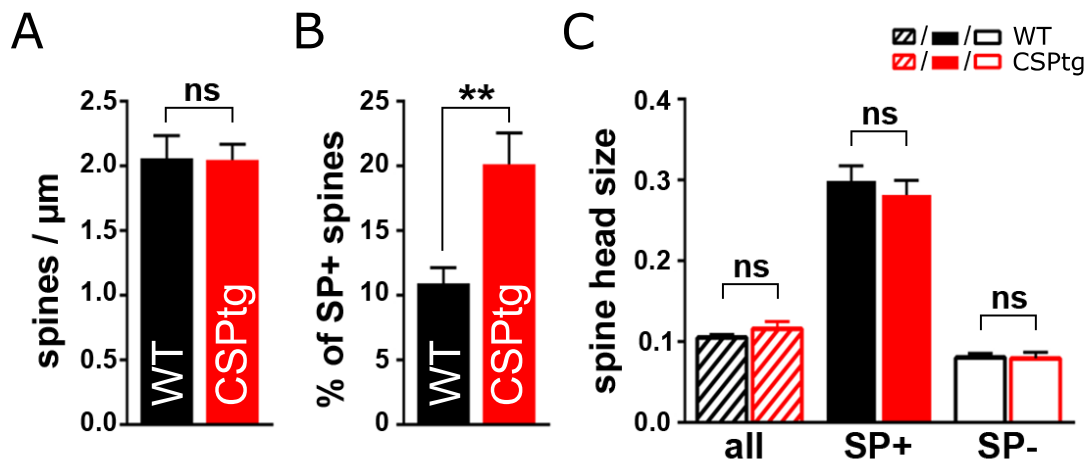
Figure 13: SP-overexpression increases the ratio of SP+ spines, while leaving spine density and mean spine head size unchanged. A: Transgenic male mice (CSPtg) showed no significant difference in density of dendritic spines, when compared to WT animals. n.s. = not significant. p = 0.699, Mann-Whitney U-test. B: Ratio of SP+ spines is nearly doubled in SP-overexpressing CSPtg mice. **p = 0.0087, Mann-Whitney U-test. C: Mean spine head size of all spines (SP+ plus SP–) was not significantly changed between transgenic and control animals. p = 0.24, Mann-Whitney U-test. The mean spine head size of SP+ spines was also not significantly different between transgenic and control animals. p = 0.59, Mann-Whitney U-test. Mean spine head size of SP– spines was also not significantly different. p = 0.59, Mann-Whitney U-test. WT: n = 6 animals, n = 18 segments, n = 1031 spines (103 SP+ spines vs. 928 SP– spines). CSPtg: n = 6 animals, n = 18 segments, n = 1050 spines (182 SP+ spines vs. 868 SP– spines). (Del Turco, Paul, Rietsche et al., unpublished)

3.1.4 In both transgenic and WT mice, mean head size of SP+ spines is increased compared to SP– spines

Previous studies showed that in dissociated hippocampal cultures of the rat[47] and in OTCs from mice[74], SP+ spines exhibit larger spine heads when compared to SP– spines. The same was shown in adult male mice expressing GFP-tagged SP at a wild type level[22]. Consistent this, average spine head size of SP+ spines was significantly larger compared to SP– spines in adult WT mice ($p < 0.0001$, Mann-Whitney U-test). In WT animals (n = 6), mean spine head size of SP+ spines was 0.299 μm^2 (n = 103 spines), while mean spine head size of SP– spines was 0.081 μm^2 (n = 928 spines). In adult CSPtg mice, the average spine head size of SP+ spines was also significantly larger when compared to SP– spines ($p < 0.0001$, Mann-Whitney U-test). In CSPtg animals (n = 6), mean spine head size of SP+ spines was 0.282 μm^2 (n = 182 spines), mean spine head size of SP– spines was 0.080 μm^2 (n = 868 spines). All results are shown in Figure 14. These data indicate that in adult male CSPtg mice, SP+ spines on GC dendrites in the OML have, <u>on average</u>, larger spine heads than SP– spines, consistent with the extant literature.
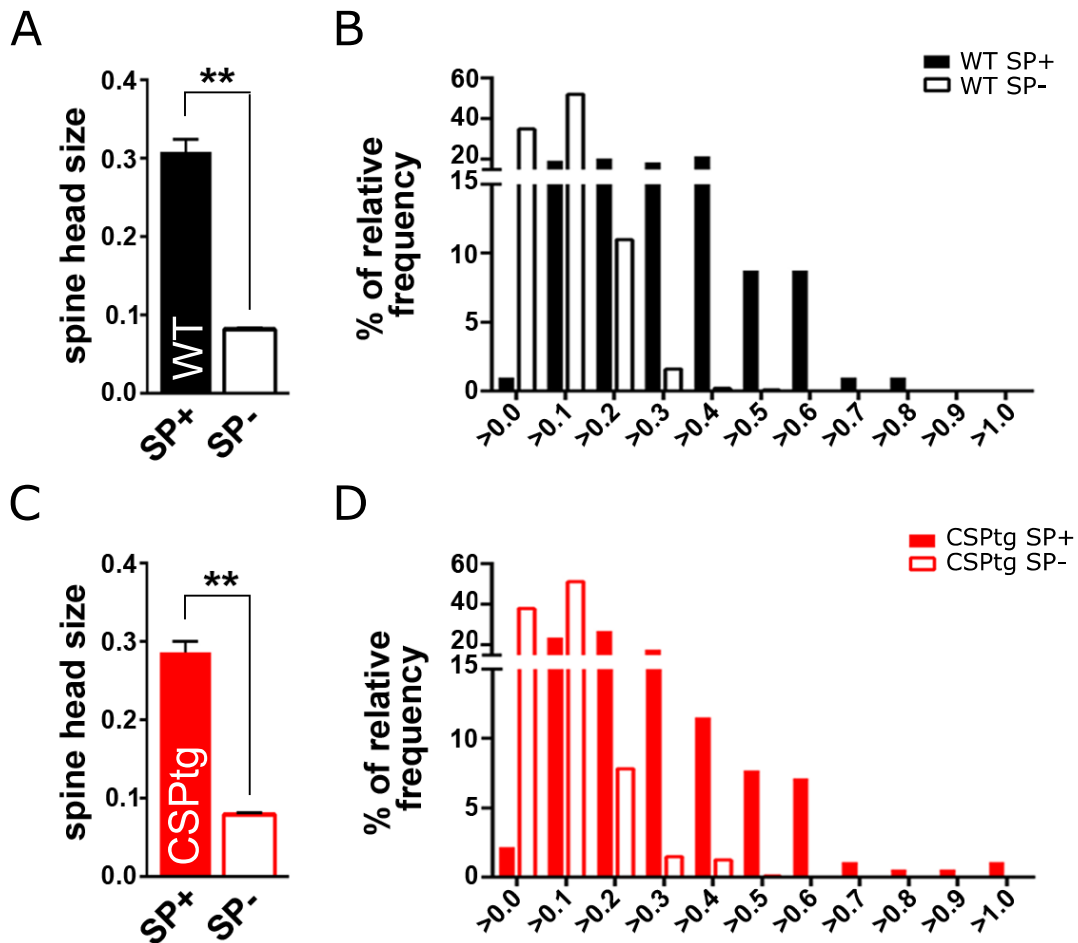
Figure 14: On average, **SP+ spines exhibit larger spine heads than SP– spines, both in WT animals and CSPtg mice.** A: Mean spine head size of SP+ spines is significantly larger when compared to SP– spines in WT animals (n = 6). ** p < 0.0001, Mann-Whitney U-test. SP+ spines: n = 103. SP– spines: n = 928. B: Cumulative distribution shows the shift of SP+ spines towards bigger head sizes in WT animals. C: Mean spine head size of SP+ spines is significantly larger when compared to SP– spines in CSPtg animals (n = 6). SP+ spines: n = 182. SP– spines: n = 868. **p < 0.0001, Mann-Whitney U-test. D: Cumulative distribution shows the shift of SP+ spines towards larger head sizes in CSPtg animals. (Del Turco, Paul, Rietsche et al., unpublished)

3.1.5 SP-overexpression changes the distribution of SP+ spines and increases the fractions of small and very large spines.

On average, SP+ granule cell spines have larger heads than SP– granule cell spines[22,47,180], which is confirmed in this thesis by the data shown in chapter 3.1.4. GC dendrites in the OML of SP-overexpressing CSPtg mice carry approximately twice as many SP+ spines compared to the control group, as shown in chapter

3.1.2. Therefore, it was hypothesized that the average head size of GC spines is larger in the CSPtg mouse. Unexpectedly, this was not the case. This prompted the investigation of the distribution of head sizes of SP+ and SP– spines in CSPtg and control GC. Do mainly large SP– spines become SP+ in a situation of SP-overexpression? Or are the spines with a middle-sized or small spine head possibly more prone to acquire SP and hence a SA?

To answer these questions, (as a first step) the relative distribution of head sizes of SP+ spines on GC dendrites from CSPtg mice was compared to the SP+ granule cell spines quantified in the control group. There was no significant difference in the SP+ head size distributions between the two groups, although a trend could be observed towards many more small SP+ spines in CSPtg and a few more very large SP+ spines (p = 0.057, Kolmogorov-Smirnov test. CSPtg: n = 182 SP+ spines. WT: n = 103 SP+ spines). This is shown in Figure 15: in CSPtg mice, the fractions of small SP+ spines with an areamax around 0.2 μm^2 or less seemed to be higher, compared to WT animals. The proportion of large spines with an areamax from 0.3 to about 0.6 μm^2 appeared to be smaller, while the fraction of rare very large spines with a head size >0.6 μm^2 seemed to be higher in CSPtg mice again, compared to WT mice.
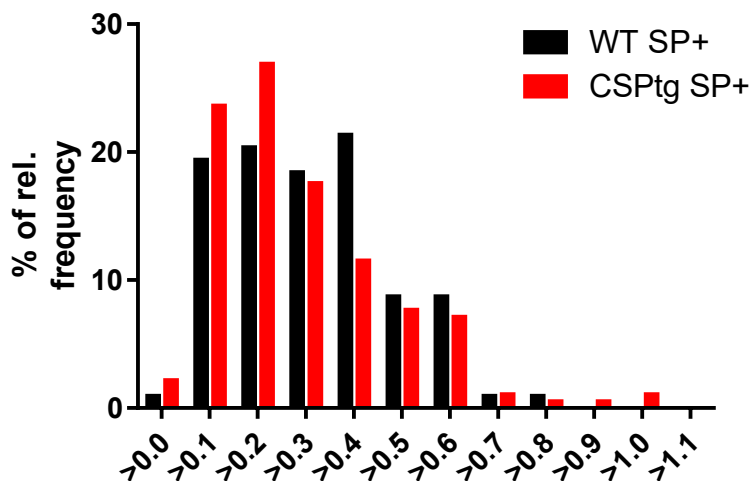
Figure 15: Relative head size distribution of SP+ spines under SP-overexpression (CSPtg) and in the control condition (WT). In CSPtg mice, the head size distribution of SP+ spines shifted towards small spines of ~0.2 μm^2 head size or lower. At the same time there was a trend towards very large spines of > 0.6 μm^2 head size. p = 0.057, Kolmogorov-Smirnov test. CSPtg: n = 182 SP+ spines; WT: n = 103 SP+ spines. (Del Turco, Paul, Rietsche et al., unpublished)

Based on these observations, and to clarify the differences in head size distribution of SP+ spines in CSPtg mice, the continuum of head sizes of all SP+ spines quantified in SP-overexpressing CSPtg mice and in the control group was divided into three size classes: small, large and very large spines. Spines with a head size < 0.2 µm^2 were classified as small spines[9], spines with head sizes from 0.2 µm^2 – 0.6µm^2 as large spines[9,140] and spines with a head size > 0.6µm^2 as very large spines. As a next step, the ratios for each size class were calculated. Small granule cell spines formed 30.1 % of all SP+ spines in WT mice (31/103 spines) and 40.1 % of all SP+ spines in CSPtg mice (73/182 spines). Large granule cell spines formed 65 % of all SP+ spines in WT mice (67/103 spines) and 53.3 % % in CSPtg mice (97/182 spines). Very large granule cell spines formed 4.9 % of all SP+ spines in WT mice (5/103 spines) and 6.6 % of all SP+ in CSPtg mice (12/182 spines). Figure 16 B illustrates the relative shift in SP+ spine head sizes under SP-overexpression towards small and very large head sizes. To quantify this relative shift, the difference of ratios between WT and CSPtg mice for small, large and very large spines was calculated as Δ% (Figure 16 B). The fraction of small spines increased by 33 % under SP-overexpression in CSPtg mice compared to WT. The fraction of large spines decreased by 18 % under SP-overexpression in CSPtg mice compared to WT. The minor fraction of very large spines increased by 36 % under SP-overexpression in CSPtg mice, compared to WT (Figure 16 B). This indicates that the increase in the number of SP+ spines in CSPtg mice is caused by an increase in the number of small and very large SP+ spines. The increase in the number of both small and very large SP+ spines also explains why the average spine head size of SP+ spines was not significantly different between genotypes.

In contrast to SP+ spines, the relative distribution of SP– spines stayed at comparable levels in both WT and CSPtg male mice. Small spines formed 95 % of all SP– spines and large spines formed 5 % of all SP– spines in both groups. Very large SP– spines with a head size > 0.6 µm^2 were never observed in this material, neither in WT nor in CSPtg mice (Figure 16 C).
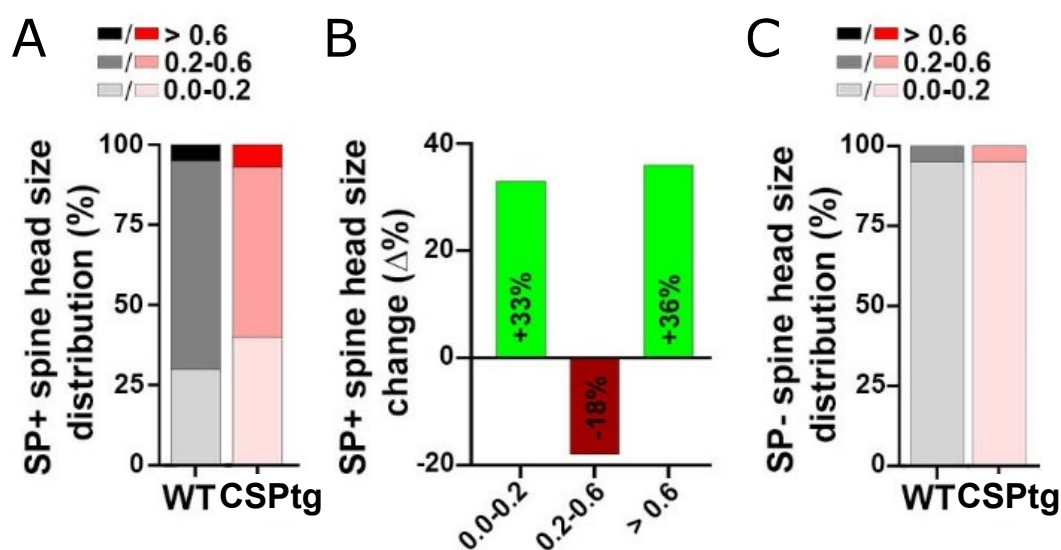
Figure 16: SP-overexpressing mice exhibit more small and very large SP+ spines. A: Ratios of small spines (< 0.2 µm^2), large spines (0.2-0.6 µm^2) and very large spines (> 0.6 µm^2) on granule cell dendrites of WT and CSPtg mice. In CSPtg animals, the ratio of small and very large spines increases, while the ratio of large spines decreases. B: Relative shift calculated as the difference of ratios (Δ%) between small, large and very large SP+ spines in CSPtg mice, compared to WT. C: Ratios of small and large SP– spines on CSPtg and WT granule cell dendrites in the OML. Note the very similar ratios. (Del Turco, Paul, Rietsche et al., unpublished)

As the relative distribution of SP– granule cell spines stays the same in the OML of both WT and CSPtg mice, it is not surprising that the average spine head size of SP– granule cell spines is not significantly different between the two groups (Chapter 3.1.3., Figure 13 C).

Taken together, the observed increase in the number of SP+ spine under SP-overexpression occurs preferentially in small spines, which under WT-conditions are less likely to contain SP and a SA, presumably. SP-acquisition under SP-upregulation may support small spine-compartments in processes of plasticity[47,181] and spine stability[22].

3.1.6 Mean SP-puncta size of SP+ granule cell spines is not significantly changed in SP-overexpressing mice.

The next question of interest was if SP-overexpression influences SP-puncta size. Would SP+ spines in the OML of CSPtg-mice exhibit, on average, larger SP-puncta? SP-KO mice lacking SP were shown to be unable to form SA[60]. As SP is an essential component in the dense plates of the SA, one could assume

that under SP-overexpression, the average size of immunolabeled SP-puncta could be altered when compared to WT animals.

To test this hypothesis, the areamax of SP-clusters of each individual SP+ spine was determined as described in the methods (WT: n = 103; CSPtg: n = 182). Similar to the findings concerning average spine head size, there was no significant difference in average SP-puncta size of SP+ granule cell spines in the OML of adult male CSPtg mice compared to WT mice (p = 0.3095, Mann-Whitney U-test). In WT animals (n = 6), mean SP-puncta size of SP+ spines was 0.074 μm^2. In CSPtg mice, mean SP-puncta size of SP+ spines was 0.066 μm^2. Results are shown in Figure 17, including the relative frequency distribution of SP-puncta sizes in CSPtg and WT mice.
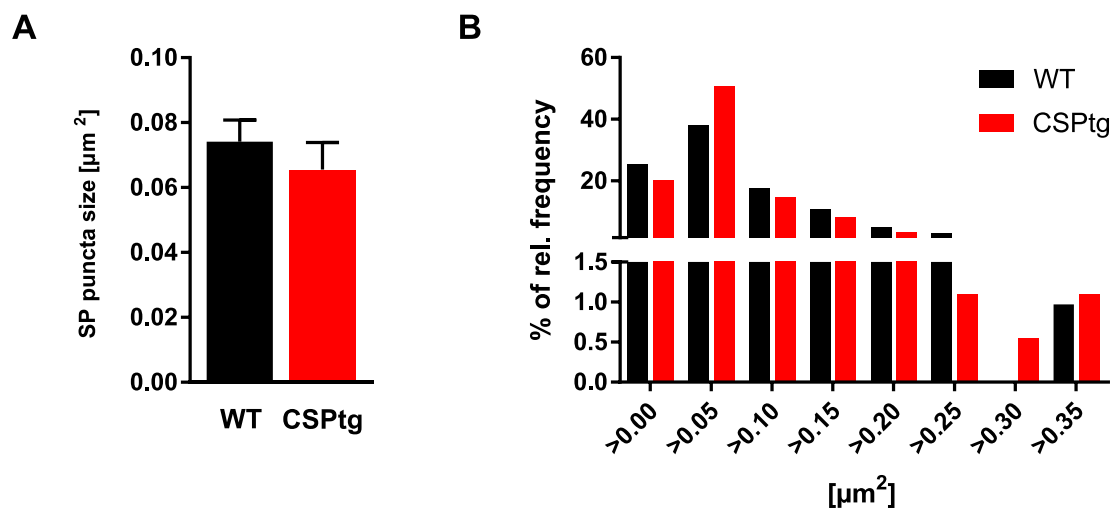
Figure 17: SP-overexpression does not change mean SP-puncta size of SP+ spines on granule cell dendrites in the OML. A: Transgenic CSPtg-mice (n = 6) and WT animals (n = 6) did not show a significant difference of mean SP-puncta sizes of SP+ spines. p = 0.3095, Mann-Whitney U-test. B: Relative frequency distribution of SP-puncta sizes. WT: n = 103, CSPtg n = 182. (Del Turco, Paul, Rietsche et al., unpublished)

3.1.7 Spine head size correlates with SP-puncta size in both transgenic and WT animals

This thesis could show that SP+ spines – assumingly equipped with a cytosolic SA-organelle[17,53,56,69] – exhibit larger spine heads than SP– spines in both WT and CSPtg adult male mice (see Fig. 14). Consistent with this, in dissociated cultured hippocampal neurons of the rat, a positive correlation between the presence of SP and spine head size had been shown before[47]. More recently, a

positive correlation between spine head size and the SP-puncta size of SP+ spines has been shown in organotypic slice cultures of the hippocampus and *ex vivo* in adult male mice, in a mouse-mutant expressing SP at a wild type level.[22] However, it remains unknown if this correlation is still present in neurons overexpressing SP.

To address this question, the areamax of each SP-puncta was correlated with the spine head size (areamax) of its spine, in both CSPtg and WT animals (WT: n = 102 SP+ spines, n = 18 dendritic segments, n = 6 animals. CSPtg: n = 182 SP+ spines, n = 18 dendritic segments, n = 6 animals). Notably, the absolute number of SP+ spines found in CSPtg animals reflects the approximately 2-fold increase in density of SP+ granule cell spines in the OML of CSPtg animals compared to WT. As shown in Figure 18, there is a clear correlation between SP-puncta size and spine head size in both groups. For WT, there was a significant correlation of spine head size with SP-puncta size with a Pearson r = 0.4965, R squared = 0.2466, P (two-tailed) < 0.0001. For CSPtg mice, granule cell spine head size and SP-puncta size of SP+ spines were significantly correlated with a Pearson r = 0.5094, R squared = 0.2595, P (two-tailed) < 0.0001.

These results indicate that in SP+ spines with large spine heads, it is more probable to also observe a large SP-puncta co-localizing with it. This finding is consistent with recently published data from Yap, Rietsche et al. (2020)[22] and Smilovic, Rietsche et al. (2021)[180]. Moreover, the linear correlation is quite similar between SP-overexpressing CSPtg mice and WT animals exhibiting wild type levels of SP, indicating that increased levels of SP do not affect the aforementioned positive correlation.
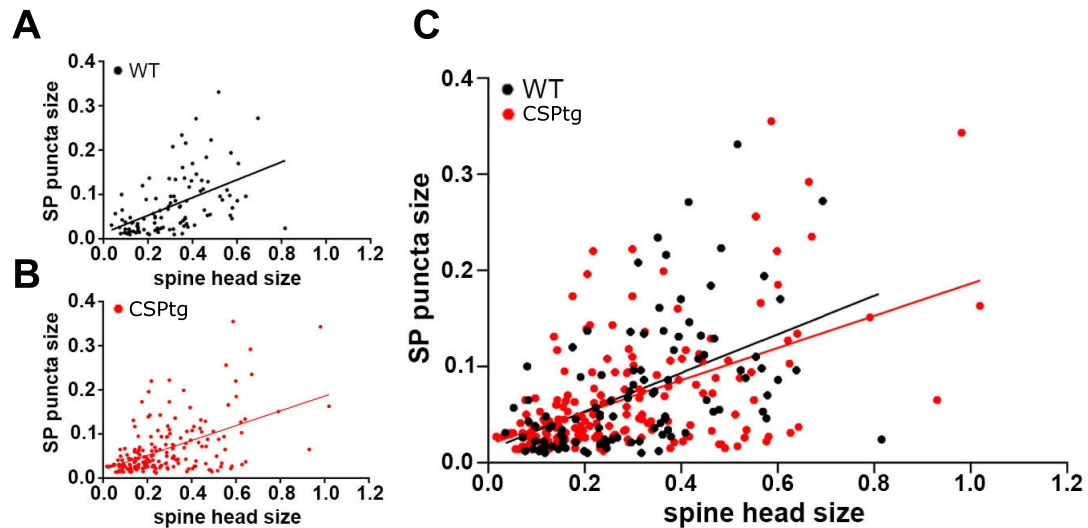
Figure 18: In the OML of the dentate gyrus of adult male mice, SP-puncta size correlates with spine head size, a phenomenon that persists under SP-overexpression in CSPtg animals. A: GC spine head size and SP-puncta size were correlated in WT animals in a linear fashion. n = 103 SP+ spines, n = 18 segments, n = 6 animals. p < 0.0001, Pearson r = 0.4965, R squared = 0.2466. B: In the OML of CSPtg mice, granule cell spine head size and SP-puncta size were correlated in a linear fashion as well. n = 103 SP+ spines, n = 18 segments, n = 6 animals. p < 0.0001, Pearson r = 0.5094, R squared = 0.2595. C: Data from A and B merged in one diagram. In both SP-overexpressing CSPtg mice and WT animals, spine head size of SP+ spines correlated with SP-puncta size in a very similar fashion (WT: R squared = 0.2466, CSPtg: R squared = 0.2466). (Del Turco, Paul, Rietsche et al., unpublished)

3.2 Dentate gyrus: Effects of Synaptopodin-deficiency on granule cell dendrites

In the first series of experiments conducted for this thesis, in a gain-of-function approach, it could be shown that overexpression of SP, thus increased levels of SP present in granule cells of the dentate gyrus (suprapyramidal blade), did not significantly change average head size of dendritic spines in adult male CSPtg mice (see also chapter 3.1.3). In a second series of experiments a loss-of-function approach was employed to investigate the effects of SP-deficiency on average spine head size of dendritic granule cell spines.

Previous studies showed that SP knock-out mice (SP-KO) have normal spine densities and normal spine lengths in CA1 pyramidal cells of the hippocampus[60,182]. However, it remained unknown which effect SP-deficiency has on spine density of GC and their average spine head size.

To answer this question, adult male SP-KO mice and WT animals were perfused, followed by intracellular labeling of individual GCs in the suprapyramidal blade of the dentate gyrus in fixed brain slices, as described in the method section (Figure 19 A shows an example of an A568-labeled granule cell). Imaging of dendritic segments in the OML was performed as indicated in chapter 2.5.1 (representative example shown in Figure 19 B), and spine head sizes were quantified as specified in chapter 2.6.1. Average spine head size per animal was calculated and tested for significant differences between SP-KO and WT mice.

As shown in Figure 19 C, the average spine head size of SP-KO (n = 8 animals, three dendritic segments per animal, 2158 spines) and WT mice (n = 8 animals, three dendritic segments per animal, 1885 spines) was not significantly different (p = 0.291, Mann-Whitney U-test). Both groups showed a similar distribution of spine head sizes, as indicated in Figure 19 D.
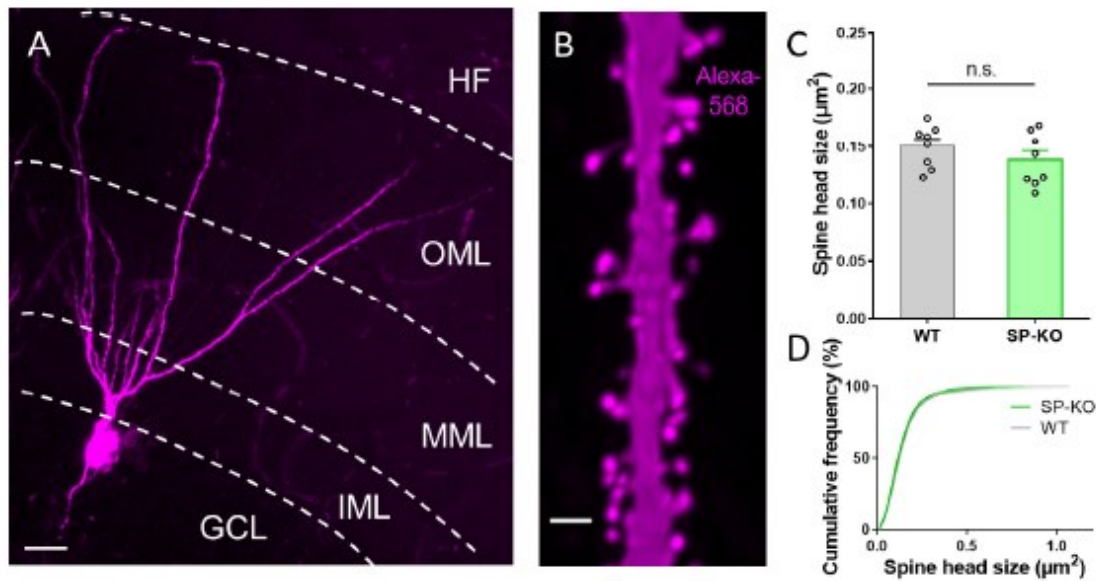
Figure 19: SP-deficiency does not change mean spine head size of granule cell dendrites
(A) Dentate granule cell intracellularly labeled in the dentate gyrus (suprapyramidal blade) of a SP-knock-out mouse (SP-KO) with the fluorescent dye Alexa568-Hydrazide in fixed tissue. Maximum intensity projection of a z-stack (after image deconvolution). Dendritic segments imaged in the outer molecular layer (OML) were used for analysis. MML, middle molecular layer; IML, inner molecular layer; GCL, granule cell layer; HF, hippocampal fissure. Scale bar = 20 µm. (B) Dendritic segment of a SP-KO granule cell shown at higher magnification. Scale bar = 1 µm; Maximum intensity projection of a deconvolved z-stack. (C) Mean spine head size of WT and SP-KO mice did not differ significantly. n.s., not significant; p = 0.291, Mann-Whitney U-test. WT mice and SP-KO mice, n = 8 per group (three dendritic segments per animal; 1885 WT spines, 2158 SP-KO spines). (D) Cumulative frequency distribution of spine head sizes of WT (grey) and SP-KO (green) mice. Modified from Yap, Rietsche et al. (2020).

In line with the data from SP-overexpressing animals, these results suggest that the level of SP-expression does not have a major impact on average spine head size of GC-spines in the OML of the DG (suprapyramidal blade) of male adult mice.

3.3 Pyramidal neurons of the dorsal CA2-subregion: Sex-dependent- and layer-specific-differences in density and head size of dendritic spines and SP distribution

The dCA2-subregion of the hippocampus has been shown to be essential for social recognition memory in numerous studies[101,110,112,113,183]. CA2 has also been implicated in other mnemonic functions, such as contextual memory and fear learning[114]. In most studies, adult male mice were used. However, sociability and social recognition differs significantly between female and male mice[111,159]. In addition, sex hormones such as estrogen or testosterone have been shown to influence dendritic spines[129,140], synaptic plasticity[134], learning and memory[132,184] as well as social behaviour[111,159] in rodents. Recently, sex-specific differences in CA2-dependent fear-conditioning have been shown in adult male and female mice (strain not specified)[122]. In guinea pigs, a sexual dimorphism in the branching pattern of apical CA2-dendrites has been shown [123] (using the classical CA2-definition of Lorente de Nó[10], see also chapter 1.4).

Besides this, nothing is known so far about sex-dependent differences concerning the molecularly defined dCA2 area in mice, especially concerning the basal compartment, i.e. *so*, and concerning layer-specific differences of dendritic spine morphology.
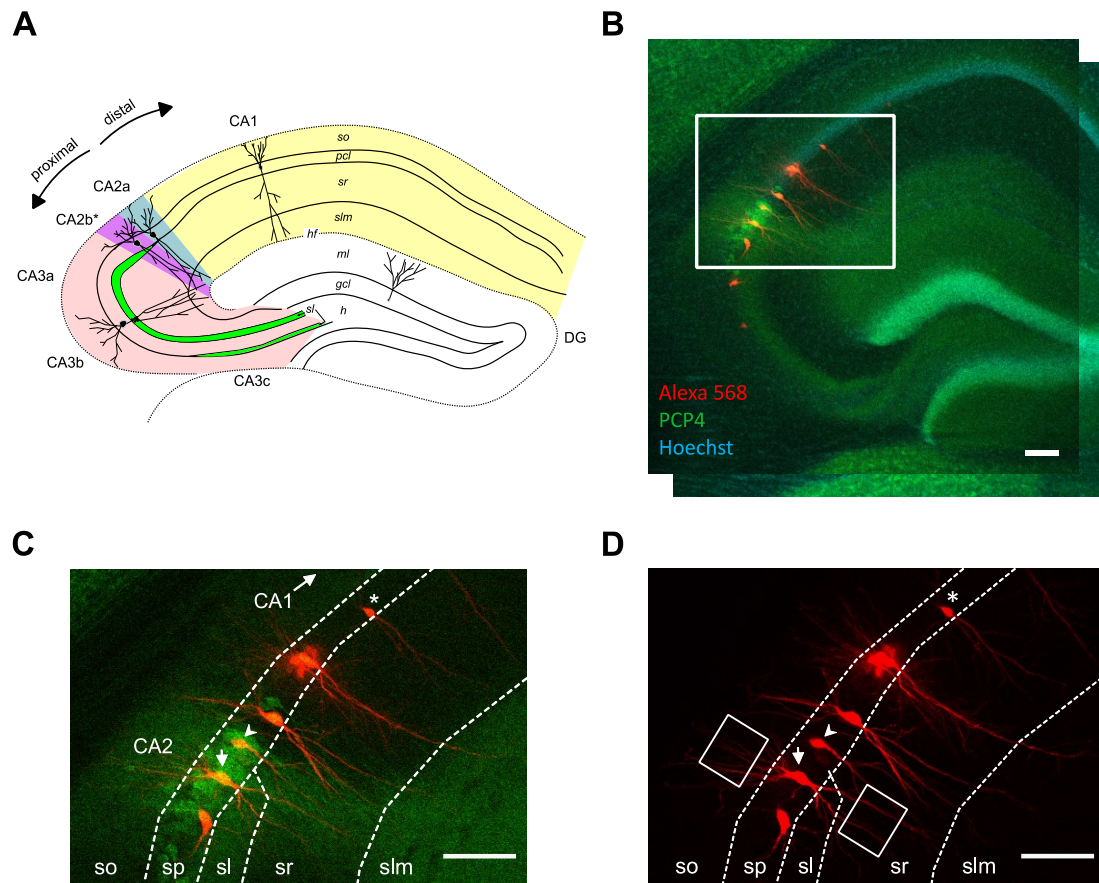
Figure 20: Intracellular labeling of pyramidal neurons in the CA2-region, post-hoc identified using the molecular marker Purkinje-cell-protein 4 (PCP4). A: Schematic of the hippocampal formation in rodents (mice and rats). CA2a (blue) corresponds to the classical CA2-subregion as defined by Lorente de Nó (1934), showing big pyramidal cells without thorny excrescences in Golgi-stainings[10]. Molecular markers applied in male C57BL/6J -mice revealed that the CA2-subregion extends towards CA3 (red). As a result, the formerly very distal portion of CA3a in mice is now called CA2b[89,92] (violet). CA2b therefore includes a section of the stratum lucidum (*sl*, green) which is tapering out, thus CA2b-pyramidal cells receive input from the dentate gyrus[92]. B: A568-injected pyramidal neurons (red) in dorsal CA3a, CA2b/a and CA1c in a fixed 250 µm thick slice of mouse hippocampus. Boxed area shown at higher magnification in C, D. The molecular marker PCP4 labels the entire CA2 area (green). Cyan: Nuclear staining (Hoechst). Merged maximum-intensity-projection of a z-stack. C, D: A568-injected pyramidal cells shown at higher magnification (boxed area in B). PCP4-positive pyramidal cells with a big soma are found in an area with *sl* (= CA2b-cell, arrow) or without *sl* (= CA2a-cell, arrowhead). A CA1c-cell (*) was also injected. Note the smaller soma compared to CA2 cells. Boxes in D mark representative locations for z-stack-imaging of basal (*so*) or apical (*sr*) dendrites of PCP4-positive CA2-cells. *so*: stratum oriens. *sp*: stratum pyramidale. *sl*: stratum lucidum. *sr*: stratum radiatum. *slm*: stratum lacunosum-moleculare. Scale bars in B-D = 100 µm.

3.3.1 Dendritic spines in stratum radiatum show smaller spine head sizes than in Stratum oriens of dCA2 in a sex-independent manner in both male mice and female animals in diestrus.

In rodents dCA2 receives layer-specific synaptic input from intra- and extrahippocampal brain regions[89,110]. Basal dendrites in *so* receive extrahippocampal input from the supramamillary nucleus[99] (with Substance-P as neurotransmitter), as well as axonic collaterals from interneurons[4,95]. In *sr*, apical dCA2-dendrites receive bilateral input from Schaffer collaterals from CA3[10,89]. Axons from ECII project to the *slm[109]*. In *sl* of dCA2b, mossy fibers from the DG form functional synapses with apical dCA2-dendrites[92,110]. Layer-specific regulation of LTP was shown for the dCA2-region. LTP is tightly regulated in *sr[96,103,185]*, whereas it could be quite easily be elicited in *slm[109]*. However, nothing is known for female animals and/or sex-specific differences in this regard. Sometimes the sex of the animals investigated was not specified by the authors[96]. Other studies used male animals mice only[109,185].

The first question to ask was if there exists a layer-specific difference in average spine head size and spine density between the apical dendritic compartment in *sr* and the basal dendritic compartment in *so*, and whether there are sex-differences between male and female animals. To address these questions, adult male and female mice were perfused and 250 μm thick brain slices containing the hippocampal formation were obtained. Female animals were controlled for the diestrus stage of the estrous cycle (Prof. Dr. David Slattery and Dr. Aet O'Leary (Group of Translational Psychiatry, Department of Psychiatry, Psychosomatic Medicine and Psychotherapy, University Hospital, Goethe University, Frankfurt, Germany). Only female mice in diestrus were included in the experiments. Individual dCA2-pc were intracellularly injected (see Figure 8 and Figure 20 B-D). After re-slicing of the sections into 40μm brain slices, injected pc were post-hoc-verified as CA2-pc by immunostaining for the molecular marker PCP4 (PCP4+ CA2-cells[93]; Figure 20 B,C). Subsequently, confocal z-stacks of basal dendritic segments (3rd dendritic order or higher) in *so* and apical dendritic segments (3rd dendritic order or higher) in *sr* were acquired (Figure 9D). The density of dendritic spines, spine morphology and spine head size were quantified with the investigator (M.R.) blind to genotype.

In male mice, as shown in Figure 21 A, the average spine head size in *sr* was significantly smaller when compared to dendritic spines in *so* (p < 0.0001, Mann-Whitney U-test; *sr*: mean = 0.130 µm^2, *so*: mean = 0.197 µm^2). Male spine head size-distributions in *sr* and *so* were significantly different (p < 0.0001, Kolmogorov-Smirnov test), in the way that *sr*-spine head sizes were left-shifted towards smaller head sizes (Figure 21 B). In female (diestrus) mice, layer-specific spine head size differences were strikingly similar to those observed in male mice. As shown in Figure 21 C, average spine head size in *sr* was significantly smaller when compared to dendritic spines in *so* (p = 0.0002, Mann-Whitney U-test; *sr*: mean = 0.113 µm^2, *so*: mean = 0.160 µm^2). Female (diestrus) spine head size-distributions in *sr* and *so* were also significantly different (p < 0.0001, Kolmogorov-Smirnov test), with *sr*-spine head sizes being left-shifted towards smaller head sizes, just as in adult male mice (Figure 21 D).

These data show that mean spine head size of pyramidal cell dendrites in *sr* is significantly larger than in *so*, and that spine head size-distributions are right-shifted towards larger head sizes, for both male and female (diestrus) mice in a comparable fashion. This suggests that differences in spine head size, which are reported here for the first time between the apical and basal compartment of molecularly defined dCA2 in mice, are not different between sexes.
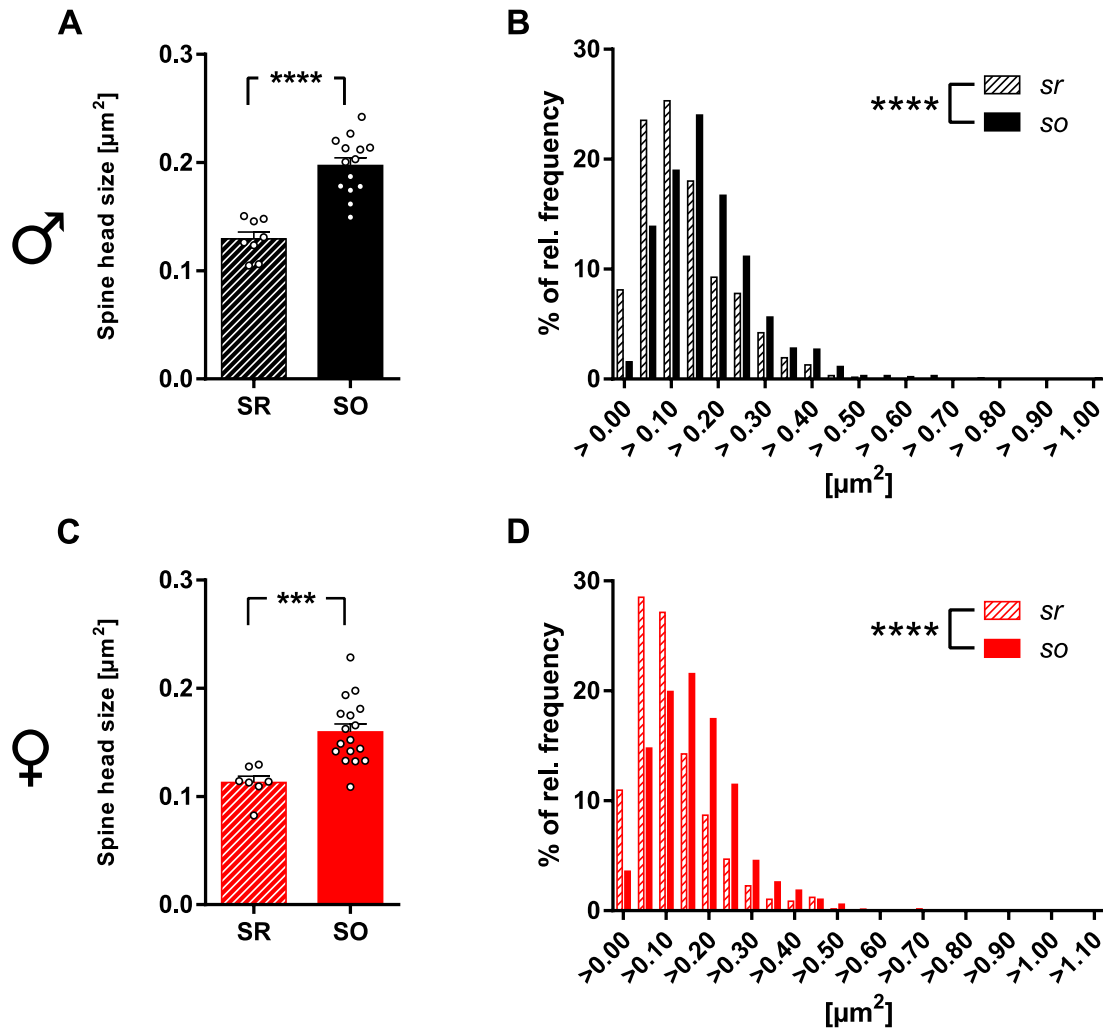
Figure 21: In *sr* of dCA2 pyramidal cell dendrites show smaller spine heads than in *so*, in both male and female mice (diestrus). A,C: Male (A, black) and female (diestrus) mice (C, red) exhibit smaller *sr*-spines (hatched columns) than s*o*-spines (filled columns) in their respective hippocampus. B,D: In both sexes, head size distributions of apical spines in *sr* are shifted towards smaller head sizes, compared to basal spines in *so*. A: ****p = < 0.0001, Mann-Whitney U-test; SR: n = 8 segments from n = 4 animals, SO: n = 14 segments from n = 6 animals. B: ****p < 0.0001, Kolmogorov-Smirnov test; SR: n = 616 spine heads, SO: n = 958 spine heads. C: ***p = 0.0002, Mann-Whitney U-test; SR: n = 7 segments from n = 3 animals, SO: n = 17 segments from n = 6 animals. D: ****p < 0.0001, Kolmogorov-Smirnov test; SR: n = 575 spine heads, SO: n = 340 spine heads.

3.3.2 Sex-dependent differences in spine head size and spine density on basal dendrites of dCA2-pc in Stratum oriens in adult C57BL/6J mice.

The layer-specific spine head size differences between apical *sr*-dendrites and basal *so*-dendrites of dCA2-pc, i.e. *sr*-spine heads being significantly smaller than

so-spine heads, were observed in both males and females (diestrus) in a strikingly similar fashion (Figure 21).

However, due to the aforementioned sex-differences in social recognition[111,159] and CA2-dependent fear-conditioning[122], another aim of this thesis was to expand the sparse microanatomical data regarding molecularly defined dCA2 pc in mice[89] in a sex- and layer-specific manner. To do so, sex-dependent differences of dendritic spines in both the apical and basal compartments of dCA2, the subregion essential for proper social recognition memory function[110], were investigated.

3.3.2.1 Stratum oriens: No significant difference in spine density or density of spine-subclasses between females (diestrus) and males

As axo-spinous synapses form the majority of excitatory synapses in telencephalic neurons, spine density has been used as an estimate for the number of excitatory synapses formed alongside a given dendritic segment[20]. Sex-hormones, including the widely-investigated hormone 17β-estradiol, are capable to influence spine density[186,187] and synaptic plasticity[132]. In addition, sex-hormone-dependent changes in spine morphology, in terms of the frequency of predefined spine classes, have been shown for CA1[140,153,186].

Therefore, the next questions of interest were (1) if spine densities of basal dendrites of dCA2-pc differ in a sex-specific manner, (2) whether the distribution of spine size groups (see also Figure 10) is sex-dependent. An investigator (M.R.) blind to the sex of the animal investigated spine densities. As elaborated in chapters 1.2, a more functional view of the spine population as a dynamic continuum has grown recently[19,20]. Therefore, each dendritic spine included for analysis of spine density was identified as either a mature spine (i.e. exhibiting a spine head, separated from the dendritic shaft by a narrower spine neck, irrespective of head size), an immature spine (i.e. not exhibiting a distinguishable spine neck) or a not-classifiable spine (see also Figure 10).

In *so*, as shown in Figure 22 A, the density of spines on basal pyramidal cell dendrites of dCA2 between females (diestrus) and males was not significantly different (p = 0.5633, Mann-Whitney U-test; male: mean = 2.65 spines/µm, female (diestrus): mean = 2.52 spines/µm). Figure 22 B illustrates the relative distribution of the spine groups observed on basal dendrites in *so* of male and

female (diestrus) dCA2, plotted as average relative ratios. Mature spines: 72.70 % (males) vs. 74.78 % (females). Immature spines: 16.06 % (males) vs. 15.66 % (females). Non-classifiable: 11.03 % (males) vs. 9.56 % (females).

As Figure 22 C-E displays, no significant sex-specific differences could be shown for each spine group, in so of dCA2-pc's of females (diestrus) compared to males: Mature spines (Figure 22 C, $p = 0.9761$, Mann-Whitney U-test; male: mean = 1.97 spines/μm, female (diestrus): mean = 1.91 spines/μm), Immature spines (Figure 22 D, $p = 0.7993$, Mann-Whitney U-test; male: mean = 0.394 spines/μm, female (diestrus): mean = 0.373 spines/μm) and Non-classifiable spines (Figure 22 E, $p = 0.3989$, Mann-Whitney U-test; male: mean = 0.286 spines/μm, female (diestrus): mean = 0.24 spines/μm). These data show that in so of dCA2, spine density on basal pyramidal cell dendrites did not differ significantly between female (diestrus) mice and male animals. The different spine groups seemed to occur in a similar fashion in both so of males and females (diestrus), as spine density for each spine group was not significantly different between both sexes.
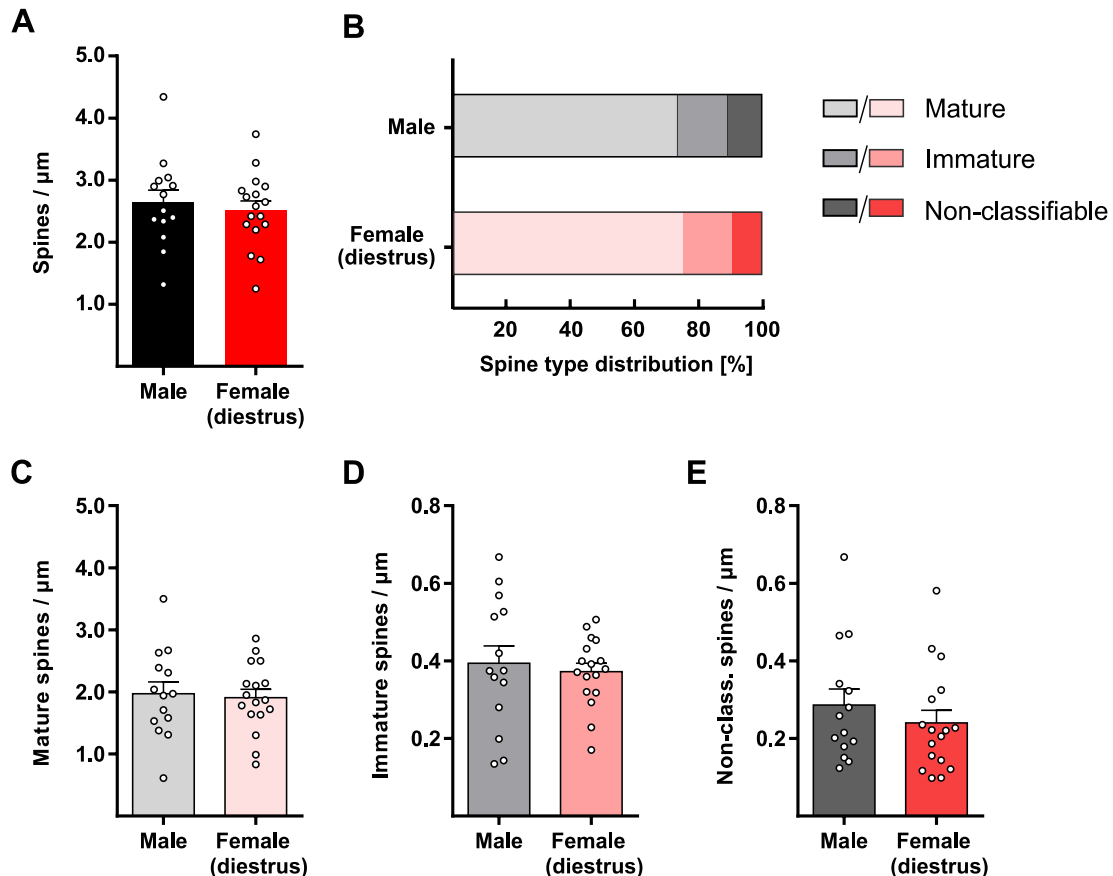
Figure 22: Pyramidal cell dendrites located in *so* of dCA2 do not show a sex-specific difference in spine density. A: Density of dendritic spines was not significantly different between female and male animals in *so*. p = 0.5633, Mann-Whitney U-test. B: Distribution ratios of spine groups[20]. Mature spines: 72.70 % (males) vs. 74.78 % (females). Immature spines: 16.06 % (males) vs. 15.66 % (females). Non-classifiable spines: 11.03 % (males) vs. 9.56 % (females). C-E: In *so* of dCA2, the densities of mature, immature and non-classifiable spines were not significantly different in adult female (diestrus) mice (different shades of red), compared to males (different shades of black). C: Mature spines, p = 0.9761. D: Immature spines, p = 0.7993. E: Non-classifiable spines, p = 0.3989. C-E: Mann-Whitney U-test, male: n = 14 segments, female (diestrus): n = 17 segments. n = 6 animals each group.

3.3.2.2 Stratum oriens: Female mice in diestrus show a decreased mean spine head size, compared to males

Sex-specific regulation of LTP has been shown in a previous work[153]. Long-lasting increase in spine head size is considered a structural correlate of LTP (sLTP)[21,188]. Also, sexual dimorphisms in social recognition have been described[111,159], and there are sex-specific differences in CA2-dependent fear-conditioning[122]. However, nothing is known about sex-specific differences in spine head size in dCA2.

Therefore, the next question of interest was if average spine head size differs significantly on basal dendrites of dCA2-pc in *so* between males and females (diestrus). Mature spines showing a spine head separated from the dendritic shaft by a spine neck[16,20] were included in the analysis and spine head size quantification was performed as detailed in the methods chapter.

In *so* of dCA2, as shown in Figure 23 A, average spine head size on basal pyramidal cell dendrites was significantly smaller in females (diestrus) when compared to males (p = 0.0014, Mann-Whitney U-test; male: mean = 0.197 μm^2, female (diestrus): mean = 0.159 μm^2). Figure 23 B illustrates the relative frequency of spine head sizes in bins of 0.05 μm^2. Note the right-shift in males towards larger spine head sizes.
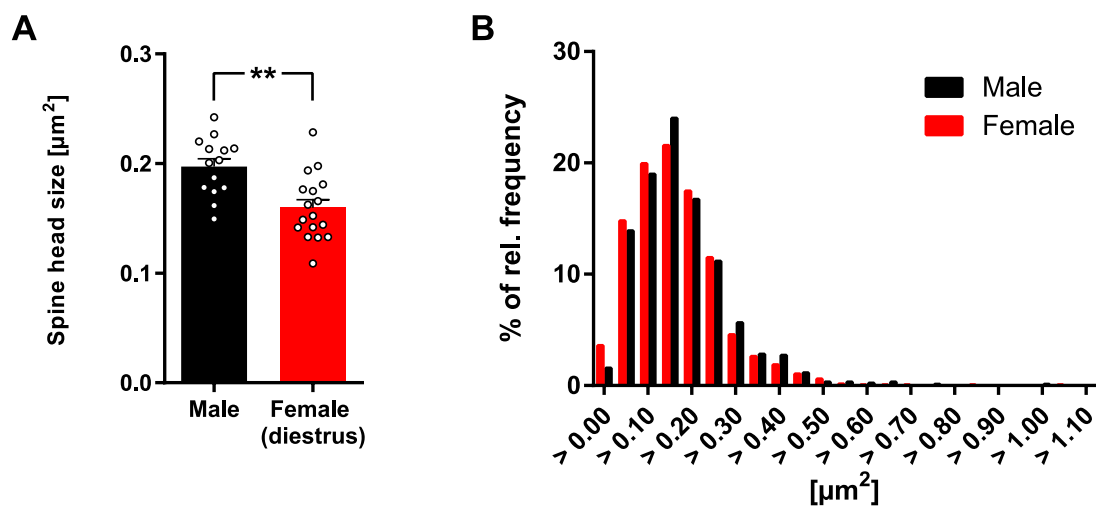
Figure 23: In Stratum oriens (*so*) of dCA2, mean head size of pyramidal cell spines is significantly smaller in females (diestrus) when compared to males. A: In *so*, female animals (red) showed significantly smaller spine heads, compared to males (black) **p = 0.0014, Mann-Whitney U-test. B: Cumulative distribution of spine head sizes of male and female (diestrus) animals in *so*. Female (diestrus): n = 6 animals, n = 17 dendritic segments, 1340 spines. Male: n = 6 animals, n = 14 dendritic segments, 958 spines.

3.3.2.3 Stratum oriens: Female (diestrus) and male animals exhibit similar ratios of SP+ spines

Hippocampal neurons of both male and female rodents synthesize Estrogen *de novo* using the enzyme aromatase[155]. SP seems to be responsive to estrogens[156,157]. Mechanistically, Ca^{2+} transients from internal stores are thought to control aromatase activity in hippocampal neurons of adult mice, while in turn, aromatase is capable to regulate SP expression[158].

However, aromatase-dependent SP regulation was shown to take place in a sex-independent manner[158]. In *sr* of dCA1, a higher fluorescence level of SP punctae has been reported in adult female mice, compared to adult males[158]. In contrast, at the EM-level the number of SA did not show any differences between male and female adult mice in *sr* of CA1[140]. In both studies, females were not controlled for estrous cycle-stage[140,158].

Therefore, the next goal of this thesis was to investigate sex-dependent differences of dendritic SP-distribution in dCA2 in a cycle-controlled manner. After analyzing spine density and spine head size in *so* as previously described, the ratio of SP+ spines on A568-injected basal dendritic segments of PCP4+ dCA2-pc (see also Figure 20) was determined in males (black) and females (diestrus) (red). In *so* of male mice, the average ratio of SP+ spines per dendritic segment was 8.65 % (Median 7.55 %, with a range of 2.08 %-19.35 %). In *so* of female (diestrus) mice, the average ratio of SP+ spines per dendritic segment was 9.27 % (Median 7.88 %, with a range of 3.03 %-15.69 %). There was no significant difference in the ratio of SP+ spines in *so* of females (diestrus) compared to males (p = 0.4928, Mann-Whitney U-test), as shown in Figure 24 A. Consistent with the presumably sex-independent regulation of SP by aromatase in CA1, the dendritic distribution of SP in spines seems to occur in a sex-independent manner in so of dCA2 of male and female (diestrus) mice.
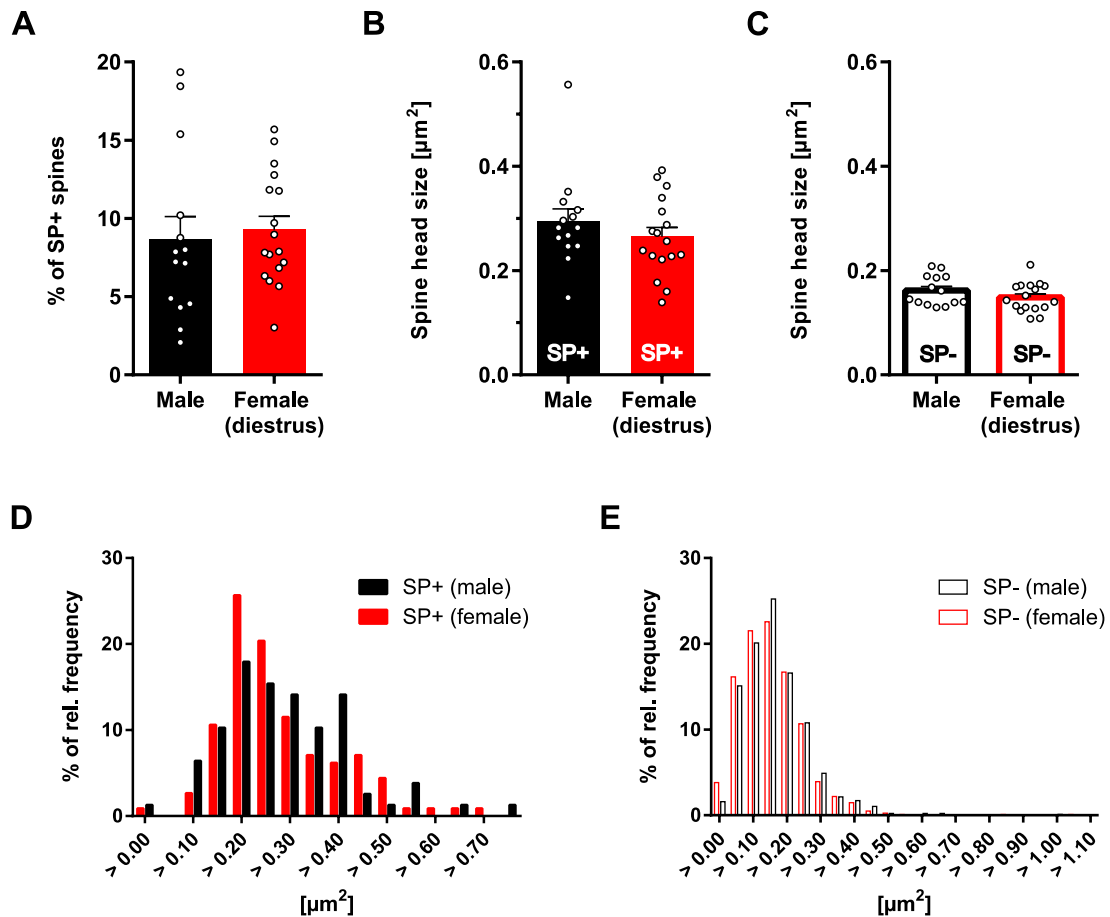
Figure 24: In so of dCA2, the ratio of SP+ spines and spine head sizes of SP+ and SP– spines are not significantly different between the sexes. A: The ratio of SP+ spines on basal pyramidal dendrites in *so* of dCA2 in females (diestrus) (red), compared to males (black) did not show a significant difference. p = 0.4928, Mann-Whitney U-test. B: There was no significant difference in SP+ spine head size/segment in *so* of females (diestrus) compared to males. p = 0.3771, Mann-Whitney U-test. C: No significant difference was observed in SP– spine head size in *so* of females (diestrus), compared to males. p = 0.2621, Mann-Whitney U-test. A-C: Male: n = 14 segments, 1 segment per PCP4+ dCA2pc, n = 6 animals. Female (diestrus): n = 17 segments, 1 segment per PCP4+ dCA2pc, n = 6 animals. D: Relative frequency distribution of head sizes of SP+ spines in males and females (diestrus) in bins of 0.05 %. Male: n = 78 SP+ spines. Female (diestrus): n = 113 SP+ spines. E: Relative frequency distribution of SP– spines in males and females (diestrus) in bins of 0.05 %. Male: n = 880 SP– spines. Female (diestrus): n = 1227 SP– spines.

3.3.2.4 The average spine head size of SP+ and SP– spines did not show sex-specific differences.

Chapter 3.3.2.3 showed that the ratio of SP+ spines did not differ significantly in *so* of females (diestrus), when compared to males (Figure 24 A). Even under the condition of SP-overexpression in male CSPtg mice, leading to a ~2-fold increase

in the ratio of SP+ granule cell spines in the OML of the dentate gyrus (Figure 13 B), no significant increase in spine head size of SP+ granule cell spines was observed when compared to WT mice (see chapter 3.1.3 and Figure 13 C). However, as ratios of SP+ spines in *so* of dCA2 were similar between males and females (diestrus) (Figure 24 A), it still remained possible that the observed sex-dependent difference in spine head size/segment in *so* of dCA2 was due to a sex-specific difference in the head size of SP+ spines. To examine this possibility, head sizes of SP+ and SP– spines were determined with the investigator (M.R.) blind to genotype and, importantly, with the investigator blind to the SP-content of a given spine. To assure this, spine head quantification was completed and finalized before performing SP-analysis. For males n = 6 animals, n = 14 dendritic segments (one segment for each individual PCP4+ dCA2pc) were analyzed. For females (diestrus) n = 6 animals, n = 17 dendritic segments (one segment each individual PCP4+ dCA2pc) were analyzed. Then, the average spine head size of SP+ and SP– spines, respectively, were calculated per segment and tested for significance.

In *so* of male mice, the average spine head size of SP+ spines was 0.294 μm^2. In *so* of female (diestrus) mice, the average spine head size of SP+ spines was 0.265 μm^2. There was no significant difference in *so* of females (diestrus) compared to males (p = 0.3771, Mann-Whitney U-test,), as shown in Figure 24 B. The head size-distribution of SP+ spines is shown in Figure 24 D.

In *so* of male mice, the average spine head size of SP– spines was 0.162 μm^2. In *so* of female (diestrus) mice, the average spine head size of SP– spines was 0.149 μm^2. Again, there was no significant difference between the two groups (p = 0.2621, Mann-Whitney U-test), as shown in Figure 24 C. The head size-distribution of SP– spines is shown in Figure 24 E.

Therefore, it could be ruled out that the observed sex-dependent difference in spine head size in *so* of dCA2 is due to sex-dependent differences in spine head size of SP+ and SP– spines.

3.3.2.5 *Average SP-puncta size of SP+ spines in the basal compartment of dCA2 did not show sex-specific differences*

Aromatase-dependent regulation of SP seems to take place in CA1 in male and female rodents in a similar fashion[158]. However, it was unknown whether there

were sex-specific differences between adult male and female (diestrus) mice in *so* of dCA2 concerning the average amount of SP present in SP+ spines.

Thus, the SP-puncta size of each previously identified SP+ spine on PCP4+ basal dendrites of dCA2-pc's that was included in the spine head quantification was quantified in a semi-automatic manner using a custom-made macro for Fiji-Software developed in-house by Dr. Tassilo Jungenitz. Macro-parameters were optimized to ensure optimal detection of SP-punctae. The same parameters were applied to all image-stacks included for SP-analysis. Colocalization was verified again by hand in all dimensions using x-y, x-z and y-z planes. In the rare case that the macro did not properly detect a SP-puncta, it was corrected by hand using the macro's threshold of gray level as a cutoff to keep measurements as comparable as possible. At all times, the investigator (M.R.) was blind to the genotype of the sample. As a final step, average SP-puncta size was determined and tested for significance.

In *so* of male mice, the average SP-puncta size was 0.038 µm^2. In *so* of female (diestrus) mice, mean SP-puncta size/segment was 0.039 µm^2. There was no significant difference in SP-puncta size in *so* in females (diestrus), compared to males ($p = 0.6314$, Mann-Whitney U-test), as shown in Figure 25 A. The relative frequency distribution of SP-puncta sizes of SP+ spines is shown in Figure 25 B.
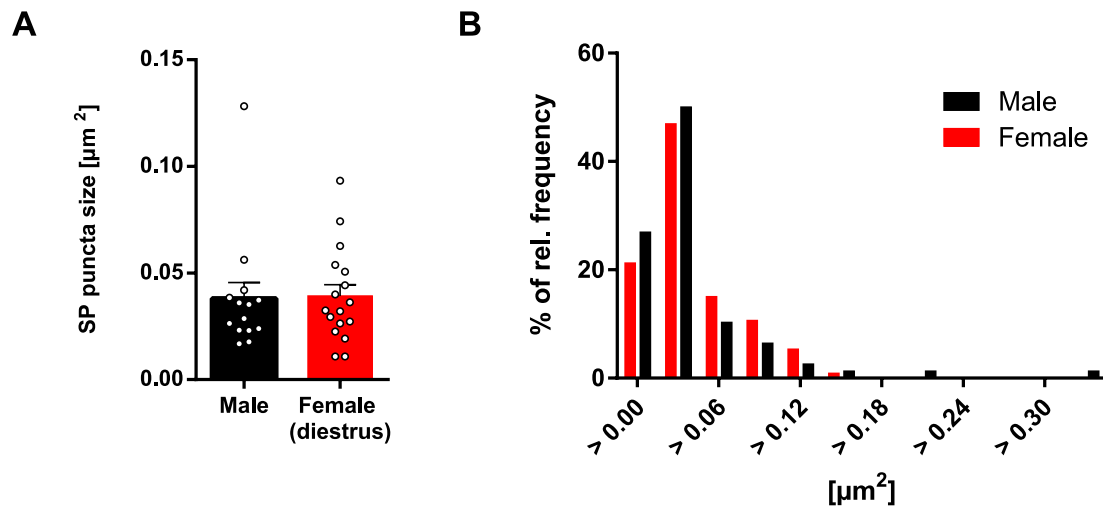
Figure 25: No sex-specific difference in SP-puncta size of basal SP+ pyramidal cell spines in dCA2 between females (diestrus) and males. A: In *so* of dCA2, mean SP-puncta size was not significantly different in females (diestrus) compared to males. p = 0.6314, Mann-Whitney U-test. Male: n = 14 dendritic segments from n = 6 animals. Female (diestrus): n = 17 dendritic segments from n = 6 animals. B: Relative frequency distribution of SP-puncta sizes in males and females (diestrus) in bins of 0.03 %. Male: n = 78 SP-puncta. Female (diestrus): n = 113 SP-puncta.

3.3.2.6 In Stratum oriens of male and female (diestrus) mice, SP+ spines have larger spine heads than SP– spines

Consistent with previous findings[22], in chapter 3.1.4 of this thesis it could be shown that SP+ granule cell spines exhibit significantly larger spine heads than SP– spines, in a very comparable manner in both SP-overexpressing adult male CSPtg-mice and male control animals. However, similar data were missing concerning dCA2. Thus, the next question was if spine head sizes of SP+ spines are larger in dCA2 of male adult mice compared to SP– spines, and if there is a sex-specific difference when compared to female (diestrus) mice.

In *so* of male mice, the average head size of SP+ spines was 0.294 μm^2, whereas the average head size of SP– spines was 0.162 μm^2. In *so* of female (diestrus) mice, the average head size of SP+ spines was 0.265 μm^2, whereas the average head size of SP– spines was 0.149 μm^2. For both groups, SP+ spines were significantly larger than SP– spines (Male: Figure 26 A, p = 0.0001. Female (diestrus): Figure 26 C, p < 0.0001; Wilcoxon matched-pairs signed rank test). The relative spine head size distribution of SP+ and SP– spines are shown in Figure 26 B (male) and Figure 26 D (female (diestrus). In both males and females

(diestrus), head sizes of SP+ spines were right-shifted towards larger spine head sizes compared to SP– spines (Male: p < 0.0001. Female (diestrus): p < 0.0001. Kolmogorov-Smirnov test). For every dendritic *so*-segment included in the analysis, the mean spine head size of SP– spines was always smaller than the mean spine head size of its SP+ spines in both sexes (Figure 26 E and F).

Thus in *so* of dCA2 SP+ spines exhibit larger heads than SP– spines in a sex-independent manner in both adult male and female (diestrus) C57BL/6J mice. This is consistent with earlier literature[17,47], recently published findings[22,180], and with the results from the dentate gyrus of adult male mice reported earlier in this thesis (see chapter 3.1.7 and Figure 18). Thus, the phenomenon of average spine head size of SP+ spines being significantly larger compared to SP- spines seems to occur independently of sex, region, and SP-expression-level.
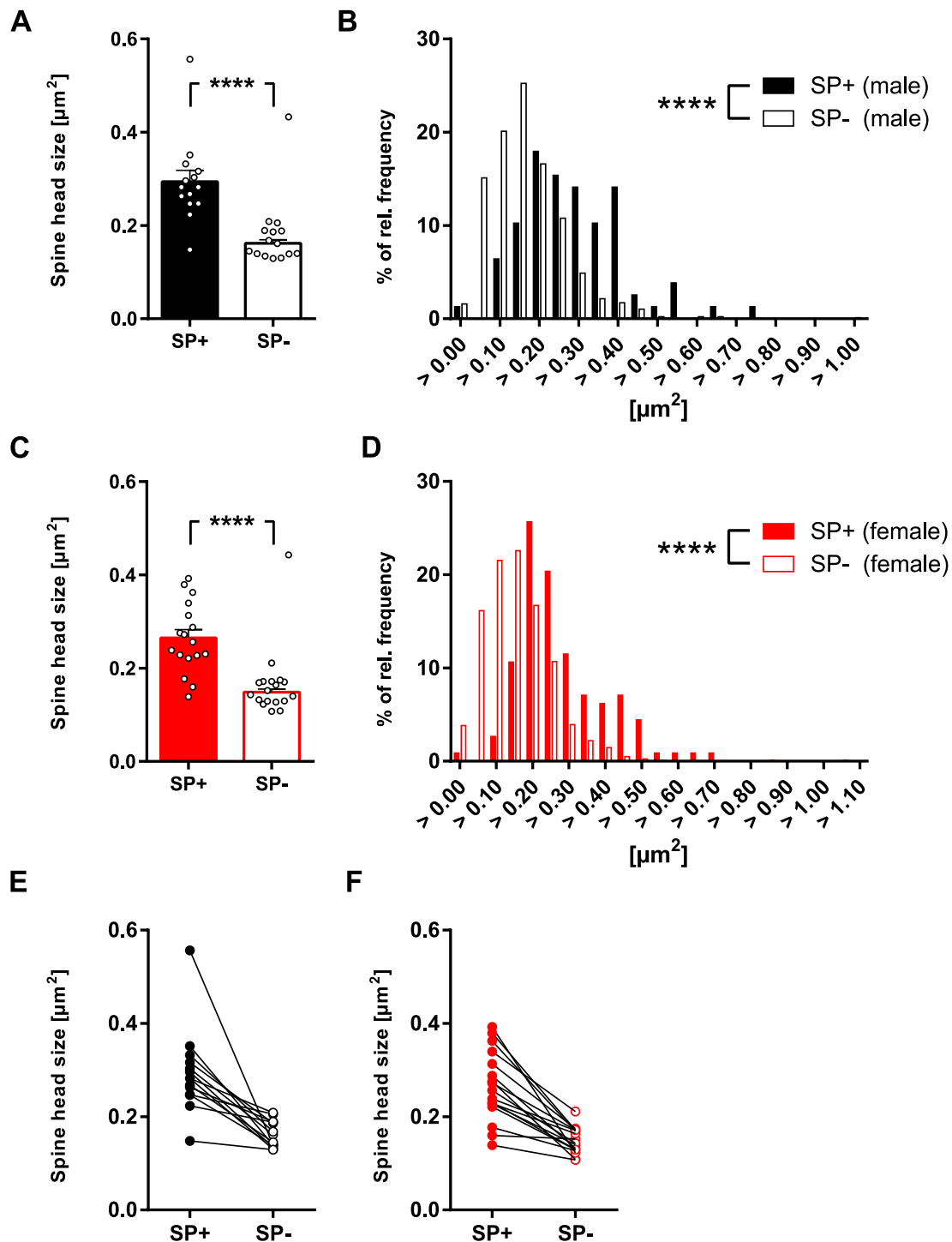
Figure 26: SP+ spines have larger spine heads than SP– spines in *so* of male and female (diestrus) mice. A: In males, *so*-spine head size of SP+ spines (black filled columns) was significantly larger compared to *so*-SP– spines (black-framed columns). ****p = 0.0001, Wilcoxon matched-pairs signed rank test. n = 14 dendritic segments from 6 male animals, for each segment SP+ and SP– spines were quantified. B: In males the relative *so*-spine head size distribution of SP+ spines is significantly right-shifted towards larger spine head sizes. ****p < 0.0001, Kolmogorov-Smirnov test. n = 78 SP+ spines. n = 880 SP– spines. C: In females (diestrus), *so*-spine head size of SP+ spines (red filled columns) is significantly larger when compared to *so*-

SP– spines (red-framed columns). ****p < 0.0001, Wilcoxon matched-pairs signed rank test. n = 17 dendritic segments from 6 female (diestrus) animals, for each segment SP+ and SP– spines were quantified. D: In comparison to male mice, in females (diestrus) animals the relative *so*-spine head size distribution of SP+ spines was significantly right-shifted towards larger spine head sizes. ****p < 0.0001, Kolmogorov-Smirnov test. n = 113 SP+ spines. n = 1227 SP– spines. E, F: Even on single segment-level for every dendritic *so*-segment included in the analysis, in both males (E) and females (diestrus) (F), the mean head size of the SP– spines of a given segment was always smaller than the mean spine head size of its SP+ spines.

3.3.2.7 Spine head size correlates with SP puncta size in females

Consistent with recently published findings from our group[22,180], in SP+ DG-spines in the OML of adult male mice, spine head size showed a positive correlation with SP-puncta size. This phenomenon seemed unaffected by expression levels of SP, as it occurred in both CSPtg and WT animals in a comparable way (see chapter 3.1.7 and Figure 18). However, similar data for dCA2 is missing so far. In addition, nothing is known about putative sex-differences of such a correlation.

To close this gap, we addressed the question whether spine head size correlates with SP-puncta size in *so* of dCA2 in adult male mice, and whether this is also the case in adult female (diestrus) mice. Thus, we correlated SP-puncta size (areamax) with its spine head size (areamax) for both sexes. (Male: n = 78 SP+ spines, n = 14 dendritic segments, n = 6 animals. Female (diestrus): n = 113 SP+ spines, n = 17 dendritic segments, n = 6 animals). In *so* of male animals, no significant correlation between SP-puncta size and spine head size was observed, although the p-value was very close to the significance level (p = 0.0536, Spearman r = 0.2195, R squared = 0.0007. Figure 27 A). In *so* of female (diestrus) animals, there was a significant correlation between SP-puncta size and spine head size, although linear Goodness of Fit was quite weak (p = 0.0474, Spearman r = 0.1869, R squared = 0.0234. Figure 26 B).
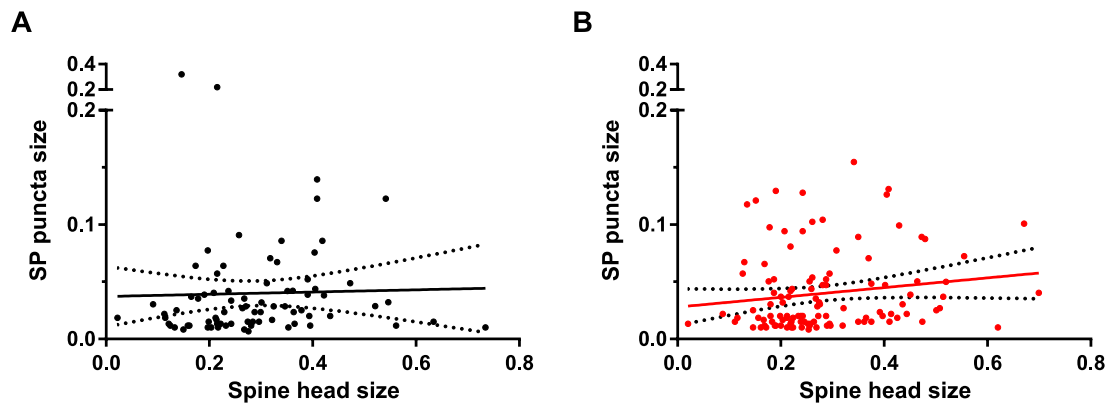
Figure 27: Correlation of SP-puncta size with spine head size in *so* of male (black) and female (diestrus) mice (red). A: In so of male animals, there was no significant correlation between SP-puncta size and spine head size (p = 0.0536, Spearman r = 0.2195, R squared = 0.0007). B: In so of female (diestrus) animals, SP-puncta size positively correlated with spine head size, although linear Goodness of Fit was weak (*p = 0.0474, Spearman r = 0.1869, R squared = 0.0234).

Based on this dataset, one could postulate a putative sex-specific difference in the correlation of SP-puncta size with spine head size of SP+ spines, in a way that in dCA2 it does exist in females (diestrus) (although it is not as robust as in GC-spines in the OML in adult male mice[22,180]), but not in males. However, for both groups p-values are quite close to one another, around the preset significance level of alpha = 0.05. Secondly, fitted linear regressions show similar slopes in both groups. This suggests that larger datasets and a greater power of the test are necessary to address this question and to avoid a type II statistical error.

3.3.3 Stratum radiatum: Sex differences of dendritic spines

3.3.3.1 Spine density is increased in females (diestrus) compared to males

As shown in chapter 3.3.2.1, in the basal compartment of dCA2-pc's, no sex-specific difference in spine densities was observed between adult male and female (diestrus) mice (Figure 22 A). However, region- and layer-specific sexual dimorphisms have previously been shown in the rodent hippocampus[138]. In line with this, estrous cycle-dependent changes in spine density in CA1 of adult female rats were only observed in the apical compartment (*slm*), whereas in the basal compartment of CA1-pc's, the density of *so*-spines was not significantly different. In CA3, no significant changes in spine density could be observed for dendrites located in either layer [129]. Therefore, the next question was if dCA2 in adult mice exhibits a layer-specific sexual dimorphism in spine density similar to what has been shown for CA1 in rat.

To answer this, in analogy to the analysis performed in the basal compartment, spine densities on apical dendrites of the 3rd-6th dendritic orders were quantified in *sr* of dCA2. All spines included for analysis were assigned to the aforementioned spine groups: I) Mature spines with a spine head, which probably form functional synapses[20], II) Immature spines without a distinguishable spine head, which probably do <u>not</u> form functional synapses[20], or III) Non-classifiable spines due to methodological reasons. In *sr* of adult female (diestrus) mice, dCA2-pc's showed a significantly higher spine density on apical pyramidal cell dendrites than in adult males (Figure 28 A, p = 0.0289, Mann-Whitney U-test; males: mean = 2.40 spines/µm, females (diestrus): mean = 2.95 spines/µm). Figure 28 B illustrates the relative frequency of mature, immature and non-classifiable spines observed on apical dendrites in *sr* of male and female (diestrus) dCA2, plotted as the average relative ratio of dendritic spine groups. Mature spines: 82.24 % (males) vs. 76.22 % (females). Immature spines: 11.68 % (males) vs. 14.51 % (females). Non-classifiable spines: 8.08 % (males) vs. 9.27 % (females). Female (diestrus) mice showed a significantly higher density of mature spines compared to male animals (Figure 28 C, p = 0.0289, Mann-Whitney U-test; males: mean = 1.92 spines/µm, females (diestrus): mean = 2.23 spines/µm). Immature spines (Figure 28 D, p = 0.0541, Mann-Whitney U-test; males: mean = 0.29 spines/µm, females (diestrus): mean = 0.44 spines/µm) and even non-classifiable spines (Figure 28 E,

p = 0.3357, Mann-Whitney U-test, males: mean = 0.19 spines/μm, females (diestrus): mean = 0.29 spines/μm) followed the same trend in females (diestrus) mice, occurring in higher numbers than in male animals, although not reaching significance.

These data, obtained by the author of this thesis applying the spine analysis paradigm detailed in the method section, show that in the apical compartment of dCA2 neurons in adult mice, a sex-specific difference in *sr*-spine density exists between female (diestrus) and male animals. The higher spine density in females (diestrus) was driven by a significantly higher density of mature spines, although also densities of immature and non-classifiable spines followed the same trend towards higher densities in females (diestrus).
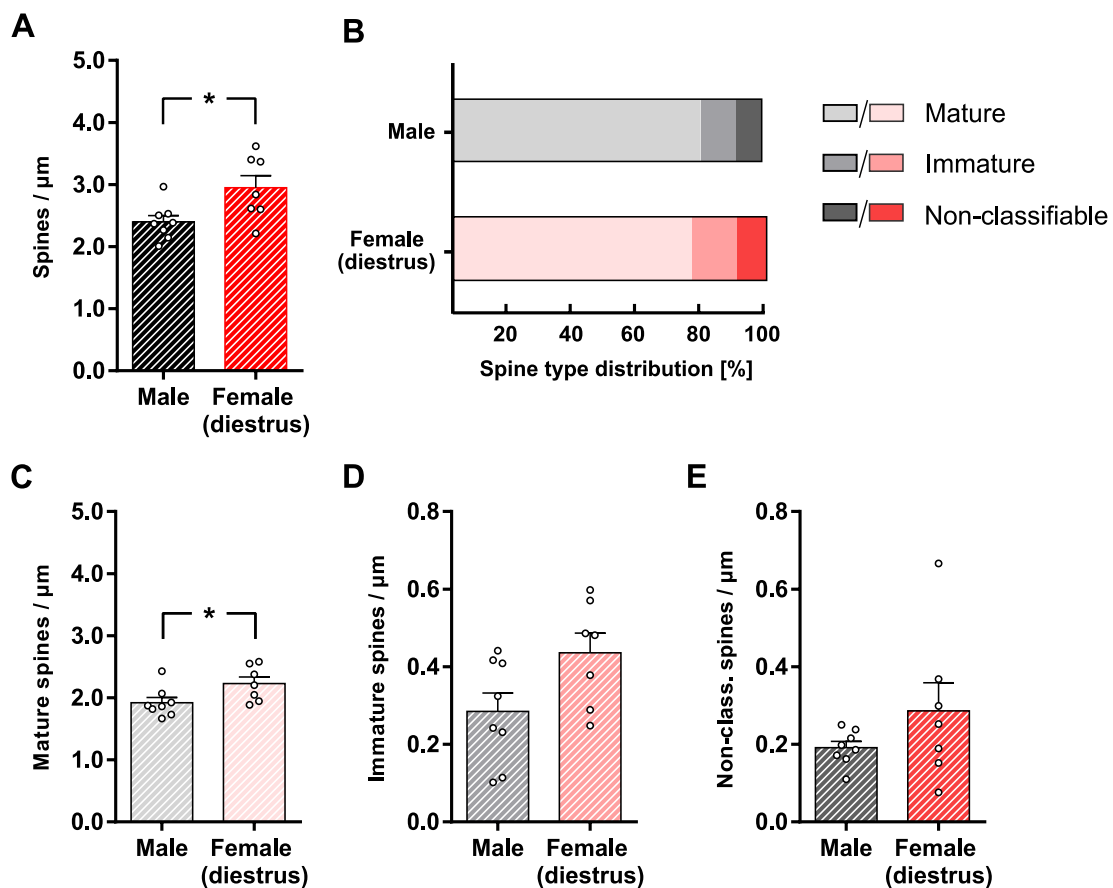
Figure 28: **Spine density *sr* of dCA2-pc's shows a sex-specific difference in females (diestrus) adult mice, compared to males.** A: Female (diestrus) animals show a higher spine density in *sr*, compared to male controls. *p = 0.0289, Mann-Whitney U-test. Male: n = 8 dendritic segments from n = 3 animals, Female (diestrus): n = 7 dendritic segments from n = 4 animals. B: Average relative ratio of predefined spine groups[20]. Mature spines: 80.24 % (males) vs. 76.22 % (females). Immature spines: 11.68 % (males) vs. 14.51 % (females).

Non-classifiable spines: 8.08 % (males) vs. 9.27 % (females). C: Density of mature dendritic spines is increased in *sr* of females (diestrus), compared to males. *p = 0.0289, Mann-Whitney U-test. D and E: In *sr* of dCA2 in females (diestrus), density of immature and non-classifiable spines show the same trend towards higher spine density compared to males, although not reaching the significance level. D: p = 0.0541, E: p = 0.3357, Mann-Whitney U-test.

3.3.3.2 In Stratum radiatum of dCA2, spine head size-distribution in female (diestrus) mice is shifted towards smaller spine head sizes.

For *so* of dCA2, a sex-specific difference in spine head size could be shown, i.e. females (diestrus) exhibiting significantly smaller spine head size per segment (Figure 23). It was also shown that *sr*-spines seem to have smaller spine heads than *so*-spines in general, independent of the sex of the animals investigated (Figure 21).

Therefore, the last aim of this thesis was to investigate whether in *sr* of dCA2 there is a sex-specific difference in spine head size. To test this hypothesis, head sizes of dendritic spines included for spine head analysis were quantified in analogy to *so* (Figures 9-11) and the mean spine head size/segment was calculated. In *sr* of dCA2 (Figure 29 A) spine head size on apical pyramidal cell dendrites showed a trend towards smaller spine head size in females (diestrus) (red hatched column, mean = 0.113 μm^2, n = 7 dendritic segments from n = 4 animals) compared to males (black hatched column, mean = 0.130 μm^2, n = 8 dendritic segments from n = 3 animals). This difference did not reach the level of significance (p = 0.1893, Mann-Whitney U-test). In line with this, in female (diestrus) mice, the relative frequency of spine head sizes was significantly shifted towards smaller values when compared to male control animals (Figure 29 B): Small spines with a head size $\leq 0.15\ \mu m^2$ formed a larger proportion of the spine population in females (diestrus) than those observed in males. Accordingly, larger spines with a head size $> 0.15\ \mu m^2$ occurred more often in male mice than in female (diestrus) animals. ***p = 0.0004, Kolmogorov-Smirnov test; Female (diestrus): n = 575 spines, Male: n = 616 spines.

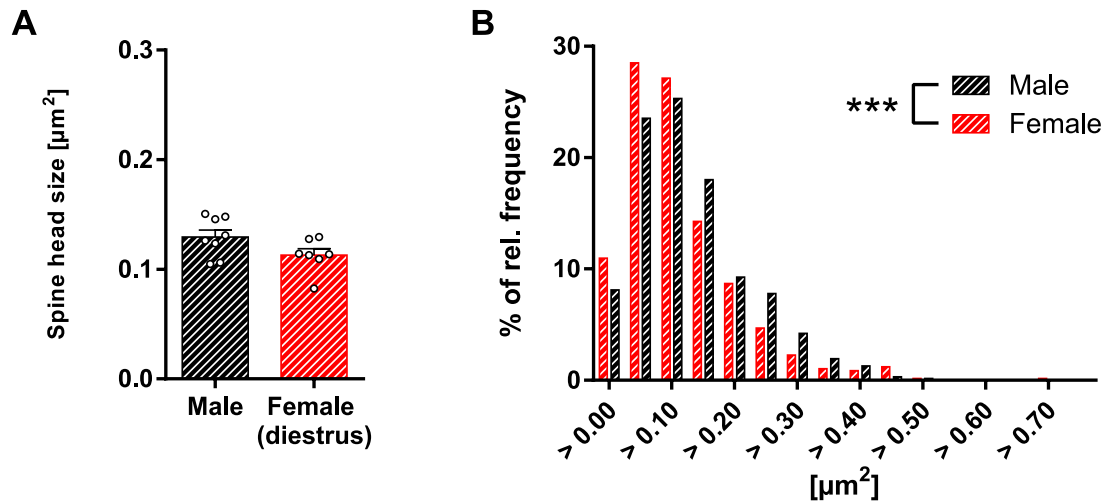**Figure 29: Spine head size-distribution in female (diestrus) mice is shifted towards smaller spine head sizes in stratum radiatum.** A: Female animals show a trend towards a smaller mean spine head size, although not significant. p = 0.1893, Mann-Whitney U-test. B: However, in females (diestrus), spine head sizes are significantly shifted towards smaller values compared to male animals. ***p = 0.0004, Kolmogorov-Smirnov test.

4 Discussion

The results presented in the first part of this thesis describe in detail, for the first time, the effects of SP-overexpression on dendritic spine parameters and on the fraction of spines containing SP (SP+ spines). In the OML of the DG, SP-overexpression in transgenic adult male CSPtg-mice resulted in doubling the fraction of SP+ spines, without affecting total spine density, average spine head size and average SP-puncta size.

Consistent with the unaltered average spine head size under conditions of SP-overexpression, the recently published results[22] presented in the second part of this thesis show, for the first time, that SP-deficiency in granule cells of adult male SP-KO animals has no significant effect on this parameter.

Interestingly, under the condition of overexpression in adult male CSPtg mice, the additional SP is sorted towards many small spines and a few large spines. In other words, under SP-overexpression, many small spines and a few large spines become SP+, assumingly assembling a SA. This could indicate an activation of silent synapses, potentially giving DG-neurons of CSPtg-mice the ability to improve the formation of environment-dependent granule cell-ensembles[68].

The results presented in the third part of this thesis reveal, for the first time, sex-specific differences in spine density and spine morphology in dCA2, the hippocampal subregion that is essential for social recognition memory[115] and other cognitive functions[114]. Strikingly, the observed sex-differences occurred in a layer-specific manner: In male adult mice, pyramidal cell spines of the basal dCA2-compartment (*so*) showed larger spine heads than spines in female mice in the diestrus stage of their cycle (females (diestrus), while spine density was not significantly different. In the apical dCA2-compartment (*sr*), females (diestrus) showed an increased spine density, while spine head size was still shifted towards larger head sizes in males. Future experiments including females (proestrus) will be needed to control for cycle-dependent changes of spine density and spine morphology. In addition, more dynamic experiments conducted on a behavioral and/or electrophysiological level would be needed to unfold the functional implications of the microanatomical findings presented here.

Despite sex-specific differences of dCA2 between males and females (diestrus), the results presented here show a significant layer-specific difference in spine

head size in a sex-independent manner: In both females (diestrus) and males, spine head size in the apical *sr* was significantly smaller than in the basal *so*. Though dCA2 is a hippocampal subregion that is known for strict layer-specific regulation of plasticity in the apical compartment, the structural data presented here could imply a yet unknown compartment-specific difference in synaptic plasticity in the basal compartment. This could be of great interest as the basal *so*, together with the *pcl*, is preferentially targeted by neuromodulatory input from extrahippocampal sources such as the PVN or SUM[99,101,170,189-195].

For the basal compartment (i.e. *so*) of dCA2, there was no sex-specific difference in SP-puncta size or in the ratio of SP+ spines. These data indicate that SP is distributed in a sex-independent manner in dCA2 in adult mice, which is consistent with the previous finding that SP seems to be regulated by the enzyme aromatase in a similar fashion in CA1 of male and female mice[158].

Taken together, this thesis investigated the distribution of SP in hippocampal neurons. The dendritic distribution of SP and its influence on spine density and spine head size were studied. These parameters are of interest, since they have functional correlates, i.e. the number of excitatory synapses (spine density), and synaptic strength (spine head size). Three different conditions were investigated in hippocampus of adult mice *ex vivo*: 1) SP-overexpression (gain-of-function), 2) SP-deficiency (loss-of-function), and 3) SP-expression at wild type-level in male and female mice (sex-differences in dCA2).

4.1 The effect of SP-overexpression on GC-spine morphology and spinous SP-distribution in the OML of adult male mice *ex vivo*

GCs have been shown to upregulate the transcription of SP in response to environmental stimuli, forming ensembles of GCs which express the activity marker arc along with somatic SP-clusters[68]. These arc/SP-positive GC-ensembles potentially encode a given environmental context[68]. The transgenic mouse model used in the first part of this thesis was designed by Del Turco, Paul, Bas-Orth, Deller et al. (unpublished): The CSPtg mouse, generated on the C57BL/6J background, expresses CFP-tagged SP under the Thy1-promoter[196], resulting in a strong neuron-specific transgene-expression.

Experiments conducted by Del Turco, Paul, Deller et al. (unpublished) demonstrated that CFP-SP is expressed in a WT-like manner in CSPtg-animals.

They also showed that CFP is distributed to spines and forms a SA at the ultrastructural level. Therefore, the CSPtg-mouse appears to be a suitable gain-of-function model to study the effect of SP-overexpression on granule cells (first part of this thesis). For this purpose, intracellular injection of fluorescence dye in fixed tissue[22,161,167,180] was used as a technique to label single granule cells in adult male CSPtg hippocampi. Confocal imaging and systematic analysis of 3D-image stacks were subsequently employed to reveal the effects of SP-overexpression on GC spines and on the distribution of SP into the spinous compartment.

4.1.1 Dendritic spine density as well as average spine head size is unchanged by different protein levels of SP in dentate granule cells

Previous studies have shown that SP-deficiency does not alter spine density[22,60,61,73,74]. Consistent with this, it could be shown in this thesis that elevated protein levels of SP in adult male CSPtg mice do not change spine density in the OML of the DG (Figure 13 A), demonstrating that SP levels do not influence this neuronal parameter. Since the number of spines also corresponds to the number of excitatory synapses, it can also be concluded that the density of glutamatergic axo-spinous synapses impinging on granule cells is most likely unaffected[20,175].

Concerning GC spine head size, recently published data[22] acquired for and presented in this thesis could show that SP-deficiency does not change average spine head size in adult male SP-KO mice *ex vivo* (Figure 19). Consistent with these findings, this thesis could also show that under SP-overexpression, average GC spine head size is unchanged in adult male CSPtg-mice *ex vivo* (Figure 13 C). However, SP was mostly observed in larger spines. Consistent with this finding and previous studies[22,47,180], the average head size of SP+ spines was significantly higher than that of SP– spines in both CSPtg and WT mice. (Figure 14). This is in line with recently published data obtained *ex vivo* and *in vitro* in adult male transgenic mice which expressed SP at a wild type level, showing that the presence of SP stabilizes large spines, rather than actively increasing average spine head size[22].

The positive correlation of spine head size and SP-puncta size was preserved under SP-overexpression (Figure 18). Concurrently, the average size of SP puncta was also unchanged (Figure 17).

Taken together, these findings indicate that in the CSPtg mouse model, despite elevated protein levels, SP is expressed in a fashion similar to the WT-condition, and that the transgenic CFP-SP is probably distributed towards the spinous compartment in a physiological manner. This underscores the advantage and usability of this transgenic mouse model (Del Turco, Paul, Rietsche et al., unpublished).

4.1.2 Elevated levels of SP-protein lead to an preferential increase of small SP+ spines in adult male CSPtg-mice

In SP-overexpressing CSPtg-mice, the ratio of SP+ GC-spines was ~2-fold higher than under WT-conditions (Figure 13 B). As mentioned before, average spine head size was unchanged under SP-overexpression (Figure 13 C). This appears counterintuitive at first, as other data in this thesis show that SP+ GC-spines exhibited larger spine heads than SP– GC-spines, in a similar fashion in both CSPtg and WT mice (Figure 14). One would have expected that if the number of larger SP+ spines rises from ~10 % to ~20%, this should have an effect on average spine head size.

However, this contradiction could be resolved following a more detailed investigation of the head size distribution of SP+ spines in CSPtg mice: The distribution of SP+ spines is changed in the SP-overexpressing mutant and the number of small SP+ spines is increased in a disproportionate fashion (Figures 15 and 16 A). This increase in small spines also counteracts the subtle increase in the number of very large SP+ spines, thus leading to an unchanged average spine head size of SP+ spines. In comparison, the proportions of small and large SP– spines remained stable in both CSPtg and WT animals (Figure 16 C), underscoring that all significant findings observed in CSPtg mice are linked to the presence of SP.

In previous studies, SP has been shown to affect synaptic strength by organizing the SA, which in turn functions as an intra-spinous calcium store[45,47,74,197]. Furthermore, SP facilitates AMPA-Receptor (AMPA-R) trafficking to the excitatory postsynapse[47] and SP+ spines show an increased synaptic strength[47].

On the other hand, small spines are unlikely to be equipped with SP or a SA[39]. Thus, if more small GC-spines contain SP and – potentially - a SA, it could strengthen the excitatory axo-spinous synapses in the ML, making them more prone to receive presynaptic input from the perforant path (PP)[20,50,198]. As small spines have been characterized as part of rather weak synapses, some may potentially be even silent[50,85,199]. Thus, SP-acquisition of a small spine could activate a previously "dormant" synapse. Electrophysiological data will be required to test this hypothesis.

As a novel environment leads to an upregulation of SP in GCs in adult male mice[68], a subsequently increased protein-level of SP could lead to a higher ratio of (small) SP+ spines, making axo-spinous PP-GC synapses more prone for plastic changes[199]. This could support the integration of SP-upregulating GCs into ensembles encoding a given environment[68].

4.2 Sex- and layer-specific differences in dCA2, the hippocampal area crucial for social recognition memory, in adult male and female mice

The hippocampal subregion dCA2 has received scientific attention during the last decade, initially due to its essential role in social recognition memory processes[110]. This has now earned it a status as a functionally distinct hippocampal subregion[115,191] instead of being a mere transition zone between CA3 and CA1. Recently, various other functional implications have been suggested for CA2[114,118,192], such as computation of saliency or novelty[116,200,201] or temporal sequence learning[117]. In the process of "re-discovering CA2"[89(p1)], several molecular markers were established for CA2, such as PCP 4 and RGS 14[91-93]. Both proteins have been implicated in one unique feature of CA2: layer-specific regulation of LTP in *sr*, but not *slm*[96]. These molecular CA-markers labeled also the adjacent most-distal portion of CA3a in mice, thus it was proposed to extend the boundaries of CA2 towards CA3, including the off-tapering *sl*.[92] The region classically identified as CA2[10] is now referred to as CA2a, the region including the most distal part of the sl is now called CA2b[89]. In other words, CA3a lost its most distal part to CA2, due to a molecular and functional re-definition[89,91-93] of the hippocampal subregions. Although much knowledge has been created concerning the apical compartment of CA2, mostly on a functional level (i.e. *sr, slm* and, for CA2b, the *sl*), only little is known about

the basal compartment (i.e. the *so*), both on a structural-microanatomical and on a functional level.

Various intra- and extrahippocampal afferents target dCA2 in rodents[170], usually in a layer-specific manner[166]. However, exact knowledge which layer is targeted by the various (neuromodulary) extrahippocampal afferents is sparse, although some appear to target *so[166]*. Also, as Dudek et al (2016) point out, little is known about the relative functions of the apical and basal compartment[89]. Therefore, the third part of this thesis focused on the structural analysis of basal and apical dendrites of molecularly defined dCA2 in adult mice. Since structure and function are intimately linked, structural differences between the layers could indicate functional difference. This could help to identify promising targets for future research.

Sex-dependent differences are known in social recognition[111,159] and CA2-dependent fear-conditioning[122]. Sex-specific regulation of synaptic plasticity via sex-hormones has been reported in previous studies[153]. In adult female rats and monkeys, estradiol is capable to influence spine density in CA1-pc and memory processes.[202-204] At the same time, SP was shown to be regulated by activity of aromatase[158], the estrogen-synthesizing enzyme. In turn, estrogens were reported to alter spine density, but also to influence processes of learning and memory[132,202,204]. As a steroid hormone, peripherally-produced estradiol can easily cross the blood brain barrier[135]. In vertebrates, aromatase is expressed widely across the brain, including the hippocampus, and the role of central-produced sex neurosteroids in rodents has been recently highlighted[134].

Thus, it appeared of interest to not only investigate the basal and apical dendritic compartments of dCA2, with focus on the plasticity-related protein SP and on dendritic spines, the most important postsynaptic site of excitatory synaptic plasticity, but also to shine a light on potential sex-specific differences in a cycle-controlled manner in order to take into account the cycle-dependent sex-hormone levels of female mice.

84

4.2.1 The layer-specific, sex-independent difference in average spine head size between the apical and basal compartment of dCA2: a putative structural correlate to layer-specific regulation of synaptic plasticity

After establishing the intracellular injection technique of fluorescent dye in fixed brain tissue for dCA2[161,162,167], individual dCA2-pc were labeled, post-hoc verified using the CA2-marker PCP4[93], and confocal z-stacks of apical and basal dendrites of dCA2-pc were acquired. A standardized spine analysis algorithm was applied. A significant layer-specific head size-difference between *sr*-spines and *so*-spines was observed in both adult males and females (diestrus) C57BL/6J mice in a comparable fashion, i.e. *sr*-spines showing a smaller average head size than *so*-spines. It can be concluded from these data that the layer-specific difference in spine head size does not depend on the sex of adult mice.

Spine head size has been associated with the strength of the associated synapse.[19,31,37]. The head size, in turn, depends on synaptic activity and strong afferent activity, e.g. LTP, can induce spine head size growth, i.e. sLTP[21,24,47]. The expression of LTP is influenced by neurosteroids in a sex-dependent fashion: In CA1 of female rodents, LTP can be influenced by neuron-derived estrogens, but not androgens. In contrast, in males LTP is affected by neuron-derived androgens, but not estrogens.[153] However, such a sex-specific regulation of (s)LTP should occur across the whole dendritic tree, i.e. not in a layer-specific fashion. The observed phenomenon is therefore more likely due to sex-independent factors, such as layer-specific afferents existing in both sexes in a similar fashion, or due to sex-independent regulation or facilitation of synaptic plasticity in *sr* vs. *so*.

Interestingly, reduced and tightly regulated synaptic plasticity on CA3-CA2 synapses in *sr* has already been shown in male mice.[96] At the same time, a layer-specific differential regulation of LTP has been demonstrated, as the *slm* with its ECII-CA2 synapses is prone to synaptic plasticity[109]. Therefore, average spine head size being smaller in *sr*, compared to *so*, could be a morphological correlate for the tightly regulated LTP in *sr*, leading to smaller spine head sizes when compared to other layers. Under this assumption, this implies that in *so*, similar as in *slm*, LTP is not as highly regulated as in *sr*. Future investigation of average spine head size of *slm* may complete the picture. In addition, new data on the

regulation of LTP in the basal compartment of dCA2 could help to elucidate this issue.

4.2.2 Layer-specific sex-differences in spine density of dCA2-pc's: Females (diestrus) show a higher spine-density in the apical compartment, while basal spine density is comparable in both sexes.

In *so* of dCA2, the spine density of basal pc-dendrites was similar in adult male mice and females (diestrus) (Figure 22 A). In line with this, the density of mature and immature spines was also comparable in both sexes. (Figure 22 B and C).

Compared to the basal dendrites, females (diestrus) showed a higher spine density on apical dendrites in *sr* of dCA2. The analysis of the different spine types revealed that this increase was caused by an increase in the number of mature spines (Figure 28). Immature and non-classifiable spines followed the same trend, but did not reach level of significance ($p < 0.05$).

Estrogens are able to influence mechanisms of synaptic plasticity, ultimately leading to changes in structure and spine density[132]. In naïve (i.e. non-ovarectomized) adult female rats, cycle-dependent changes in *slm* of CA1 (but not *so*) were observed previously[129]. However, estrogen-dependent changes of spine density were shown to be region- and layer-specific[131,138] and were already observed in the pioneering studies[129,203]: in intact female rats, spine density was not significantly changed in *so* of CA1 or in *slm* and *so* of CA3[129] throughout the estrous cycle.

Consistent with this, the findings presented in this thesis indicate that at least during diestrus of female mice, *so*-spine density of dCA2pc's does not seem to be affected by sex-specific variables. However, in theory, increasing serum-levels of estradiol during proestrus and estrus could still lead to changes in spine density[131,204], which is why ongoing research in our lab is addressing this question at the moment.

At least for females (diestrus), one could speculate that spine density and frequency of spine classes are regulated in the *so* of dCA2 in a sex-independent manner – or, alternatively, being regulated in a gender-specific way at similar levels, leading to comparable structural changes on dendritic spines. The sex-specific difference in spine density in *sr* of dCA2 could be an estrogen-driven

effect along the estrous cycle, comparable to the findings of Woolley et al. (1990) in area CA1 of female rats. Importantly, recent research conducted in adult male and female mice did not show a cycle-dependent fluctuation of spine density in CA1 of female mice[140] if all spine classes were considered. However, a cycle-dependent fluctuation was found for spines with a large spine head, defined by the authors as > 0.6μm diameter. Interestingly, peak spine density of so-defined large spines was found in the diestrus stage of the estrous cycle.[140] The investigation of potential estrous cycle-dependent fluctuations of spine density in dCA2 is a topic of ongoing research.

4.2.3 Increased spine head size in dCA2 of male mice: Sex-specific differences in LTP-regulation, neuromodulation, presynaptic input or actin-remodeling?

Although spine density was at comparable levels in *so* of both sexes, basal spine heads were significantly larger in males than in females (diestrus) (Figure 23). Such a sex-specific difference in spine head size has not been shown before in dCA2 of adult animals *ex vivo*. Similar to the findings in *so* of dCA2, spine head sizes of *sr*-spines in males were significantly shifted towards larger spine head sizes (Figure 29 B). However, average *sr*-spine head size was not significantly different compared to females (diestrus) (Figure 29 A).

As spine head size has been correlated with the area of the PSD and synaptic strength[19,31,37], the aforementioned findings could imply stronger synapses in *so* of dCA2 in adult male C57BL/6J mice, compared to females (diestrus). Electrophysiological experiments in *so* of dCA2 would therefore be of high interest.

Stronger synapses in males, compared to females (diestrus) could be either due to a stronger presynaptic input projecting onto basal dendrites of dCA2, or a somehow increased postsynaptic potentiation to the same level of presynaptic input. Therefore, the first possibility would be that for *so* of dCA2, synaptic potentiation results in a larger average spine head size, i.e. sLTP is regulated in a sex-specific manner. In CA1-pc, LTP was shown to be regulated in a sex-specific fashion via estrogenic neurosteroids in females and androgenic neurosteroids in males[153,205]. However, the magnitude of LTP appeared to be in

comparable ranges[153]. Similar experiments for dCA2 have not been published so far.

The actin cytoskeleton provides the basis for the size, shape, or stability of dendritic spines[206,207]. Actin polymerization is also the basis for spine head expansion and, thus, sLTP[21]. Estrogens influence actin remodeling rapidly via intracellular signaling cascades[208,209]. Therefore, it is conceivable that sex-specific differences in estrogen-levels or estrogen-receptors result in differences in actin-regulation, eventually leading to differences in spine head size.

Adding to this, the morphology of dendritic spines was shown to depend on protein synthesis[210,211]. Estrogens were shown to increase protein synthesis[212], both genomically-driven[213] and via local protein synthesis[214,215].

Furthermore, differences in afferent input, e.g. by the various neuromodulators such as Substance-P from the SUM or AVP from PVN, could be responsible for this effect. As stated before, *so* receives input from the SUM. Overall, only little is known about the afferents projecting onto the many spines in *so* and further research in that area is needed to elucidate potential mechanisms of structural plasticity in either sex. As PNN's occur in high numbers in dCA2 and were shown to suppress synaptic plasticity at excitatory synapses of dCA2-pc's[107,216], sex-specific differences concerning PNN's of dCA2 could have an impact on spine head size. Future research including electrophysiology and tracing experiments are needed to clarify these questions.

As another possibility, the observed head size-difference could be due to fluctuations in spine head size during the estrous cycle, e.g. due to fluctuating levels of serum-hormones and/or neurosteroids via GnRH[134].

Concerning the more subtle sex-specific effect observed on apical dendrites in *sr* of dCA2, one reason could lie within the well-described tight regulation of LTP in the *sr* of dCA2[93,96,105,160,217-219]. As synaptic potentiation is followed by a spine head increase (i.e. sLTP), one could expect a smaller range of possible spine head sizes in a region of restricted plasticity, such as the *sr* of dCA2. Assuming the same (yet unknown) sex-dependent factor influences spine head size in *sr* in a similar fashion as in *so*, i.e. in favor of larger average spine head size in males, a smaller range of putative spine head-expansion, due to LTP-restriction, could lead to more subtle, but still noticeable sex-differences in spine head sizes in *sr*.

However, this remains purely speculative until more experiments have been conducted.

4.2.4 The distribution of SP is sex-independent in *so* of dCA2

The main finding in *sr* of dCA2 of this thesis is the sex-difference in spine density on apical dendrites, with females (diestrus) exhibiting a higher spine density compared to males (Figure 22). Spine density, however, seems to be unaffected by expression-levels of SP[60] (Figure 13 A). As there were no sex-differences in any quantified SP-parameters on basal dCA2-dendrites (Figures 24-26), no further investigations on the distribution of SP in dCA2 were performed.

The size of an immunolabeled SP-puncta of a given SP+ spine correlates with the size of the SA in a spine[9,69,220,221]. Although SP puncta size of SP+ spines did correlate with spine head size in the DG (Figure 18), consistent with recent findings[22,180,220,221], SP-overexpression did not affect average spine head size in the DG of CSPtg mice (Figure 13). Conversely, differences in average spine head size should not necessarily affect SP-parameters. Indeed, no sex-specific differences of any SP-parameter were observed on basal dendrites of dCA2-pc's of adult mice (Figures 24-26). These findings indicate that SP is distributed to dCA2-pc-dendrites in a sex-independent fashion, at least in the basal compartment. This is in line with the finding that aromatase regulates SP in a comparable way in both male and female rodents[158]. Therefore, I postulate that the observed layer-specific sex-differences in dCA2 are not related to levels of dendritic SP-distribution.

No sex-specific differences were found in the basal compartment of dCA2, the *so*, for the ratio of SP+ spines between adult male and female (diestrus) mice. This is consistent with ultrastructural findings from Brandt et al. (2020) in *sr* of CA1 in adult male and female mice: the number of SA observed was similar in male and female adult mice[140]. However, a direct comparison to the present study is limited due to different methodological approaches, different layer/subregion, and the fact that the cycle-stage of the female mice (n = 3) used for EM-analysis was not stated[140].

Interestingly, in *sr* of dCA1, a sex-specific difference in the number of immunolabeled SP puncta has been shown: Adult female C57BL/6J-mice exhibited more SP puncta than adult male animals[158]. However, adult females

were not controlled for estrous cycle-stage in this study, hence the study probably included data from different cycle-stages. As diestrus lasts longest, one could speculate that the majority of female mice had been in diestrus at the time of perfusion, making the findings of this thesis and those of Fester et al. (2017)[158] more comparable. Also of importance, SP-clusters were observed in the dendritic shaft (shaft-SP) on a regular basis in the material used for this thesis. Therefore, quantification of SP puncta alone in a given layer probably does not directly correspond to the ratio of SP+ spines. So far, sex-specific differences of SP located in dendritic shafts have not been studied in detail.

Despite limitations in comparison, these findings are in line with the known phenomenon of region- and layer-specific sex-differences, and may point to a layer-specific and/or subregion-specific sexual dimorphism of SP-regulation between *sr* of dCA1 and *so* of dCA2. This would be consistent with the increasingly accepted view of region-specific differences between the sexes[131]. As one example, orchiectomy in male rats affected the apical and basal dendritic arborization of CA3-pc's, but left both apical and basal CA1-dendrites unchanged[222]. In ovarectomized females, dendritic arborization was not significantly changed, neither in CA3 nor in CA1[222].

Average spine head size of SP+ *so*-spines was not significantly different between males and females (diestrus), neither was the average head size of SP– spines. Consistent with the findings in the DG (see chapter 4.1), there was also no difference in SP-puncta size of SP+ spines in *so* of dCA2 between males and females (diestrus). However, SP+ spines on basal dendrites of dCA2 exhibited significantly larger spine heads than SP– spines, in both males and females (diestrus) (Figure 26). These findings are consistent with the extant literature[17,47] and recently published findings[22,180], as well as with the findings shown in this thesis for the DG (suprapyramidal blade) of adult male mice (see chapter 3.1.7 and Figure 18). Thus, I propose that the phenomenon of average spine head size of SP+ spines being significantly larger than SP- spines seems to be independent of sex, region, and expression-levels of SP.

Taken together, the lack of sex-specific differences regarding several SP-parameters implies that the observed sex-dependent differences in spine density (in *sr*, but not in *so*) and in spine head size (both in *sr* and *so*) is not directly related

to the ratio of SP+ spines, and not due to a sex-specific sorting of SP into dendritic spines.

However, as SP was shown to influence synaptic plasticity via various pathways, and as SP is capable of stabilizing dendritic spines[22], dynamic investigation such as time-lapse imaging and loss-of-function approaches would be necessary to corroborate this hypothesis. In addition, having investigated only female mice in diestrus, a cycle-dependent difference in the ratio of SP+ spines, and thus a sex-specific role of SP in *so* of dCA2, could have been missed. Future research should address these questions.

4.3 Outlook

In this thesis, sex-specific differences in spine density and spine head size were analyzed in dCA2, the hippocampal subregion essential for social recognition memory. Males and females (diestrus) were studied and spine parameters of basal dendrites (*so*) and apical dendrites (*sr*) were compared.

The next step is now to include females in other stages of the estrous cycle, in particular in proestrus, to investigate the effect of increasing levels of serum-estradiol on spine density and spine head size on apical and basal dendrites of dCA2. This would reveal whether the sex-specific differences reported in this thesis are cycle-dependent. Specifically, it should be analyzed whether the sex-independent head size-difference between *sr* and *so* of dCA2 persists in females that are in the proestrus phase of their cycle. If females in proestrus also exhibited a larger average spine head size in *sr*-spines, further evidence for the hypothesis that the observed head size difference is sex-independent would be provided.

Obtaining electrophysiological data on dCA2 will also be important. It will be of profound interest to investigate the basal compartment of dCA2 on an electrophysiological level, e.g. testing the "LTP-capability" of basal axo-spinous dCA2-pc synapses, compared to the very restricted compartment of the apical *sr,* and the highly plastic *slm*.

Another topic would be to dissect potential sex-specific differences in spine parameters of vCA1, where social memory engrams are thought to be stored[112,113,119].

Taken together, the part of this thesis addressing dCA2 provided structural data regarding the cellular anatomy of identified neurons in male and female (diestrus) mice. This work can now be extended in various directions, as suggested above.

5 Tables

5.1 Table 1: Overview of solutions

Name of solution	Substance	Amount per liter
0.1 M PBS	Dulbeccos´s Phosphate Buffered Saline (1x)	9,55g
	Millipore-fitrated H_2O	Ad 1000 ml
TBS	Tris	6.055 g
	NaCl	9 g
	Millipore-fitrated H_2O	955 ml
	1 M HCl	44 ml (target pH = 7.40)
4 % PFA	PFA	40g
	1 M NaOH	3 drops (target pH = 7.40)
	0.1 M PBS	ad 1000 ml

5.2 Table 2: List of animals

	CSPtg [n]	WT [n]	Total [n]
Dentate gyrus (gain-of-function)	6	6	12
	SP-KO [n]	WT [n]	Total [n]
Dentate gyrus (loss-of-function)	8	8	16
	Female (diestrus) [n]	Male [n]	Total [n]
CA2: Str. oriens	6	6	12
CA2: Str. radiatum	4*	3*	7*

* Subset of animals used for Str. oriens

5.3 Table 3: Quantitative analysis in the DG of CSPtg-animals (gain-of-function)

	Segments (n)	Spines [n]	SP-puncta [n]
CSPtg	18	1050	182
WT	18	1031	103

5.4 Table 4: Quantitative analysis in the DG of SP-KO-animals (loss-of-function)

	Segments (n)	Spines [n]
SP-KO	24	2158
WT	24	1885

5.5 Table 5: Quantitative analysis in *so* and sr of dCA2

	Segments (n)	Spines [n]	SP-puncta [n]
Male: *so*	14	958	78
Female (diestrus): *so*	17	1340	113
Male: *sr*	8	616	n/a

Female (diestrus): *sr*	7	575	n/a

6 Abbreviations

A568 = Alexa Fluor 658 Hydrazide

AMPA = alpha-amino-3-hydroxy-5-methyl-4-isoxazolpropionic acid

AMPA-R = AMPA-receptor

areamax = maximum cross-sectional area

Arc = activity-regulated cytoskeleton protein

BBB = blood brain barrier

CA = cornu ammonis

CSPtg = CFP-SP-transgenic mice

CNS = central nervous system

d = transverse diameter

dCA2 = dorsal CA2-subregion

dHC = dorsal hippocampus

gcl = granule cell layer

DG = dentate gyrus

EC = entorhinal cortex

ECM = extracellular matrix

ECII = Layer II of the entorhinal cortex

ER = endoplasmatic reticulum

GC = dentate granule cell

gcl = granule cell layer

h = dentate hilus

HC = hippocampus

hf = hippocampal fissure

F = filopodia-like protrusions

female (diestrus) = female mice in diestrus stage of the estrous cycle

l = longitudinal diameter

IEG = immediate early gene

IML = inner molecular layer

lat = lateral

LEC = lateral entorhinal cortex

LTD = long term depression

LTP = long term potentiation

M = mushroom-shaped spine

MEC = medial entorhinal cortex

med = medial

ml = molecular layer

MML = middle molecular layer

n.s. = not significant

NAc = Nucleus accumbens

OML = outer molecular layer

pA = polyadenylation sequence

PBS = phosphate buffered saline

pcl = pyramidal cell layer

PCP 4 = purkinie-cell-protein 4

pl = polymorphic cell layer

PFA = paraformaldehyde

pc = pyramidal neuron / pyramidal cell

PNN = perineural nets

PP = perforant path

PSD = postsynaptic density

PVN = periventricular nucleus

RGS 14 = regulator of G-protein signaling 14

RT = room temperature

S = stubby-shaped spine

SA = Spine apparatus

SEM = standard error of the mean

sER = smooth endoplasmatic reticulum

slm = stratum lacunosum-moleculare

sLTP = structural long term potentiation

SP = Synaptopodin (the brain-specific isoform, if not stated otherwise)

SP+ = Synaptopodin-positive, i.e. containing Synaptopodin

SP– = Synaptopodin-negative, i.e. not containing Synaptopodin

SP-KO = SP-deficient mice

sr = stratum radiatum

STED = Stimulated emission depletion (STED) microscopy

SUM = supramammillary nucleus

T = thin-shaped spine

TBS = Tris-buffered saline

UTR = untranslated region

vCA1 = ventral CA1

WT = wild-type animals

7 References

1. Scoville WB, Millner B. Loss of recent memory after bilateral hippocampal lesions. *J Neurol Neurosurg Psychiatry*. 1957;20(1):11-21. doi:10.1136/jnnp.20.1.11.

2. van Strien NM, Cappaert NLM, Witter MP. The anatomy of memory: an interactive overview of the parahippocampal-hippocampal network. *Nat Rev Neurosci*. 2009;10(4):272-282. doi:10.1038/nrn2614.

3. Bird CM, Burgess N. The hippocampus and memory: insights from spatial processing. *Nat Rev Neurosci*. 2008;9(3):182-194. doi:10.1038/nrn2335.

4. Andersen P, Morris RGM, Amaral DG, Bliss T, O'Keefe J, eds. *The Hippocampus book*. Oxford, NewYork, Auckland, Cape Town, Dar es Salaam, Hong Kong, Karachi: Oxford University Press; 2007. http://www.loc.gov/catdir/enhancements/fy0725/2006007088-d.html.

5. Amaral DG, Scharfman HE, Lavenex P. The dentate gyrus: fundamental neuroanatomical organization (dentate gyrus for dummies). *Prog Brain Res*. 2007;163:3-22. doi:10.1016/S0079-6123(07)63001-5.

6. Beining M, Jungenitz T, Radic T, et al. Adult-born dentate granule cells show a critical period of dendritic reorganization and are distinct from developmentally born cells. *Brain Struct Funct*. 2017;222(3):1427-1446. doi:10.1007/s00429-016-1285-y.

7. Claiborne BJ, Amaral DG, Cowan WM. Quantitative, three-dimensional analysis of granule cell dendrites in the rat dentate gyrus. *J Comp Neurol*. 1990;302(2):206-219. doi:10.1002/cne.903020203.

8. Scharfman HE. The enigmatic mossy cell of the dentate gyrus. *Nat Rev Neurosci*. 2016;17(9):562-575. doi:10.1038/nrn.2016.87.

9. Jungenitz T, Beining M, Radic T, et al. Structural homo- and heterosynaptic plasticity in mature and adult newborn rat hippocampal granule cells. *Proc Natl Acad Sci U S A*. 2018;115(20):E4670-E4679. doi:10.1073/pnas.1801889115.

10. Lorente De Nó R. Studies on the structure of the cerebral cortex. II. Continuation of the study of the ammonic system. *Journal für Psychologie und Neurologie*. 1934;(46):113-177.

11. Chicurel ME, Harris KM. Three-dimensional analysis of the structure and composition of CA3 branched dendritic spines and their synaptic relationships

with mossy fiber boutons in the rat hippocampus. *J Comp Neurol*. 1992;325(2):169-182. doi:10.1002/cne.903250204.

12. Rollenhagen A, Sätzler K, Rodríguez EP, Jonas P, Frotscher M, Lübke JHR. Structural determinants of transmission at large hippocampal mossy fiber synapses. *J Neurosci*. 2007;27(39):10434-10444. doi:10.1523/JNEUROSCI.1946-07.2007.

13. Amaral DG, Witter MP. The three-dimensional organization of the hippocampal formation: a review of anatomical data. *Neuroscience*. 1989;31(3):571-591. doi:10.1016/0306-4522(89)90424-7.

14. Ishizuka N, Cowan WM, Amaral DG. A quantitative analysis of the dendritic organization of pyramidal cells in the rat hippocampus. *J Comp Neurol*. 1995;362(1):17-45. doi:10.1002/cne.903620103.

15. Ramon y Cajal S. Estructura de los centros nerviosos de las aves. *Rev. Trim. Histol. Norm. Pat.* 1888;(1):1-10.

16. Yuste R. *Dendritic spines*. Cambridge, Mass.: MIT Press; 2010.

17. Jedlicka P, Deller T. Understanding the role of synaptopodin and the spine apparatus in Hebbian synaptic plasticity - New perspectives and the need for computational modeling. *Neurobiol Learn Mem*. 2017;138:21-30. doi:10.1016/j.nlm.2016.07.023.

18. Segal M. Dendritic spines: Morphological building blocks of memory. *Neurobiol Learn Mem*. 2017;138:3-9. doi:10.1016/j.nlm.2016.06.007.

19. Pchitskaya E, Bezprozvanny I. Dendritic Spines Shape Analysis-Classification or Clusterization? Perspective. *Front Synaptic Neurosci*. 2020;12:31. doi:10.3389/fnsyn.2020.00031.

20. Berry KP, Nedivi E. Spine Dynamics: Are They All the Same? *Neuron*. 2017;96(1):43-55. doi:10.1016/j.neuron.2017.08.008.

21. Bosch M, Castro J, Saneyoshi T, Matsuno H, Sur M, Hayashi Y. Structural and molecular remodeling of dendritic spine substructures during long-term potentiation. *Neuron*. 2014;82(2):444-459. doi:10.1016/j.neuron.2014.03.021.

22. Yap K, Drakew A, Smilovic D, et al. The actin-modulating protein synaptopodin mediates long-term survival of dendritic spines. *Elife*. 2020;9. doi:10.7554/eLife.62944.

23. Maiti P, Manna J, Ilavazhagan G, Rossignol J, Dunbar GL. Molecular regulation of dendritic spine dynamics and their potential impact on synaptic

plasticity and neurological diseases. *Neurosci Biobehav Rev*. 2015;59:208-237. doi:10.1016/j.neubiorev.2015.09.020.

24. Holtmaat A, Svoboda K. Experience-dependent structural synaptic plasticity in the mammalian brain. *Nat Rev Neurosci*. 2009;10(9):647-658. doi:10.1038/nrn2699.

25. Yuste R, Bonhoeffer T. Genesis of dendritic spines: insights from ultrastructural and imaging studies. *Nat Rev Neurosci*. 2004;5(1):24-34. doi:10.1038/nrn1300.

26. Peters A, Kaiserman-Abramof IR. The small pyramidal neuron of the rat cerebral cortex. The perikaryon, dendrites and spines. *The American Journal of Anatomy*. 1970;127(4):321-355. doi:10.1002/aja.1001270402.

27. Harris KM, Jensen FE, Tsao B. Three-dimensional structure of dendritic spines and synapses in rat hippocampus (CA1) at postnatal day 15 and adult ages: implications for the maturation of synaptic physiology and long-term potentiation [published erratum appears in J Neurosci 1992 Aug;12(8):following table of contents]. *J Neurosci*. 1992;12(7):2685-2705. doi:10.1523/jneurosci.12-07-02685.1992.

28. Bourne J, Harris KM. Do thin spines learn to be mushroom spines that remember? *Curr Opin Neurobiol*. 2007;17(3):381-386. doi:10.1016/j.conb.2007.04.009.

29. Yoshihara Y, Roo M de, Muller D. Dendritic spine formation and stabilization. *Curr Opin Neurobiol*. 2009;19(2):146-153. doi:10.1016/j.conb.2009.05.013.

30. Hayashi Y, Majewska AK. Dendritic spine geometry: functional implication and regulation. *Neuron*. 2005;46(4):529-532. doi:10.1016/j.neuron.2005.05.006.

31. Arellano JI, Benavides-Piccione R, DeFelipe J, Yuste R. Ultrastructure of dendritic spines: correlation between synaptic and spine morphologies. *Front Neurosci*. 2007;1(1):131-143. doi:10.3389/neuro.01.1.1.010.2007.

32. Hering H, Sheng M. Dendritic spines: structure, dynamics and regulation. *Nat Rev Neurosci*. 2001;2(12):880-888. doi:10.1038/35104061.

33. Tønnesen J, Katona G, Rózsa B, Nägerl UV. Spine neck plasticity regulates compartmentalization of synapses. *Nat Neurosci*. 2014;17(5):678-685. doi:10.1038/nn.3682.

34. Holtmaat A, Bonhoeffer T, Chow DK, et al. Long-term, high-resolution imaging in the mouse neocortex through a chronic cranial window. *Nat Protoc*. 2009;4(8):1128-1144. doi:10.1038/nprot.2009.89.

35. Schätzle P, Esteves da Silva M, Tas RP, et al. Activity-Dependent Actin Remodeling at the Base of Dendritic Spines Promotes Microtubule Entry. *Curr Biol*. 2018;28(13):2081-2093.e6. doi:10.1016/j.cub.2018.05.004.

36. Gray E. G. Electron Microscopy of Synaptic Contacts on Dendrite Spines of the Cerebral Cortex. *Nature*. 1959;(183):1592-1593.

37. Kharazia VN, Weinberg RJ. Immunogold localization of AMPA and NMDA receptors in somatic sensory cortex of albino rat. *J Comp Neurol*. 1999;412(2):292-302. doi:10.1002/(sici)1096-9861(19990920)412:2<292:aid-cne8>3.0.co;2-g.

38. Noguchi J, Nagaoka A, Watanabe S, et al. In vivo two-photon uncaging of glutamate revealing the structure-function relationships of dendritic spines in the neocortex of adult mice. *J Physiol (Lond)*. 2011;589(Pt 10):2447-2457. doi:10.1113/jphysiol.2011.207100.

39. Spacek J, Harris KM. Three-Dimensional Organization of Smooth Endoplasmic Reticulum in Hippocampal CA1 Dendrites and Dendritic Spines of the Immature and Mature Rat. *J Neurosci*. 1997;17(1):190-203. doi:10.1523/JNEUROSCI.17-01-00190.1997.

40. Holbro N, Grunditz A, Oertner TG. Differential distribution of endoplasmic reticulum controls metabotropic signaling and plasticity at hippocampal synapses. *Proc Natl Acad Sci U S A*. 2009;106(35):15055-15060. doi:10.1073/pnas.0905110106.

41. Strehl A, Lenz M, Itsekson-Hayosh Z, et al. Systemic inflammation is associated with a reduction in Synaptopodin expression in the mouse hippocampus. *Exp Neurol*. 2014;261:230-235. doi:10.1016/j.expneurol.2014.04.033.

42. Lenz M, Eichler A, Kruse P, et al. All-trans retinoic acid induces synaptopodin-dependent metaplasticity in mouse dentate granule cells. *Elife*. 2021;10. doi:10.7554/eLife.71983.

43. Tsuboi M, Hirabayashi Y. New insights into the regulation of synaptic transmission and plasticity by the endoplasmic reticulum and its membrane

contacts. *Proc Jpn Acad Ser B Phys Biol Sci*. 2021;97(10):559-572. doi:10.2183/pjab.97.028.

44. Berridge MJ. Neuronal calcium signaling. *Neuron*. 1998;21(1):13-26. doi:10.1016/s0896-6273(00)80510-3.

45. Basnayake K, Mazaud D, Kushnireva L, et al. Nanoscale molecular architecture controls calcium diffusion and ER replenishment in dendritic spines. *Sci Adv*. 2021;7(38). doi:10.1126/sciadv.abh1376.

46. Pierce JP, van Leyen K, McCarthy JB. Translocation machinery for synthesis of integral membrane and secretory proteins in dendritic spines. *Nat Neurosci*. 2000;3(4):311-313. doi:10.1038/73868.

47. Vlachos A, Korkotian E, Schonfeld E, Copanaki E, Deller T, Segal M. Synaptopodin regulates plasticity of dendritic spines in hippocampal neurons. *J Neurosci*. 2009;29(4):1017-1033. doi:10.1523/JNEUROSCI.5528-08.2009.

48. Cui-Wang T, Hanus C, Cui T, et al. Local zones of endoplasmic reticulum complexity confine cargo in neuronal dendrites. *Cell*. 2012;148(1-2):309-321. doi:10.1016/j.cell.2011.11.056.

49. Bosch M, Hayashi Y. Structural plasticity of dendritic spines. *Curr Opin Neurobiol*. 2012;22(3):383-388. doi:10.1016/j.conb.2011.09.002.

50. Kasai H, Matsuzaki M, Noguchi J, Yasumatsu N, Nakahara H. Structure-stability-function relationships of dendritic spines. *Trends Neurosci*. 2003;26(7):360-368. doi:10.1016/S0166-2236(03)00162-0.

51. Mundel P, Heid HW, Mundel TM, Krüger M, Reiser J, Kriz W. Synaptopodin: an actin-associated protein in telencephalic dendrites and renal podocytes. *J Cell Biol*. 1997;139(1):193-204. doi:10.1083/jcb.139.1.193.

52. Asanuma K, Kim K, Oh J, et al. Synaptopodin regulates the actin-bundling activity of alpha-actinin in an isoform-specific manner. *J Clin Invest*. 2005;115(5):1188-1198. doi:10.1172/JCI23371.

53. Deller T, Mundel P, Frotscher M. Potential role of synaptopodin in spine motility by coupling actin to the spine apparatus. *Hippocampus*. 2000;10(5):569-581. doi:10.1002/1098-1063(2000)10:5<569:AID-HIPO7>3.0.CO;2-M.

54. Czarnecki K, Haas CA, Bas Orth C, Deller T, Frotscher M. Postnatal development of synaptopodin expression in the rodent hippocampus. *J Comp Neurol*. 2005;490(2):133-144. doi:10.1002/cne.20651.

55. Sidhu VK, Huang BX, Desai A, Kevala K, Kim H-Y. Role of DHA in aging-related changes in mouse brain synaptic plasma membrane proteome. *Neurobiol Aging*. 2016;41:73-85. doi:10.1016/j.neurobiolaging.2016.02.007.

56. Deller T, Merten T, Roth SU, Mundel P, Frotscher M. Actin-associated protein synaptopodin in the rat hippocampal formation: Localization in the spine neck and close association with the spine apparatus of principal neurons. *J Comp Neurol*. 2000;418(2):164-181. doi:10.1002/(SICI)1096-9861(20000306)418:2<164:AID-CNE4>3.0.CO;2-0.

57. Deller T, Bas Orth C, Vlachos A, et al. Plasticity of synaptopodin and the spine apparatus organelle in the rat fascia dentata following entorhinal cortex lesion. *J Comp Neurol*. 2006;499(3):471-484. doi:10.1002/cne.21103.

58. Bas Orth C, Vlachos A, Del Turco D, et al. Lamina-specific distribution of Synaptopodin, an actin-associated molecule essential for the spine apparatus, in identified principal cell dendrites of the mouse hippocampus. *J Comp Neurol*. 2005;487(3):227-239. doi:10.1002/cne.20539.

59. Fukazawa Y, Saitoh Y, Ozawa F, Ohta Y, Mizuno K, Inokuchi K. Hippocampal LTP Is Accompanied by Enhanced F-Actin Content within the Dendritic Spine that Is Essential for Late LTP Maintenance In Vivo. *Neuron*. 2003;38(3):447-460. doi:10.1016/S0896-6273(03)00206-X.

60. Deller T, Korte M, Chabanis S, et al. Synaptopodin-deficient mice lack a spine apparatus and show deficits in synaptic plasticity. *Proc Natl Acad Sci U S A*. 2003:10494-10499. doi:10.1073/pnas.1832384100.

61. Vlachos A, Ikenberg B, Lenz M, et al. Synaptopodin regulates denervation-induced homeostatic synaptic plasticity: Supporting Information. *Proc Natl Acad Sci U S A*. 2013:8242-8247. doi:10.1073/pnas.1213677110.

62. Schlüter A, Del Turco D, Deller T, Gutzmann A, Schultz C, Engelhardt M. Structural Plasticity of Synaptopodin in the Axon Initial Segment during Visual Cortex Development. *Cereb Cortex*. 2017;27(9):4662-4675. doi:10.1093/cercor/bhx208.

63. Sánchez-Ponce D, Blázquez-Llorca L, DeFelipe J, Garrido JJ, Muñoz A. Colocalization of α-actinin and synaptopodin in the pyramidal cell axon initial segment. *Cereb Cortex*. 2012;22(7):1648-1661. doi:10.1093/cercor/bhr251.

64. Sánchez-Ponce D, DeFelipe J, Garrido JJ, Muñoz A. In vitro maturation of the cisternal organelle in the hippocampal neuron's axon initial segment. *Mol Cell Neurosci*. 2011;48(1):104-116. doi:10.1016/j.mcn.2011.06.010.

65. Bas Orth C, Schultz C, Müller CM, Frotscher M, Deller T. Loss of the cisternal organelle in the axon initial segment of cortical neurons in synaptopodin-deficient mice. *J Comp Neurol*. 2007;504(5):441-449. doi:10.1002/cne.21445.

66. Palay SL, Sotelo C, Peters A, Orkand PM. The axon hillock and the initial segment. *J Cell Biol*. 1968;38(1):193-201. doi:10.1083/jcb.38.1.193.

67. Jungenitz T, Bird A, Engelhardt M, Jedlicka P, Schwarzacher SW, Deller T. Structural plasticity of the axon initial segment in rat hippocampal granule cells following high frequency stimulation and LTP induction. *Front Neuroanat*. 2023;17:1125623. doi:10.3389/fnana.2023.1125623.

68. Paul MH, Choi M, Schlaudraff J, Deller T, Del Turco D. Granule Cell Ensembles in Mouse Dentate Gyrus Rapidly Upregulate the Plasticity-Related Protein Synaptopodin after Exploration Behavior. *Cereb Cortex*. 2020;30(4):2185-2198. doi:10.1093/cercor/bhz231.

69. Falahati H, Wu Y, Feuerer V, Simon H-G, Camilli P de. Proximity proteomics of synaptopodin provides insight into the molecular composition of the spine apparatus of dendritic spines. *Proc Natl Acad Sci U S A*. 2022;119(42):e2203750119. doi:10.1073/pnas.2203750119.

70. Chirillo M, Bourne J, Lindsey L, Harris K. Complexity of dendritic SER increases at enlarging synapses during LTP. *bioRxiv*. 2015. doi:10.1101/015974.

71. Deller T, Haas CA, Deissenrieder K, et al. Laminar distribution of synaptopodin in normal and reeler mouse brain depends on the position of spine-bearing neurons. *J Comp Neurol*. 2002;453(1):33-44. doi:10.1002/cne.10362.

72. Jedlicka P, Schwarzacher SW, Winkels R, et al. Impairment of in vivo theta-burst long-term potentiation and network excitability in the dentate gyrus of synaptopodin-deficient mice lacking the spine apparatus and the cisternal organelle. *Hippocampus*. 2009;19(2):130-140. doi:10.1002/hipo.20489.

73. Zhang X, Pöschel B, Faul C, Upreti C, Stanton PK, Mundel P. Essential role for synaptopodin in dendritic spine plasticity of the developing hippocampus.

J Neurosci. 2013;33(30):12510-12518. doi:10.1523/JNEUROSCI.2983-12.2013.

74. Korkotian E, Frotscher M, Segal M. Synaptopodin regulates spine plasticity: mediation by calcium stores. *J Neurosci*. 2014;34(35):11641-11651. doi:10.1523/JNEUROSCI.0381-14.2014.

75. Okubo-Suzuki R, Okada D, Sekiguchi M, Inokuchi K. Synaptopodin maintains the neural activity-dependent enlargement of dendritic spines in hippocampal neurons. *Mol Cell Neurosci*. 2008;38(2):266-276. doi:10.1016/j.mcn.2008.03.001.

76. Asanuma K, Yanagida-Asanuma E, Faul C, Tomino Y, Kim K, Mundel P. Synaptopodin orchestrates actin organization and cell motility via regulation of RhoA signalling. *Nat Cell Biol*. 2006;8(5):485-491. doi:10.1038/ncb1400.

77. Faul C, Asanuma K, Yanagida-Asanuma E, Kim K, Mundel P. Actin up: regulation of podocyte structure and function by components of the actin cytoskeleton. *Trends Cell Biol*. 2007;17(9):428-437. doi:10.1016/j.tcb.2007.06.006.

78. Konietzny A, González-Gallego J, Bär J, et al. Myosin V regulates synaptopodin clustering and localization in the dendrites of hippocampal neurons. *J Cell Sci*. 2019;132(16). doi:10.1242/jcs.230177.

79. Yanagida-Asanuma E, Asanuma K, Kim K, et al. Synaptopodin protects against proteinuria by disrupting Cdc42:IRSp53:Mena signaling complexes in kidney podocytes. *The American Journal of Pathology*. 2007;171(2):415-427. doi:10.2353/ajpath.2007.070075.

80. Bramham CR. Local protein synthesis, actin dynamics, and LTP consolidation. *Curr Opin Neurobiol*. 2008;18(5):524-531. doi:10.1016/j.conb.2008.09.013.

81. Colgan LA, Yasuda R. Plasticity of dendritic spines: subcompartmentalization of signaling. *Annu Rev Physiol*. 2014;76:365-385. doi:10.1146/annurev-physiol-021113-170400.

82. Spence EF, Soderling SH. Actin Out: Regulation of the Synaptic Cytoskeleton. *J Biol Chem*. 2015;290(48):28613-28622. doi:10.1074/jbc.R115.655118.

83. Wang L, Dumoulin A, Renner M, Triller A, Specht CG. The Role of Synaptopodin in Membrane Protein Diffusion in the Dendritic Spine Neck. *PLoS ONE*. 2016;11(2):e0148310. doi:10.1371/journal.pone.0148310.

84. Vlachos A. Synaptopodin and the spine apparatus organelle-regulators of different forms of synaptic plasticity? *Ann Anat*. 2012;194(4):317-320. doi:10.1016/j.aanat.2011.10.014.

85. Kasai H, Fukuda M, Watanabe S, Hayashi-Takagi A, Noguchi J. Structural dynamics of dendritic spines in memory and cognition. *Trends Neurosci*. 2010;33(3):121-129. doi:10.1016/j.tins.2010.01.001.

86. Yamazaki M, Matsuo R, Fukazawa Y, Ozawa F, Inokuchi K. Regulated expression of an actin-associated protein, synaptopodin, during long-term potentiation. *J Neurochem*. 2001;79(1):192-199. doi:10.1046/j.1471-4159.2001.00552.x.

87. Ramirez-Amaya V, Angulo-Perkins A, Chawla MK, Barnes CA, Rosi S. Sustained transcription of the immediate early gene Arc in the dentate gyrus after spatial exploration. *J Neurosci*. 2013;33(4):1631-1639. doi:10.1523/JNEUROSCI.2916-12.2013.

88. Cole AJ, Saffen DW, Baraban JM, Worley PF. Rapid increase of an immediate early gene messenger RNA in hippocampal neurons by synaptic NMDA receptor activation. *Nature*. 1989;340(6233):474-476. doi:10.1038/340474a0.

89. Dudek SM, Alexander GM, Farris S. Rediscovering area CA2: unique properties and functions. *Nat Rev Neurosci*. 2016;17(2):89-102. doi:10.1038/nrn.2015.22.

90. Shinohara Y, Hosoya A, Yahagi K, et al. Hippocampal CA3 and CA2 have distinct bilateral innervation patterns to CA1 in rodents. *Eur J Neurosci*. 2012;35(5):702-710. doi:10.1111/j.1460-9568.2012.07993.x.

91. Lein ES, Callaway EM, Albright TD, Gage FH. Redefining the boundaries of the hippocampal CA2 subfield in the mouse using gene expression and 3-dimensional reconstruction. *J Comp Neurol*. 2005;485(1):1-10. doi:10.1002/cne.20426.

92. Kohara K, Pignatelli M, Rivest AJ, et al. Cell type-specific genetic and optogenetic tools reveal hippocampal CA2 circuits. *Nat Neurosci*. 2014;17(2):269-279. doi:10.1038/nn.3614.

93. San Antonio A, Liban K, Ikrar T, Tsyganovskiy E, Xu X. Distinct physiological and developmental properties of hippocampal CA2 subfield revealed by using anti-Purkinje cell protein 4 (PCP4) immunostaining. *J Comp Neurol*. 2014;522(6):1333-1354. doi:10.1002/cne.23486.

94. Chevaleyre V, Piskorowski RA. Hippocampal Area CA2: An Overlooked but Promising Therapeutic Target. *Trends Mol Med*. 2016;22(8):645-655. doi:10.1016/j.molmed.2016.06.007.

95. Ishizuka N, Weber J, Amaral DG. Organization of intrahippocampal projections originating from CA3 pyramidal cells in the rat. *J Comp Neurol*. 1990;295(4):580-623. doi:10.1002/cne.902950407.

96. Zhao M, Choi Y-S, Obrietan K, Dudek SM. Synaptic plasticity (and the lack thereof) in hippocampal CA2 neurons. *J Neurosci*. 2007;27(44):12025-12032. doi:10.1523/JNEUROSCI.4094-07.2007.

97. Dang R, Zhou Y, Zhang Y, et al. Regulation of Social Memory by Lateral Entorhinal Cortical Projection to Dorsal Hippocampal CA2. *Neurosci Bull*. 2022;38(3):318-322. doi:10.1007/s12264-021-00813-6.

98. Bartesaghi R, Gessi T. Parallel activation of field CA2 and dentate gyrus by synaptically elicited perforant path volleys. *Hippocampus*. 2004;14(8):948-963. doi:10.1002/hipo.20011.

99. Vertes RP. Major diencephalic inputs to the hippocampus: supramammillary nucleus and nucleus reuniens. Circuitry and function. *Prog Brain Res*. 2015;219:121-144. doi:10.1016/bs.pbr.2015.03.008.

100. Benoy A, Dasgupta A, Sajikumar S. Hippocampal area CA2: an emerging modulatory gateway in the hippocampal circuit. *Exp Brain Res*. 2018;236(4):919-931. doi:10.1007/s00221-018-5187-5.

101. Smith AS, Williams Avram SK, Cymerblit-Sabba A, Song J, Young WS. Targeted activation of the hippocampal CA2 area strongly enhances social memory. *Mol Psychiatry*. 2016;21(8):1137-1144. doi:10.1038/mp.2015.189.

102. Carstens KE, Dudek SM. Regulation of synaptic plasticity in hippocampal area CA2. *Curr Opin Neurobiol*. 2019;54:194-199. doi:10.1016/j.conb.2018.07.008.

103. Caruana DA, Alexander GM, Dudek SM. New insights into the regulation of synaptic plasticity from an unexpected place: hippocampal area CA2. *Learn Mem*. 2012;19(9):391-400. doi:10.1101/lm.025304.111.

104. Robert V, Cassim S, Chevaleyre V, Piskorowski RA. Hippocampal area CA2: properties and contribution to hippocampal function. *Cell Tissue Res*. 2018;373(3):525-540. doi:10.1007/s00441-017-2769-7.

105. Simons SB, Escobedo Y, Yasuda R, Dudek SM. Regional differences in hippocampal calcium handling provide a cellular mechanism for limiting plasticity. *Proc Natl Acad Sci U S A*. 2009;106(33):14080-14084. doi:10.1073/pnas.0904775106.

106. Evans PR, Parra-Bueno P, Smirnov MS, et al. RGS14 Restricts Plasticity in Hippocampal CA2 by Limiting Postsynaptic Calcium Signaling. *eNeuro*. 2018;5(3). doi:10.1523/ENEURO.0353-17.2018.

107. Carstens KE, Phillips ML, Pozzo-Miller L, Weinberg RJ, Dudek SM. Perineuronal Nets Suppress Plasticity of Excitatory Synapses on CA2 Pyramidal Neurons. *J Neurosci*. 2016;36(23):6312-6320. doi:10.1523/JNEUROSCI.0245-16.2016.

108. Domínguez S, Rey CC, Therreau L, et al. Maturation of PNN and ErbB4 Signaling in Area CA2 during Adolescence Underlies the Emergence of PV Interneuron Plasticity and Social Memory. *Cell Rep*. 2019;29(5):1099-1112.e4. doi:10.1016/j.celrep.2019.09.044.

109. Chevaleyre V, Siegelbaum SA. Strong CA2 pyramidal neuron synapses define a powerful disynaptic cortico-hippocampal loop. *Neuron*. 2010;66(4):560-572. doi:10.1016/j.neuron.2010.04.013.

110. Hitti FL, Siegelbaum SA. The hippocampal CA2 region is essential for social memory. *Nature*. 2014;508(7494):88-92. doi:10.1038/nature13028.

111. Karlsson SA, Haziri K, Hansson E, Kettunen P, Westberg L. Effects of sex and gonadectomy on social investigation and social recognition in mice. *BMC Neurosci*. 2015;16:83. doi:10.1186/s12868-015-0221-z.

112. Meira T, Leroy F, Buss EW, Oliva A, Park J, Siegelbaum SA. A hippocampal circuit linking dorsal CA2 to ventral CA1 critical for social memory dynamics. *Nat Commun*. 2018;9(1):4163. doi:10.1038/s41467-018-06501-w.

113. Okuyama T, Kitamura T, Roy DS, Itohara S, Tonegawa S. Ventral CA1 neurons store social memory. *Science*. 2016;353(6307):1536-1541. doi:10.1126/science.aaf7003.

114. Lehr AB, Kumar A, Tetzlaff C, Hafting T, Fyhn M, Stöber TM. CA2 beyond social memory: Evidence for a fundamental role in hippocampal information processing. *Neurosci Biobehav Rev*. 2021;126:398-412. doi:10.1016/j.neubiorev.2021.03.020.

115. Middleton SJ, McHugh TJ. CA2: A Highly Connected Intrahippocampal Relay. *Annu Rev Neurosci*. 2020;43:55-72. doi:10.1146/annurev-neuro-080719-100343.

116. Boehringer R, Polygalov D, Huang AJY, et al. Chronic Loss of CA2 Transmission Leads to Hippocampal Hyperexcitability. *Neuron*. 2017;94(3):642-655.e9. doi:10.1016/j.neuron.2017.04.014.

117. DeVito LM, Konigsberg R, Lykken C, Sauvage M, Young WS, Eichenbaum H. Vasopressin 1b receptor knock-out impairs memory for temporal order. *J Neurosci*. 2009;29(9):2676-2683. doi:10.1523/JNEUROSCI.5488-08.2009.

118. MacDonald CJ, Tonegawa S. Crucial role for CA2 inputs in the sequential organization of CA1 time cells supporting memory. *Proc Natl Acad Sci U S A*. 2021;118(3). doi:10.1073/pnas.2020698118.

119. Watarai A, Tao K, Wang M-Y, Okuyama T. Distinct functions of ventral CA1 and dorsal CA2 in social memory. *Curr Opin Neurobiol*. 2021;68:29-35. doi:10.1016/j.conb.2020.12.008.

120. Arszovszki A, Borhegyi Z, Klausberger T. Three axonal projection routes of individual pyramidal cells in the ventral CA1 hippocampus. *Front Neuroanat*. 2014;8:53. doi:10.3389/fnana.2014.00053.

121. Wang Q, Ding S-L, Li Y, et al. The Allen Mouse Brain Common Coordinate Framework: A 3D Reference Atlas. *Cell*. 2020;181(4):936-953.e20. doi:10.1016/j.cell.2020.04.007.

122. Alexander GM, Riddick NV, McCann KE, Lustberg D, Moy SS, Dudek SM. Modulation of CA2 neuronal activity increases behavioral responses to fear conditioning in female mice. *Neurobiol Learn Mem*. 2019;163:107044. doi:10.1016/j.nlm.2019.107044.

123. Bartesaghi R, Ravasi L. Pyramidal neuron types in field CA2 of the guinea pig. *Brain Research Bulletin*. 1999;50(4):263-273. doi:10.1016/S0361-9230(99)00198-7.

124. Gemmati D, Varani K, Bramanti B, et al. "Bridging the Gap" Everything that Could Have Been Avoided If We Had Applied Gender Medicine, Pharmacogenetics and Personalized Medicine in the Gender-Omics and Sex-Omics Era. *Int J Mol Sci*. 2019;21(1). doi:10.3390/ijms21010296.

125. McCarthy MM. Incorporating Sex as a Variable in Preclinical Neuropsychiatric Research. *Schizophr Bull*. 2015;41(5):1016-1020. doi:10.1093/schbul/sbv077.

126. May T, Adesina I, McGillivray J, Rinehart NJ. Sex differences in neurodevelopmental disorders. *Curr Opin Neurol*. 2019;32(4):622-626. doi:10.1097/WCO.0000000000000714.

127. Bushnell CD, Chaturvedi S, Gage KR, et al. Sex differences in stroke: Challenges and opportunities. *J Cereb Blood Flow Metab*. 2018;38(12):2179-2191. doi:10.1177/0271678X18793324.

128. Regitz-Zagrosek V, Kararigas G. Mechanistic Pathways of Sex Differences in Cardiovascular Disease. *Physiol Rev*. 2017;97(1):1-37. doi:10.1152/physrev.00021.2015.

129. Woolley CS, Gould E, Frankfurt M, McEwen BS. Naturally occurring fluctuation in dendritic spine density on adult hippocampal pyramidal neurons. *J Neurosci*. 1990;10(12):4035-4039.

130. Choleris E, Galea LAM, Sohrabji F, Frick KM. Sex differences in the brain: Implications for behavioral and biomedical research. *Neurosci Biobehav Rev*. 2018;85:126-145. doi:10.1016/j.neubiorev.2017.07.005.

131. Sheppard PAS, Choleris E, Galea LAM. Structural plasticity of the hippocampus in response to estrogens in female rodents. *Mol Brain*. 2019;12(1):22. doi:10.1186/s13041-019-0442-7.

132. Finney CA, Shvetcov A, Westbrook RF, Jones NM, Morris MJ. The role of hippocampal estradiol in synaptic plasticity and memory: A systematic review. *Front Neuroendocrinol*. 2020;56:100818. doi:10.1016/j.yfrne.2019.100818.

133. Hojo Y, Kawato S. Neurosteroids in Adult Hippocampus of Male and Female Rodents: Biosynthesis and Actions of Sex Steroids. *Front Endocrinol (Lausanne)*. 2018;9:183. doi:10.3389/fendo.2018.00183.

134. Fester L, Rune GM. Sex neurosteroids: Hormones made by the brain for the brain. *Neurosci Lett*. 2021;753:135849. doi:10.1016/j.neulet.2021.135849.

135. Banks WA. Brain meets body: the blood-brain barrier as an endocrine interface. *Endocrinology*. 2012;153(9):4111-4119. doi:10.1210/en.2012-1435.

136. Zhou L, Fester L, Blittersdorff B von, et al. Aromatase inhibitors induce spine synapse loss in the hippocampus of ovariectomized mice. *Endocrinology*. 2010;151(3):1153-1160. doi:10.1210/en.2009-0254.

137. Alexander BH, Barnes HM, Trimmer E, et al. Stable Density and Dynamics of Dendritic Spines of Cortical Neurons Across the Estrous Cycle While Expressing Differential Levels of Sensory-Evoked Plasticity. *Front Mol Neurosci*. 2018;11:83. doi:10.3389/fnmol.2018.00083.

138. van Eijk L, Hansell NK, Strike LT, et al. Region-specific sex differences in the hippocampus. *Neuroimage*. 2020;215:116781. doi:10.1016/j.neuroimage.2020.116781.

139. Yagi S, Galea LAM. Sex differences in hippocampal cognition and neurogenesis. *Neuropsychopharmacology*. 2019;44(1):200-213. doi:10.1038/s41386-018-0208-4.

140. Brandt N, Löffler T, Fester L, Rune GM. Sex-specific features of spine densities in the hippocampus. *Sci Rep*. 2020:11405. doi:10.1038/s41598-020-68371-x.

141. Sorra KE, Harris KM. Overview on the structure, composition, function, development, and plasticity of hippocampal dendritic spines. *Hippocampus*. 2000;10(5):501-511. doi:10.1002/1098-1063(2000)10:5<501:AID-HIPO1>3.0.CO;2-T.

142. Prendergast BJ, Onishi KG, Zucker I. Female mice liberated for inclusion in neuroscience and biomedical research. *Neurosci Biobehav Rev*. 2014;40:1-5. doi:10.1016/j.neubiorev.2014.01.001.

143. Becker JB, Prendergast BJ, Liang JW. Female rats are not more variable than male rats: a meta-analysis of neuroscience studies. *Biol Sex Differ*. 2016;7:34. doi:10.1186/s13293-016-0087-5.

144. Machida T, Yonezawa Y, Noumura T. Age-associated changes in plasma testosterone levels in male mice and their relation to social dominance or subordinance. *Horm Behav*. 1981;15(3):238-245. doi:10.1016/0018-506x(81)90013-1.

145. Shansky RM. Are hormones a "female problem" for animal research? *Science*. 2019;364(6443):825-826. doi:10.1126/science.aaw7570.

146. Allen E. The oestrous cycle in the mouse. *The American Journal of Anatomy*. 1922;(30):297-371.

147. Shaikh AA. Estrone and estradiol levels in the ovarian venous blood from rats during the estrous cycle and pregnancy. *Biol Reprod*. 1971;5(3):297-307. doi:10.1093/biolreprod/5.3.297.

148. Cora MC, Kooistra L, Travlos G. Vaginal Cytology of the Laboratory Rat and Mouse: Review and Criteria for the Staging of the Estrous Cycle Using Stained Vaginal Smears. *Toxicol Pathol*. 2015;43(6):776-793. doi:10.1177/0192623315570339.

149. Gururajan A, Reif A, Cryan JF, Slattery DA. The future of rodent models in depression research. *Nat Rev Neurosci*. 2019;20(11):686-701. doi:10.1038/s41583-019-0221-6.

150. Byers SL, Wiles MV, Dunn SL, Taft RA. Mouse Estrous Cycle Identification Tool and Images. *PLoS ONE*. 2012. doi:10.1371/journal.pone.0035538.g001.

151. Goldman JM, Murr AS, Cooper RL. The rodent estrous cycle: characterization of vaginal cytology and its utility in toxicological studies. *Birth Defects Res B Dev Reprod Toxicol*. 2007;80(2):84-97. doi:10.1002/bdrb.20106.

152. Hayashi Y. Molecular mechanism of hippocampal long-term potentiation - Towards multiscale understanding of learning and memory. *Neurosci Res*. 2022;175:3-15. doi:10.1016/j.neures.2021.08.001.

153. Brandt N, Vierk R, Fester L, et al. Sex-specific Difference of Hippocampal Synaptic Plasticity in Response to Sex Neurosteroids. *Cereb Cortex*. 2020;30(4):2627-2641. doi:10.1093/cercor/bhz265.

154. Vierk R, Glassmeier G, Zhou L, et al. Aromatase inhibition abolishes LTP generation in female but not in male mice. *J Neurosci*. 2012;32(24):8116-8126. doi:10.1523/JNEUROSCI.5319-11.2012.

155. Brandt N, Rune GM. Sex-dependency of oestrogen-induced structural synaptic plasticity: Inhibition of aromatase versus application of estradiol in rodents. *Eur J Neurosci*. 2020;52(1):2548-2559. doi:10.1111/ejn.14541.

156. Fester L, Zhou L, Voets C, et al. The opposing roles of estradiol on synaptic protein expression in hippocampal cultures. *Psychoneuroendocrinology*. 2009;34 Suppl 1:S123-9. doi:10.1016/j.psyneuen.2009.08.013.

157. Fester L, Labitzke J, Hinz R, et al. Estradiol responsiveness of synaptopodin in hippocampal neurons is mediated by estrogen receptor β. *J*

Steroid Biochem Mol Biol. 2013;138:455-461. doi:10.1016/j.jsbmb.2013.09.004.

158. Fester L, Zhou L, Ossig C, et al. Synaptopodin is regulated by aromatase activity. *J Neurochem*. 2017;140(1):126-139. doi:10.1111/jnc.13889.

159. Krueger-Burg D, Winkler D, Mitkovski M, et al. The SocioBox: A Novel Paradigm to Assess Complex Social Recognition in Male Mice. *Front Behav Neurosci*. 2016;10:151. doi:10.3389/fnbeh.2016.00151.

160. Chevaleyre V, Piskorowski R. Modulating excitation through plasticity at inhibitory synapses. *Front Cell Neurosci*. 2014;8:93. doi:10.3389/fncel.2014.00093.

161. Buhl EH, Lübke J. Intracellular lucifer yellow injection in fixed brain slices combined with retrograde tracing, light and electron microscopy. *Neuroscience*. 1989;28(1):3-16. doi:10.1016/0306-4522(89)90227-3.

162. Rietsche M, Hick M, Deller T. Intracellular Injection of Fluorescent Dyes: Visualization of Neuronal Morphologies in Mouse Mutants. Poster-presentation at the 4th Biennal Meeting of the rhine-main neuroscience network; 2016; Oberwesel.

163. Feng G, Mellor RH, Bernstein M, et al. Imaging Neuronal Subsets in Transgenic Mice Expressing Multiple Spectral Variants of GFP. *Neuron*. 2000;28(1):41-51. doi:10.1016/S0896-6273(00)00084-2.

164. Vuksic M, Del Turco D, Bas Orth C, et al. 3D-reconstruction and functional properties of GFP-positive and GFP-negative granule cells in the fascia dentata of the Thy1-GFP mouse. *Hippocampus*. 2008;18(4):364-375. doi:10.1002/hipo.20398.

165. Arends JJ, Jacquin MF. Lucifer yellow staining in fixed brain slices: Optimal methods and compatibility with somatotopic markers in neonatal brain. *Journal of Neuroscience Methods*. 1993;50(3):321-339. doi:10.1016/0165-0270(93)90039-t.

166. Tzakis N, Holahan MR. Social Memory and the Role of the Hippocampal CA2 Region. *Front Behav Neurosci*. 2019;13:233. doi:10.3389/fnbeh.2019.00233.

167. Hick M, Herrmann U, Weyer SW, et al. Acute function of secreted amyloid precursor protein fragment APPsα in synaptic plasticity. *Acta Neuropathol*. 2015;129(1):21-37. doi:10.1007/s00401-014-1368-x.

168. Kempermann G, Song H, Gage FH. Neurogenesis in the Adult Hippocampus. *Cold Spring Harb Perspect Biol*. 2015;7(9):a018812. doi:10.1101/cshperspect.a018812.

169. Christian KM, Ming G-L, Song H. Adult neurogenesis and the dentate gyrus: Predicting function from form. *Behav Brain Res*. 2020;379:112346. doi:10.1016/j.bbr.2019.112346.

170. Cui Z, Gerfen CR, Young WS. Hypothalamic and other connections with dorsal CA2 area of the mouse hippocampus. *J Comp Neurol*. 2013;521(8):1844-1866. doi:10.1002/cne.23263.

171. Young WS, Li J, Wersinger SR, Palkovits M. The vasopressin 1b receptor is prominent in the hippocampal area CA2 where it is unaffected by restraint stress or adrenalectomy. *Neuroscience*. 2006;143(4):1031-1039. doi:10.1016/j.neuroscience.2006.08.040.

172. Benavides-Piccione R, Fernaud-Espinosa I, Robles V, Yuste R, DeFelipe J. Age-based comparison of human dendritic spine structure using complete three-dimensional reconstructions. *Cereb Cortex*. 2013;23(8):1798-1810. doi:10.1093/cercor/bhs154.

173. Schindelin J, Arganda-Carreras I, Frise E, et al. Fiji: an open-source platform for biological-image analysis. *Nat Methods*. 2012;9(7):676-682. doi:10.1038/nmeth.2019.

174. Ruszczycki B, Szepesi Z, Wilczynski GM, et al. Sampling issues in quantitative analysis of dendritic spines morphology. *BMC Bioinformatics*. 2012;13:213. doi:10.1186/1471-2105-13-213.

175. Chidambaram SB, Rathipriya AG, Bolla SR, et al. Dendritic spines: Revisiting the physiological role. *Prog Neuropsychopharmacol Biol Psychiatry*. 2019;92:161-193. doi:10.1016/j.pnpbp.2019.01.005.

176. Deller T, Bas Orth C, Del Turco D, et al. A role for synaptopodin and the spine apparatus in hippocampal synaptic plasticity. *Ann Anat*. 2007;189(1):5-16. doi:10.1016/j.aanat.2006.06.013.

177. Honkura N, Matsuzaki M, Noguchi J, Ellis-Davies GCR, Kasai H. The subspine organization of actin fibers regulates the structure and plasticity of dendritic spines. *Neuron*. 2008;57(5):719-729. doi:10.1016/j.neuron.2008.01.013.

178. Yang Y, Liu J-J. Structural LTP: Signal transduction, actin cytoskeleton reorganization, and membrane remodeling of dendritic spines. *Curr Opin Neurobiol*. 2022;74:102534. doi:10.1016/j.conb.2022.102534.

179. Harris KM. Structural LTP: from synaptogenesis to regulated synapse enlargement and clustering. *Curr Opin Neurobiol*. 2020;63:189-197. doi:10.1016/j.conb.2020.04.009.

180. Smilovic D, Rietsche M, Drakew A, Vuksic M, Deller T. Constitutive tumor necrosis factor (TNF)-deficiency causes a reduction in spine density in mouse dentate granule cells accompanied by homeostatic adaptations of spine head size. *J Comp Neurol*. 2021. doi:10.1002/cne.25237.

181. Maggio N, Vlachos A. Synaptic plasticity at the interface of health and disease: New insights on the role of endoplasmic reticulum intracellular calcium stores. *Neuroscience*. 2014;281:135-146. doi:10.1016/j.neuroscience.2014.09.041.

182. Verbich D, Becker D, Vlachos A, Mundel P, Deller T, McKinney RA. Rewiring neuronal microcircuits of the brain via spine head protrusions--a role for synaptopodin and intracellular calcium stores. *Acta Neuropathol Commun*. 2016;4:38. doi:10.1186/s40478-016-0311-x.

183. Leroy F, Park J, Asok A, et al. A circuit from hippocampal CA2 to lateral septum disinhibits social aggression. *Nature*. 2018;564(7735):213-218. doi:10.1038/s41586-018-0772-0.

184. Frick KM, Kim J, Koss WA. Estradiol and hippocampal memory in female and male rodents. *Curr Opin Behav Sci*. 2018;23:65-74. doi:10.1016/j.cobeha.2018.03.011.

185. Chang PY, Taylor PE, Jackson MB. Voltage imaging reveals the CA1 region at the CA2 border as a focus for epileptiform discharges and long-term potentiation in hippocampal slices. *J Neurophysiol*. 2007;98(3):1309-1322. doi:10.1152/jn.00532.2007.

186. Luine V, Serrano P, Frankfurt M. Rapid effects on memory consolidation and spine morphology by estradiol in female and male rodents. *Horm Behav*. 2018;104:111-118. doi:10.1016/j.yhbeh.2018.04.007.

187. McEwen BS, Alves SE. Estrogen actions in the central nervous system. *Endocr Rev*. 1999;20(3):279-307. doi:10.1210/edrv.20.3.0365.

188.   Borovac J, Bosch M, Okamoto K. Regulation of actin dynamics during structural plasticity of dendritic spines: Signaling messengers and actin-binding proteins. *Mol Cell Neurosci*. 2018;91:122-130. doi:10.1016/j.mcn.2018.07.001.

189.   Stevenson EL, Caldwell HK. The vasopressin 1b receptor and the neural regulation of social behavior. *Horm Behav*. 2012;61(3):277-282. doi:10.1016/j.yhbeh.2011.11.009.

190.   Tirko NN, Eyring KW, Carcea I, et al. Oxytocin Transforms Firing Mode of CA2 Hippocampal Neurons. *Neuron*. 2018;100(3):593-608.e3. doi:10.1016/j.neuron.2018.09.008.

191.   Stöber TM, Lehr AB, Hafting T, Kumar A, Fyhn M. Selective neuromodulation and mutual inhibition within the CA3-CA2 system can prioritize sequences for replay. *Hippocampus*. 2020. doi:10.1002/hipo.23256.

192.   Chen S, He L, Huang AJY, et al. A hypothalamic novelty signal modulates hippocampal memory. *Nature*. 2020;586(7828):270-274. doi:10.1038/s41586-020-2771-1.

193.   Wu X, Morishita W, Beier KT, Heifets BD, Malenka RC. 5-HT modulation of a medial septal circuit tunes social memory stability. *Nature*. 2021;599(7883):96-101. doi:10.1038/s41586-021-03956-8.

194.   Pimpinella D, Mastrorilli V, Giorgi C, et al. Septal cholinergic input to CA2 hippocampal region controls social novelty discrimination via nicotinic receptor-mediated disinhibition. *Elife*. 2021;10. doi:10.7554/eLife.65580.

195.   Althammer F, Roy RK, Lefevre A, et al. Altered PVN-to-CA2 hippocampal oxytocin pathway and reduced number of oxytocin-receptor expressing astrocytes in heart failure rats. *J Neuroendocrinol*. 2022. doi:10.1111/jne.13166.

196.   Caroni P. Overexpression of growth-associated proteins in the neurons of adult transgenic mice. *Journal of Neuroscience Methods*. 1997;71(1):3-9. doi:10.1016/s0165-0270(96)00121-5.

197.   Korkotian E, Segal M. Synaptopodin regulates release of calcium from stores in dendritic spines of cultured hippocampal neurons. *J Physiol (Lond)*. 2011;589(Pt 24):5987-5995. doi:10.1113/jphysiol.2011.217315.

198.   Ganeshina O, Berry RW, Petralia RS, Nicholson DA, Geinisman Y. Differences in the expression of AMPA and NMDA receptors between

axospinous perforated and nonperforated synapses are related to the configuration and size of postsynaptic densities. *J Comp Neurol*. 2004;468(1):86-95. doi:10.1002/cne.10950.

199.   Kerchner GA, Nicoll RA. Silent synapses and the emergence of a postsynaptic mechanism for LTP. *Nat Rev Neurosci*. 2008;9(11):813-825. doi:10.1038/nrn2501.

200.   Alexander GM, Farris S, Pirone JR, Zheng C, Colgin LL, Dudek SM. Social and novel contexts modify hippocampal CA2 representations of space. *Nat Commun*. 2016;7:10300. doi:10.1038/ncomms10300.

201.   Brown LY, Alexander GM, Cushman J, Dudek SM. Hippocampal CA2 Organizes CA1 Slow and Fast γ Oscillations during Novel Social and Object Interaction. *eNeuro*. 2020;7(2). doi:10.1523/ENEURO.0084-20.2020.

202.   Luine V, Frankfurt M. Estrogenic regulation of memory: The first 50 years. *Horm Behav*. 2020;121:104711. doi:10.1016/j.yhbeh.2020.104711.

203.   Gould E, Woolley CS, Frankfurt M, McEwen BS. Gonadal steroids regulate dendritic spine density in hippocampal pyramidal cells in adulthood. *J Neurosci*. 1990;10(4):1286-1291.

204.   Frankfurt M, Luine V. The evolving role of dendritic spines and memory: Interaction(s) with estradiol. *Horm Behav*. 2015;74:28-36. doi:10.1016/j.yhbeh.2015.05.004.

205.   Vierk R, Bayer J, Freitag S, et al. Structure-function-behavior relationship in estrogen-induced synaptic plasticity. *Horm Behav*. 2015;74:139-148. doi:10.1016/j.yhbeh.2015.05.008.

206.   Rudy JW. Actin dynamics and the evolution of the memory trace. *Brain Research*. 2015;1621:17-28. doi:10.1016/j.brainres.2014.12.007.

207.   Hotulainen P, Hoogenraad CC. Actin in dendritic spines: connecting dynamics to function. *J Cell Biol*. 2010;189(4):619-629. doi:10.1083/jcb.201003008.

208.   Briz V, Baudry M. Estrogen Regulates Protein Synthesis and Actin Polymerization in Hippocampal Neurons through Different Molecular Mechanisms. *Front Endocrinol (Lausanne)*. 2014;5:22. doi:10.3389/fendo.2014.00022.

209.   Kim J, Schalk JC, Koss WA, et al. Dorsal Hippocampal Actin Polymerization Is Necessary for Activation of G-Protein-Coupled Estrogen

Receptor (GPER) to Increase CA1 Dendritic Spine Density and Enhance Memory Consolidation. *J Neurosci*. 2019;39(48):9598-9610. doi:10.1523/JNEUROSCI.2687-18.2019.

210. Lai K-O, Jordan BA, Ma X-M, Srivastava DP, Tolias KF. Molecular Mechanisms of Dendritic Spine Development and Plasticity. *Neural Plast*. 2016;2016:2078121. doi:10.1155/2016/2078121.

211. Bramham CR, Wells DG. Dendritic mRNA: transport, translation and function. *Nat Rev Neurosci*. 2007;8(10):776-789. doi:10.1038/nrn2150.

212. NOTEBOOM WD, GORSKI J. AN EARLY EFFECT OF ESTROGEN ON PROTEIN SYNTHESIS. *Proc Natl Acad Sci U S A*. 1963;50:250-255. doi:10.1073/pnas.50.2.250.

213. Nilsson S, Mäkelä S, Treuter E, et al. Mechanisms of estrogen action. *Physiol Rev*. 2001;81(4):1535-1565. doi:10.1152/physrev.2001.81.4.1535.

214. Paletta P, Sheppard PAS, Matta R, Ervin KSJ, Choleris E. Rapid effects of estrogens on short-term memory: Possible mechanisms. *Horm Behav*. 2018;104:88-99. doi:10.1016/j.yhbeh.2018.05.019.

215. Sellers K, Raval P, Srivastava DP. Molecular signature of rapid estrogen regulation of synaptic connectivity and cognition. *Front Neuroendocrinol*. 2015;36:72-89. doi:10.1016/j.yfrne.2014.08.001.

216. Cope EC, Zych AD, Katchur NJ, et al. Atypical perineuronal nets in the CA2 region interfere with social memory in a mouse model of social dysfunction. *Mol Psychiatry*. 2021. doi:10.1038/s41380-021-01174-2.

217. Piskorowski RA, Chevaleyre V. Synaptic integration by different dendritic compartments of hippocampal CA1 and CA2 pyramidal neurons. *Cell Mol Life Sci*. 2012;69(1):75-88. doi:10.1007/s00018-011-0769-4.

218. Piskorowski RA, Chevaleyre V. Delta-opioid receptors mediate unique plasticity onto parvalbumin-expressing interneurons in area CA2 of the hippocampus. *J Neurosci*. 2013;33(36):14567-14578. doi:10.1523/JNEUROSCI.0649-13.2013.

219. Nasrallah K, Piskorowski RA, Chevaleyre V. Inhibitory Plasticity Permits the Recruitment of CA2 Pyramidal Neurons by CA3. *eNeuro*. 2015;2(4). doi:10.1523/ENEURO.0049-15.2015.

220. Lenz M, Eichler A, Kruse P, et al. All-trans retinoic acid induces synaptopodin-dependent metaplasticity in mouse dentate granule cells. *Elife*. 2021;10. doi:10.7554/eLife.71983.

221. Lenz M, Kruse P, Eichler A, et al. All-trans retinoic acid induces synaptic plasticity in human cortical neurons. *Elife*. 2021;10. doi:10.7554/eLife.63026.

222. Mendell AL, Atwi S, Bailey CDC, McCloskey D, Scharfman HE, MacLusky NJ. Expansion of mossy fibers and CA3 apical dendritic length accompanies the fall in dendritic spine density after gonadectomy in male, but not female, rats. *Brain Struct Funct*. 2017;222(1):587-601. doi:10.1007/s00429-016-1237-6.

8 List of figures

9 Summary

9.1 English Version

Dendritic spines are small membranous protrusions covering the dendritic tree of principal telencephalic neurons, such as the GC or CA2-pc. The CA2-subregion is crucial for social memory. Dendritic spines are a main site of synaptic plasticity, which is a key element of learning and memory. The plasticity-related protein Synaptopodin (SP) is essential to form the spine apparatus (SA), a spine-specific organelle involved in synaptic plasticity. SP stabilizes dendritic spines. This thesis investigated, for the first time, the dendritic SP-distribution and its influence on spine density and spine head size under different conditions in adult mice *ex vivo*: 1) SP-overexpression (gain-of-function), 2) SP-deficiency (loss-of-function), and 3) wild type-level of SP-expression in male and female mice (sex-differences in dCA2). SP-overexpression in adult male CSPtg-mice led to a ~doubled ratio of SP+ spines in the OML of the DG, while the spine density, the average spine head size and the average SP-puncta size were not affected. Consistently, SP-deficiency in adult male SP-KO animals had no significant effect on average spine head size. Of importance, under SP-overexpression, many small spines and a few large spines become SP+, assumingly assembling a SA. On a functional level, this may indicate an activation of silent synapses. dCA2 showed sex-specific differences in spine density and spine morphology in a layer-specific manner: In males, pc-spines of the basal dCA2-compartment showed larger spine heads than females in the diestrus stage of their cycle (females (diestrus), while spine density was not significantly different. In the apical dCA2-compartment (*sr*), females (diestrus) showed an increased spine density, while spine head size was still shifted towards larger head sizes in males. In addition, dCA2 showed significant layer-specific differences in spine head size, but in a sex-independent manner: In both sexes, average spine head size in the apical *sr* was significantly smaller than in the basal *so*. This findings could reflect a yet unknown compartment-specific difference in synaptic plasticity in the basal compartment, which is preferentially targeted by neuromodulatory input from extrahippocampal sources such as the PVN or SUM[99,101,170,189-195]. In *so* of dCA2, there was no sex-specific difference in SP-puncta size or in the ratio of SP+

spines, indicating that SP is distributed in a sex-independent manner in dCA2 in adult mice.

9.2 German version

Dendritische Dornen sind kleine Plasmamembranprotrusionen, die auf vielen telenzephalischen Nervenzellen, wie der Körnerzelle des Gyrus dentatus oder die Pyramidenzelle der CA2-Region des Hippocampus, vorkommen. CA2 wird als unabdingbar für das Soziale Gedächtnis angesehen. Dendritische Dornen sind Schauplatz der synaptischen Plastizität. Das Protein Synaptopodin (SP) ist essentieller Bestandteil des Dornenapparats (spine apparatus, SA), einer für dendritische Dornen spezifischen Zellorganelle, die für die synaptische Plastizität eine große Rolle spielt. SP scheint zudem in der Lage zu sein, dendritische Dornen zu stabilisieren. Die vorliegende Arbeit untersuchte *ex-vivo* in Hirngewebe von ausgewachsenen Mäusen die SP-Proteinverteilung auf dendritische Dornen, deren Kopfgröße sowie die Anzahl der Dornen pro µm unter den folgenden Bedingungen: 1) SP-Überexpression (gain-of-function), 2) SP-Defizienz (loss-of-function), und 3) physiologische Expression von SP in männlichen und weiblichen Mäusen, im Hinblick auf Geschlechtsunterschiede. Eine ungefähr 2-fache Überexpression von SP in männlichen Mäusen führte zu einer ungefähr verdoppelten Rate an SP-positiven Dornen (d.h. Dornen, die sehr wahrscheinlich einen Dornapparat besitzen). Die Dichte aller Dornen, die durchschnittliche Kopfgröße sowie die durchschnittliche Größe von immungefärbtem SP in SP+ Dornen blieb unverändert. Passend hierzu zeigten männliche SP-defiziente Mäuse vergleichbar große Dornenköpfe wie ihre Kontrollgruppe. Unter SP-Überexpression wurden besonders viele kleine und wenige sehr große Dornen SP+, was auf eine Aktivierung von sog. «schweigenden Synapsen» hindeuten könnte. Die dCA2-Region zeigte geschlechts- und schichtspezifische Unterschiede: In *so* der Männchen hatten die Dornen größere Köpfe, während die Dornendichte unverändert war. In *sr* der Weibchen war die Dornendichte erhöht, während die Verteilung der Dornkopfgrößen in den Männchen signifikant unterschiedlich war, zugunsten großer Dornköpfe. Unabhängig vom Geschlecht waren die durchschnittliche Dornkopfgröße in *sr* kleiner als in *so*, was auf einen geschlechtsunabhängigen, kompartimentspezifischen Unterschied in Synaptischer Plastizität in CA2

hinweisen könnte. SP zeigte keinen Unterschied zwischen den Geschlechtern, was auf eine geschlechtsunabhängige Verteilung und/oder Funktion hindeutet.

10 Acknowledgments

11 Curriculum Vitae

Publikationen (Auswahl)

2022	Smilovic D., Rietsche M., Fellenz M., Drakew A., Vuksic M., Deller T. Loss of tumor necrosis factor (TNF)-receptor 1 and TNF-receptor 2 partially replicate effects of TNF deficiency on dendritic spines of granule cells in mouse dentate gyrus. J Comp Neurol (2022)
2022	Smilovic D., Rietsche M., Drakew A., Vuksic M., Deller T. Constitutive tumor necrosis factor (TNF)-deficiency causes a reduction in spine density in mouse dentate granule cells accompanied by homeostatic adaptations of spine head size. J Comp Neurol (2022)
2020	Yap K., Drakew A., Smilovic D., Rietsche M., Paul M.H., Vuksic M., Del Turco D., Deller T. The actin-modulating protein Synaptopodin mediates long-term survival of dendritic spines. Elife (2020)

12 Schriftliche Erklärung

Ich erkläre ehrenwörtlich, dass ich die dem Fachbereich Medizin der Johann Wolfgang Goethe-Universität Frankfurt am Main zur Promotionsprüfung eingereichte Dissertation mit dem Titel

The plasticity-related protein Synaptopodin in the dentate gyrus and area CA2 of the mouse hippocampus

in dem Institut für Anatomie I (Klinische Neuroanatomie) unter Betreuung und Anleitung von Herrn Prof. Dr. Thomas Deller mit Unterstützung durch Herrn Dr. Domenico Del Turco, Frau Dr. Mandy Paul und Frau Dr. Meike Fellenz ohne sonstige Hilfe selbst durchgeführt und bei der Abfassung der Arbeit keine anderen als die in der Dissertation angeführten Hilfsmittel benutzt habe. Darüber hinaus versichere ich, nicht die Hilfe einer kommerziellen Promotionsvermittlung in Anspruch genommen
zu haben.

Ich habe bisher an keiner in- oder ausländischen Universität ein Gesuch um Zulassung zur Promotion eingereicht. Die vorliegende Arbeit wurde bisher nicht als Dissertation eingereicht.

_____   _____
        (Ort, Datum)   (Unterschrift)